DIAGENESIS AND SEDIMENT-WATER EXCHANGES IN ORGANIC-POOR
SEDIMENTS OF LAKE SUPERIOR

A THESIS
SUBMITTED TO THE FACULTY OF THE GRADUATE SCHOOL
OF THE UNIVERSITY OF MINNESOTA
BY

JIYING LI

IN PARTIAL FULFILLMENT OF THE REQUIREMENTS
FOR THE DEGREE OF
MASTER OF SCIENCE

SERGEI KATSEV

JUNE, 2011

Acknowledgements

Abstract

To investigate early diagenetic processes and the spatial and temporal variability in organic-poor sediments of Lake Superior, we have repeatedly sampled sediments at 8 locations across the lake. Sediment geochemistry was characterized by the penetration depths and uptake rates of oxygen, and the distributions of organic carbon, dissolved Fe(II), nitrate, ammonium, soluble reactive phosphate (SRP), and solid phase Fe(III)/Fe(II) and phosphorus. Oxygen penetrated deeply into the sediments at all locations: from ~3.5 cm at near-shore stations to >12 cm in the deep basins. The total oxygen uptake ranged from 4.44 mmol m^{-2} d^{-1} to 7.68 mmol m^{-2} d^{-1}, averaging 6.10 mmol m^{-2} d^{-1}. Diffusive oxygen flux averaged 2.92 $\pm$ 0.75 mmol m^{-2} d^{-1}. Aerobic respiration accounted for >90-95% of the total carbon degradation, with denitrification and iron reduction contributing <5% of the total carbon degradation. Reactivity of the organic carbon in the upper 1 cm of sediment was calculated to be ~ 1.2 yr^{-1}, which is typical for organic material less than a year old. Sediment carbon degradation rate of 5.29$\pm$ 1.20 mmol m^{-2} d^{-1} corresponds to ~ 19% of the recently estimated primary production. More than ~ 90% of carbon reaching the lake floor is mineralized, with a sediment carbon burial flux of 0.49 mmol m^{-2} d^{-1}. Diffusive fluxes of nitrate from sediment into the overlying water averaged 0.17$\pm$ 0.07 mmol m^{-2} d^{-1}, recycling ~ 40% of nitrogen sedimentation flux. Phosphorus cycling was strongly associated with the diagenetic cycling of iron. Sediment diffusive effluxes of SRP were small ($< \sim 1.5$ x 10^{-3} mmol m^{-2} d^{-1}) and similar among stations. The efficient trapping of phosphorus in the sediment is interpreted as a result of strong adsorption of phosphorus by iron (hydro)oxides. Sediments in Lake Superior exhibit strong spatial heterogeneity on spatial scales down to hundreds of meters. The presence of multiple Fe- and Mn-rich layers, forming dense crusts and often visible to the naked eye, suggests decadal or longer variations in the sediment's physical or redox environment. Oxygen diffusive fluxes and carbon degradation rates exhibited strong seasonality, with higher oxygen fluxes and carbon degradation rates in July, and the depth of oxygen penetration varied by several mm to cm.

Table of Contents

List of Tables

List of Figures

Introduction

Organic-poor sediments underlie vast areas of the Earth's ocean floor and account for a major fraction of global carbon exchanges with the water column. For example, sediments in water depths >3000 m are responsible for 40% of the benthic organic matter mineralization in the ocean (Glud 2008). These sediments are typically characterized by a deep penetration of oxygen (> 5 cm), which is sensitive to the supplies of organic carbon and oxygen from the overlying water column (Katsev et al. 2006). Oxygen penetration, which is the most important sediment redox boundary, may fluctuate in response to temporal changes in the environment. Significant changes in the oxygen penetration depth (OPD) were suggested to occur seasonally in response to seasonality in organic sedimentation (Gehlen et al. 1997) and on a decadal scale possibly as a result of global warming (Gobeil et al. 2001; Katsev et al. 2006). Fluctuations in OPD may shift the pathways of organic matter mineralization, modify other redox reactions, and affect the rates of sediment exchanges with the water column. A better understanding of these fluctuations and their consequences is needed to understand the carbon and nutrient budgets, as well as to interpret the sediment records of past environmental changes.

Detecting the fluctuations in sediment redox boundaries is difficult. Direct observations are often lacking because of the difficulty of continuous sampling. The fluctuations may become recorded in the distributions of sediment redox sensitive elements (Mangini et al. 2001; Katsev et al. 2006), which in that case may provide at least some information on past changes over the decadal or longer time scales. The detection of seasonal fluctuations requires a repeated characterization of the sediments,

which is expensive in the deep ocean. In addition, repeated sediment sampling necessarily assumes that sediments are identical within the sampling area, so that the observed changes may be interpreted as temporal. The assumption of spatial homogeneity is rarely tested. This thesis addresses the issues of spatial and temporal variability in OPD in organic-poor sediments, and investigates their effects on early diagenetic processes and fluxes across the sediment-water interface.

Lake Superior, with its large surface area, mostly marine organic sedimentation (Zigah et al. 2011), and low organic carbon content in the open lake sediments (Evans et al. 1981; Johnson et al. 1982), provides an opportunity to investigate sediment biogeochemical processes and their spatial and temporal variability without incurring the high costs of ocean research. Whereas obvious differences exist between a freshwater lake and the deep ocean, the deep penetration of oxygen, low organic carbon content, and strong seasonality in organic sedimentation in Lake Superior make it an interesting analogue to at least some of the abyssal ocean environments, in particular the deep Arctic Ocean.

Lakes and other freshwater environments are important components of the global C cycle, yet their sediments remain understudied in terms of C burial, sequestration, and early diagenetic C remineralization. In comparison to marine environments, there is little information on the rates and pathways of C degradation in lake sediments and there have been few rigorous examinations of the relationships between C burial, water depth, sedimentation rate, primary production, and electron acceptor availability. Arguably, lakes deserve more attention than marine environments given their relative heterogeneity

and spatial and temporal complexity. Characterizing the benthic geochemical fluxes in Lake Superior is also important in the context of the carbon and nutrient cycling in this lake. The budgets of organic carbon and nitrogen in the Lake Superior water column are imbalanced: the inputs of organic carbon from primary production and other sources are thought to be lower than the total outputs (Cotner et al. 2004; Sterner 2010); the difference between nitrogen inputs and outputs is $\sim 50\%$ greater than the building up of nitrate in the water column (Sterner et al. 2007), suggesting substantial loss to sediments. As sediments actively participate in the exchanges of these substances with the water column, it is important to characterize the fluxes of these elements across the sediment-water interface and the rates and pathways of their transformations within the sediment column.

In this study we investigate the early diagenetic processes in the sediments of Lake Superior and test their spatial and temporal variability. The study was conducted on sediments sampled repeatedly at 8 sites, which ranged from coastal to open-basins, during the navigation seasons in 2009 and 2010. We characterize the oxygen penetration, porewater concentrations of dissolved inorganic nitrogen, phosphorus and iron, the fluxes within the sediments and the rates of major mineralization pathways of organic carbon. Fluxes across the sediment water interface are determined for nitrate and soluble reactive phosphorus (SRP, which is a proxy for phosphate), and their significance for the lake-wide budgets of nitrogen and phosphorus is discussed. We discuss the evidence for transient diagenesis and its possible origins: changes in the sediment redox conditions on

3

seasonal and longer time scales and physical disturbance of the sediments by bottom currents.

Whereas the main goal of this work is to characterize the primary diagenetic redox sequence -- to define the zones of principal mineralization pathways, calculate the rates of the main redox reactions and fluxes of major elements across the sediment-water interface -- in the process we analyzed our sediment samples for a number of other characteristics. Those less relevant data are presented in figures and tables but are not discussed in detail, to preserve the focus of the text on the central theme of the thesis.

The thesis is structured as follows:

Chapter 1 provides a geochemical and limnological background and formulates problems that we are addressing in this thesis. We first describe the major geochemical pathways of sediment early diagenesis, discuss the steady state and transient regimes, and focus more narrowly on organic-poor sediments. We then review the sediment geochemistry in Lake Superior. The lake-wide carbon and nutrient budgets are briefly reviewed, and presently outstanding issues are identified.

Chapter 2 describes the methodology: sampling, on-board and in-lab measurements and experiments, and approximations and parameters used in calculations.

Chapter 3 presents the experimental and calculation results.

Chapter 4 discusses the sediment diagenesis in Lake Superior. Both spatial and temporal variability is addressed. We identify the geochemical pathways of organic carbon mineralization and quantify their rates, and calculate the contributions of

sediment-water nutrient fluxes to their respective lake-wide budgets. We also discuss the

evidence for and possible causes of transient diagenesis.

Chapter 5 summarizes our conclusions and main numerical results.

Chapter 1 Background:

Steady state diagenesis in aquatic sediments

Continuous piling up of fresh sediment at the sediment-water interface results in a downward motion of sediment particles and interstitial waters relative to the sediment-water interface. When conditions can be considered constant in time, steady state diagenesis results in sediment properties (concentrations, rates, etc.) at a particular depth being constant. This is the basis for a steady state approximation, which is a good starting point for understanding the diagenetic processes. As the sediment is being buried, it undergoes biogeochemical transformations that are fuelled primarily by mineralization (oxidation) of organic matter. Microbially-catalyzed oxidation of organic carbon by several electron acceptors (Table 1) proceeds in the order of the free energy yield of the reaction (Froelich et al. 1979): the most energetic reaction occurs first until the concentration of the electron acceptor falls below a critical level, at which point the next most efficient oxidant is used. The sequence continues until all oxidants are consumed or reactive organic material is exhausted (see reactions in Table 1 and Fig. 1). Aerobic respiration (i.e. by O_2 as electron acceptor) is energetically most favorable. In organic-poor systems, including pelagic oceans, aerobic respiration is the dominant process, often accounting for $> 90\%$ of sediment carbon degradation (Bender and Heggie 1984; Archer et al. 2002; Burdige 2006). In environments with greater concentrations of organic carbon or lower concentrations of oxygen, considerable carbon oxidation occurs below the oxic

zone, anaerobically (Canfield 1994). Anaerobic mineralization is often presumed to occur at slower rates than aerobic (Wakeham and Canuel 2006).

Denitrification, which uses *nitrate* as the electron acceptor, is frequently considered as the second most energetic pathway. As N_2 is produced as an end product, which then escapes, denitrification serves as a geochemical sink for sediment nitrogen. Nitrate may be also reduced to ammonium (nitrate ammonification), but the controls of this process are poorly understood (Burdige 2006). After nitrate, the next preferable electron acceptors are poorly crystalline *manganese and iron oxides*. The zone of manganese reduction often overlaps vertically with the denitrification zone, as the two processes provide similar amounts of free energy, Mn reduction now being considered slightly more energetic (LaRowe and Van Cappellen 2011). Iron reduction typically proceeds after nitrate is completely depleted (Burdige 1993). The reduced products, Mn(II) and Fe(II), are soluble and typically diffuse upwards into the oxic zone where they can re-precipitate upon oxidation. *Sulfate* reduction and *methanogonesis* occur below the zone of Fe reduction if there is still metabolizable organic matter. In organic-poor sediments of the deep seafloor, anaerobic respirations fuelled by NO_3^-, MnO_2, FeOOH, and SO_4^{2-} rarely oxidize more than 5-10% of the deposited organic carbon (Bender and Heggie 1984).

Degradation of organic compounds releases ammonium and phosphates (Burdige 2006). The nitrogen and phosphorus, thus mobilized into the sediment interstitial water, may eventually diffuse into the water column, where they can become available for uptake by biota. In lakes, the sediment recycling of nutrients, especially phosphorus, is

often an important factor that regulates lake productivity (Hecky and Kilham 1988). As Fe oxyhydroxide strongly binds phosphates, the release of phosphorus is frequently linked to the diagenetic cycling of iron (Wetzel 2001; Caraco et al. 1993). As in the presence of oxygen the released ammonium can be oxidized within the sediment to nitrate (*nitrification*), the flux of nitrate across the sediment-water interface is controlled by the balance of nitrification and denitrification (Middelburg 1996).

The reduced products of the anaerobic respiration reactions may diffuse upwards from the deep, reduced, sediment layers upwards, where they can be oxidized in a suite of chemoautrophic reactions: methane oxidation, manganese and iron oxidation, and oxidation of several reduced forms of sulfur (Table. 1). Most of these reactions consume oxygen, and the flux of oxygen into the sediment, therefore, reflects not only aerobic respiration but also, indirectly, contributions from anaerobic metabolisms. The only exception is denitrification, where the reduced product N_2 can escape as gas. In addition to the oxidation reactions that use oxygen, inorganic oxidative reactions may involve nitrate and manganese oxides as oxidants (see Table 1 for some common reactions; Hulth et al. 1999). For example, in anaerobic ammonium oxidation (*anammox*), nitrate is used to oxidize ammonium and N_2 is released as end product (Strous et al. 1999; Dalsgaard et al. 2005).

Table 1 Primary organic matter mineralization processes, aerobic chemolithotrophic reactions, and reactions in anoxic sediments

(Modified from Burdige 2006, Katsev et al. 2006, and Hulth et al. 1999)

Process	Organic matter remineralization reaction
Aerobic respiration	$(CH_2O) + O_2 \rightarrow CO_2 + H_2O$
Denitrification	$(CH_2O) + 4/5NO_3^- \rightarrow 2/5N_2 + 4/5HCO_3^- + 1/5CO_2 + 3/5H_2O$
Manganese reduction	$(CH_2O) + 2MnO_2 + 3CO_2 + H_2O \rightarrow 2Mn^{2+} + 4HCO_3^-$
Iron reduction	$(CH_2O) + 4Fe(OH)_3 + 7CO_2 \rightarrow 4Fe^{2+} + 8HCO_3^- + 3H_2O$
Sulfate reduction	$(CH_2O) + 1/2SO_4^{2-} \rightarrow HCO_3^- + 1/2H_2S$
Methanogenesis	$(CH_2O) \rightarrow 1/2CH_4 + 1/2CO_2$
	Aerobic chemoautotrophic reactions
Nitrification	$NH_4^+ + 2O_2 + 2HCO_3^- \rightarrow NO_3^- + 2CO_2 + 3H_2O$
Iron oxidation	$4Fe^{2+} + O_2 + 8HCO_3^- + 2H_2O \rightarrow 4Fe(OH)_3 + 8CO_2$
Manganese oxidation	$Mn^{2+} + O_2 + 2HCO_3^- \rightarrow MnO_2$
Sulfide oxidation	$H_2S + 2O_2 + 2HCO_3^- \rightarrow SO_4^{2-} + 2CO_2 + 2H_2O$
	Anaerobic-inorganic reaction
Anoxic nitrification	$4MnO_2 + NH_4^+ + 6H^+ \rightarrow 4Mn^{2+} + NO_3^- + 5H_2O$
Anammox	$5NH_4^+ + 3NO_3^- + 2HCO_3^- \rightarrow 4N_2 + 11H_2O + 2CO_2$
Denitrification coupled with Fe oxidation	$NO_3^- + 5Fe^{2+} + 4HCO_3^- + 8H_2O \rightarrow 5Fe(OH)_3 + 1/2N_2 + 4CO_2$
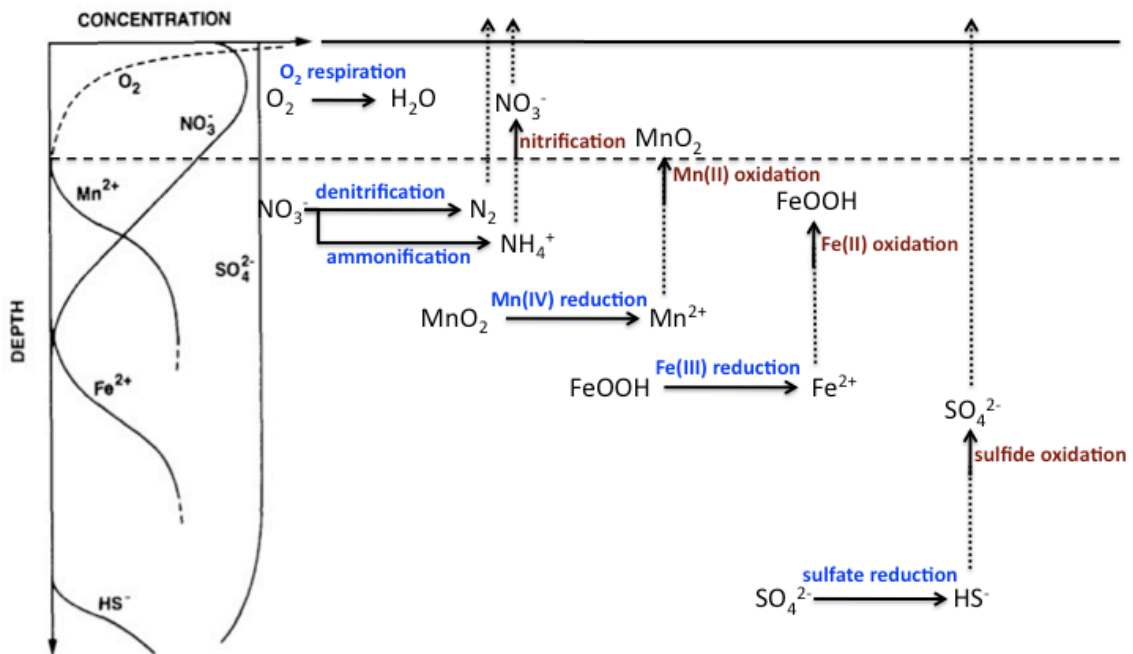
Figure 1. Schematics of primary diagenetic processes

Hypothetical profiles on left are taken from Burdige 2006. Horizontal solid line indicates the sediment-water interface; dashed line is the oxic-anoxic boundary; directions of diagenetic reactions are indicated by solid arrows; diffusion processes are indicated by dotted arrows.

Transient diagenesis in organic-poor sediments

In situations where environmental conditions vary in time, *non steady-state* processes may become important (Burdige 2006). In coastal marine sediments, for example, the depth of oxygen penetration (OPD) may fluctuate seasonally by several centimeters (Glud et al. 2003; Martens and Klump 1984). Seasonality in oxygen consumption rates was observed, for example, in abyssal sediments in the Central and Eastern North Pacific (Smith and Baldwin 1984). Longer-scale changes were inferred in the deep Arctic Ocean: distributions of redox sensitive metals suggested an upward migration of the sediment redox boundary by several tens of cm within the past 50 years, presumably as a result of an increased flux of degradable organic matter caused by thinning ice (Gobeil et al. 2001). Organic-poor sediments are particularly prone to such OPD migrations, which may be caused by variations in either sedimentation fluxes of organic carbon or bottom water oxygen availability (Katsev et al. 2006; Rabouille and Gaillard 1991).

The time scales of the OPD migrations are linked to their causes. Variations in the concentration of oxygen in the bottom water typically displace the oxygen penetration depth (OPD) on the time scale of diffusion, $t = x^2/(2D)$, where x is the distance over which the dissolved oxygen needs to diffuse and D is the diffusion coefficient. For example, for a typical value of D= 400 cm^2/yr, oxygen diffuses to x=8 cm in 1 month. Responses to organic sedimentation are determined by the magnitude of the organic carbon flux variability and the reactivity of organic carbon that reaches the sediment. For seasonal OPD variations, the deposited organic carbon must decompose on a seasonal or

11

shorter time scale (1 year) (Martin et al. 1988). For example, the North Atlantic deep-sea sediments, characterized by a carbon degradation rate constant k $\sim$5-10 yr^{-1}, were shown to exhibit seasonality in oxygen fluxes caused by the seasonal variations in the sedimentation flux of organic matter (Smith and Baldwin 1984). The North Pacific sediments with k <1 yr^{-1}, on the other hand, exhibited constant oxygen consumption rates while organic carbon fluxes varied by a factor of $\sim$3-5 (Sayles et al. 1994). Non-steady state processes on yet longer time scales include such processes as burn-down of turbidites and gravity-driven flows of organic rich sediments to the pelagic sediments (Burdige 2006).

Migrations of the oxygen penetration depth significantly affect the pathways of organic carbon mineralization, as they shift the balance between the supplies of electron acceptors and reactive organic material. For example, carbon mineralization may intensify when a downward migration of OPD supplies oxygen to the previously anoxic sediments. Shifts in the mineralization pathways may also affect the elemental sediment-water exchanges. For example as a downward movement of OPD increases the role of aerobic respiration, less nitrate is removed as N_2 by denitrification. Accumulation of nitrate in the sediments may result in an increased flux of nitrate from sediment into the water column. Migrations of the OPD also redistribute redox sensitive elements within the sediment column (Burdige 1993). For example, a shallowing redox boundary may lead to the dissolution of previously accumulated Mn(IV) phases and their re-precipitation at the new OPD (Katsev et al. 2006). In contrast, a deepening OPD does not affect the Mn oxide enrichments. For this asymmetry, where direct observations of

transient diagenesis are difficult, the distributions of sediment redox sensitive elements may become records of redox migrations. Multiple peaks in solid-phase manganese, for example, a common observation in many pelagic and hemipelagic sediments (Burdige 2006), may indicate the present/past location(s) of the manganese redox boundary (Thomson et al. 1996; Mangini et al. 2001). Non-steady state features in the distributions of other redox sensitive elements, such as Fe, Re, S and U, can also indicate redox excursions (Colley et al. 1984; Wilson et al. 1986; Gobeil et al. 2001). Investigating non-steady state redox processes in the organic-poor sediments of Lake Superior, which are expected to be sensitive to redox variations, provides an opportunity for bettering the understanding of such processes in other, less accessible, environments.

Lake Superior: carbon and nutrient cycles

Lake Superior is the world's largest freshwater lake by area (82,100 km^2) and one of the deepest, with the maximum depth of 405 m and average depth of 147 m (Matheson and Munawar 1978). It contains approximately 10% of the Earth's surface freshwater and serves as an important water resource for North America. The water temperature varies seasonally at the lake surface between 0 and 17 °C but in the bottom water remains near 3.5 °C in summer and decreases to 1°C in winter. This thermal regime results in dimictic overturns (Bennett 1978). The lake is highly oligotrophic, with productivity being significantly lower than in other Laurentian Great Lakes (Munawar and Munawar 1978; Hecky 2000). Despite a number of recent estimates for primary production (Table 2), with a most resent estimate of 9.7 Tg yr^{-1} (119 g m^{-2} yr^{-1}, Sterner 2010), the productivity

trends in Lake Superior remain poorly documented and differences in methodology make comparisons between studies difficult.

The budget of organic carbon in Lake Superior is poorly constrained and appears imbalanced, with losses exceeding inputs (Table 2). Primary production is the main source of organic carbon to the water column (Keough et al. 1996; Ostrom et al. 1998), whereas losses occur primarily through respiration in the water column (Cotner et al. 2004). Most respiration measurements were made in the western arm of the lake, where the primary production and terrestrial carbon inputs are higher, and data for winter are not yet available, so the lake-wide annual respiration may be overestimated (McManus et al. 2003). The riverine and atmospheric inputs account for ~ 6% - 9% of the total input of organic carbon (Cotner et al. 2004; Maier and Swain 1978). Benthic DOC fluxes are not well constrained, as they vary greatly seasonally and among locations, and the size of the lake floor area that accumulates sediment (depositional area) is not well constrained (Stark 2009). Sedimentation flux was estimated in the western arm in sediment traps (Heinen and McManus 2004), but may not be representative of a lake average.

The present-day lake-wide budget for nitrogen is also imbalanced (Table 3): the output of 156 mmol m^{-2} yr^{-1} does not balance the minimum total input of 192 mmol m^{-2} yr^{-1}. Nitrate concentrations in the water column have increased through the 20th century, at a buildup rate of 23.4 mmol m^{-2} yr^{-1}, stabilizing somewhat in the last two decades (Sterner et al. 2007). Still, the difference between the estimated inputs and outputs of nitrate is greater than the build up rate, suggesting that nitrogen outputs are underestimated. Total phosphorus output is two fold higher then the total input (Table 4).

Table 2. Sources and sinks of organic carbon for Lake Superior water column (Tg yr^{-1}).

Sedimentation flux is calculated from an organic carbon sedimentation rate of 2.3 mmol C m^{-2} d^{-1} (Heinen and McManus 2004). The most resent estimate for primary production (Sterner 2010) was used to calculate the total input.

Source/Sink	Input	Output	Reference
Primary Production	9.7		Sterner 2010
	5.3-8.2		Cotner et al. 2004
	3-8		Urban et al. 2005
Riverine input	0.54-0.62		Cotner et al. 2004
	0.63		Maier and Swain 1978
Atmosphere deposition	0.16-0.41		Cotner et al. 2004
Benthic DOC flux	0.71		Stark 2009
Respiration in water column		13-39	Cotner et al. 2004
Sedimentation flux		0.83	Heinen and McManus 2004
Outflow		0.12	McManus et al. 2003
Total	11.1-11.4	14.0- 40.0	

Table 3. Sources and sinks of nitrogen in Lake Superior (mmol m^{-2} yr^{-1})

Table is modified from Sterner et al. 2007. Benthic fluxes of NO$_3^-$ are calculated from Heinen and McManus (2004)'s estimates of 0.15± 0.07 mmol m^{-2} d^{-1}, and fluxes of DON was estimated by Stark (2009) as 100 mmol m^{-2} yr^{-1}. Sedimentation flux is calculated from an organic carbon sedimentation rate of 2.3 mmol C m^{-2} d^{-1} (Heinen and McManus 2004), with a C:N ratio of 13 (Heinen and McManus 2004).

Source/Sink	Input	Output
Atmospheric deposition of NO$_3^-$ and NH$_4^+$	30.1	
Watershed input of NO$_3^-$, NH$_4^+$ and organic N	32.7	
Nitrogen fixation	Unknown	
Outflow of NO$_3^-$, NH$_4^+$ and organic N		28.6
Sedimentation flux		127
Benthic flux of NO$_3^-$	55±26	
Benthic flux of DON	100	
Total	192-244	156

Table 4. Sources and sinks of phosphorus in Lake Superior (Mmol yr^{-1})

Total input includes atmospheric, point-source and riverine inputs. Total P outflow of 14 Mmol yr^{-1} is also estimated based on maximum TP concentrations of 0.2 uM (Baehr and McManus 2003) and total outflow of 6.96 x 10^{10} m^3 yr^{-1}(Maier and Swain 1978). Sedimentation flux is calculated from a organic carbon settling rate of 2.3 mmol m^{-2} d^{-1}, with a C:P ratio of 106:1 (Redfield 1934). Benthic flux of SRP is calculated from SRP flux of 0.006 mmol m^{-2} d^{-1} (Heinen 2002).

Source/Sink	Input	Output	Reference
Input	130		Chapra and Sonzogni 1979
	100		Lesht et al 1991
	100-200		Heinen and McManus 2004
Outflow		12.9	Heinen and McManus 2004
		14	Baehr and McManus 2003; Maier and Swain 1978
Sedimentation		650	Heinen and McManus 2004
Benthic flux of SRP	180		Heinen 2002
Total	380	677	

Lake Superior: sediment properties

The floor of Lake Superior exhibits high spatial heterogeneity. The western and central basins of the lake contain large, low relief abyssal plains (Johnson et al. 1982), whereas the eastern region of the lake is topographically more complex, containing deep basins and shoals, troughs and steep relief, with great spatial variability in sediment accumulation patterns over distances as small as a few kilometers (Klump et al. 1989). Sedimentation rates across the lake are generally low and non-uniform, ranging from 0.01 to 0.32 cm/yr (Fig. 2; Evans et al. 1981), with large areas of the lake considered non-depositional (Kemp et al. 1978; Thomas and Dell 1978). The western basin of the lake, which is believed to have higher phytoplankton abundance than the eastern and central basins (Munawar and Munawar 1978), accumulates more sediment (Kemp et al. 1978; Evans et al. 1981). Sedimentation rates have been estimated at 0.02-0.04 cm/yr in the open waters of the western basins, 0.01-0.02 cm/yr in that of the eastern basin and <0.03 cm/yr in the central basin (Bruland et al 1975; Kemp et al. 1978; Evans 1980; Evans et al. 1981). Shoreline erosion and re-suspension of near-shore sediments causes moderate to high (0.05-0.11 cm/yr) sedimentation rates in the western arm of lake adjacent to the Wisconsin coast; marginal bays adjoining Lake Superior (Thunder, Whitefish, and Keweenaw Bays) are regions of very high (>0.15 cm/yr) sedimentation rates (Evans et al. 1981).
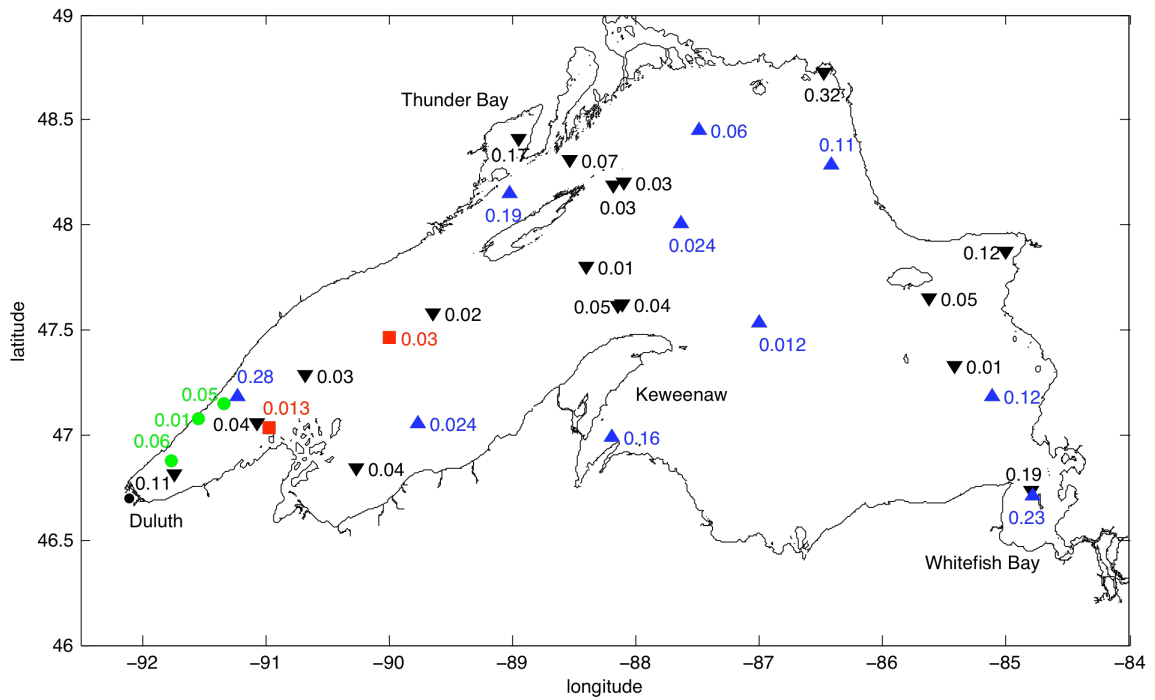
Figure 2. Sedimentation rates in Lake Superior.

Black triangles are Evans 1980, by 210Pb method; blue triangles are from Kemp et al. 1978, by pollen method; red squares are from Bruland et al. 1975 by 210Pb and pollen methods; and green circles are from Maher 1977 by pollen method.

Recent seismic surveys (van Alstine 2006) that focused on the western basin revealed that the lake floor contains multiple pockmarks, as well as linear and ring-shaped depressions that were ~2 m deep and spanned hundreds of meters. These featured are hypothesized to be expressions of glacial iceberg scouring and dewatering of post-glacial sediments (T. Johnson and N. Wattrus, pers. comm.). Analyses of sediment cores revealed that the sediment properties may vary strongly along these features, with post-glacial, organic-depleted, sediments sometimes being exposed along the depressions.

The organic carbon concentrations in the upper sediment layer in Lake Superior range 0.3-4% (Carlton et al. 1989; Richardson and Nealson 1989). Sediment carbon degradation rates were estimated to be 2.1 mmol m^{-2} d-1 in the eastern basin by diffusive oxygen uptake measurements (Klump et al. 1989) and 1.7±0.6 mmol m^{-2} d^{-1} in the western arm by incubation for oxygen consumption rates (Heinen and McManus 2004). Reported oxygen penetrations into the sediment varied between 0.8 to 2.4 cm near the Isle Royale and Keweenaw peninsula (Carlton et al. 1989), and from 2 cm to >15 cm in the eastern basin (Richardson and Nealson 1989). In the central and eastern basins, aerobic respiration was estimated to account for > 94% of the carbon mineralization in the sediments (Carlton et al. 1989). Denitrification rates ranged between 0 and 0.11 mmol m^2 d^{-1} (Carlton et al. 1989). Sulfate reduction was found to be insignificant (Carlton et al. 1989). Fluxes across the sediment water interface reported in the literature are summarized in Table 5.

Table 5. Fluxes at sediment-water interface in Lake Superior (mmol m^{-2} d^{-1})

Organic carbon settling	Oxygen uptake	DOC flux	Nitrate flux	DON flux	SRP flux	Reference
2.3	2.2 ± 0.8		0.15 ± 0.07		0.006	Heinen and McManus 2004; Heinen 2002
	2.7					Klump et al. 1989
3.0						Johson et al. 1982
	1.2-2.7					Carlton et al. 1989
		2.0	0.12	0.27		Stark 2009

The objectives of this work

This work aims to quantify the seasonality in sediment diagenesis in Lake Superior and constraining the sediment contributions to the geochemical budgets of carbon, nitrogen, and phosphorus. The specific objectives are:

- To characterize the spatial and temporal dynamics of oxygen in the deep sediments of Lake Superior in terms of the oxygen penetration depth, oxygen consumption rates, and sediment oxygen uptake.

- To evaluate evidence for transient diagenesis in Lake Superior and conclude on its causes, time scales, and sediment signatures.

- To characterize the vertical extent and the rates of the biogeochemical reactions in the primary diagenetic redox sequence in these sediments.

- To determine the rates of carbon degradation in Lake Superior sediments, their variation with depth within the sediment, the efficiency of carbon mineralization and burial, and the sediment contribution to the lake-wide carbon budget.

- To estimate nutrient fluxes across the sediment-water interface, gain insight into their controls, and improve understanding of the sediment contributions to the nutrient budgets of the lake.

Chapter 2. Methods

Sampling and sample preparation

Sediment and water column samples were taken on several cruises aboard the *R/V Blue Heron* during 2009-2010, from the eastern, western, and central basins of Lake Superior (Table 6 and Fig. 3). Sediment cores (94 mm i.d., in polycarbonate coring tubes) were recovered by Ocean Instruments Multi-corer. The lake floor was monitored by a Knudsen echosounder to avoid disturbed areas. The cores were stored at 4 °C before processing. Sediment cores were sectioned on-board after >40 minutes of equilibrating. Cores for porewater extractions were sectioned in a glove bag filled with nitrogen to avoid oxidation by atmospheric oxygen (Fig. 4a). Sediments were sectioned into 50 mL centrifuge tubes and porewaters were extracted from sediment sections using Rhizon porous polymer micro samplers with 0.1 um membrane (Fig. 4b and 4c; Dickens et al. 2007). The remaining fractions were frozen at -18 °C for further analyses. Porewater samples were stored in separate vials with storage methods appropriate for each analysis: NO_3^- and NH_4^+ samples were frozen at -18 °C, Fe^{2+} and SRP samples were acidified with 6 N HCl to 1% and stored at 4 °C. Water column oxygen concentrations and temperature were measured using a Seabird 911 CTD. Bottom water samples were taken from ~5 m above the sediment-water interface, filtered with 0.2 um GMF filter and stored for future analysis.

Separate, intact, sediment cores were split, photographed, and analyzed for magnetic susceptibility and gamma density at the LacCore facility of the University of

Minnesota. Gamma density was determined by whole-core logging on the Geotek Multi-Sensor Core Logger (MSCL) at a 0.5 cm resolution. Core tubes were grooved in a core cradle using a pair of vibrating medical cast saws and the saws were set to stop short of cutting through the whole tube to avoid tube shreds spreading into the sediments. Utility knives were used to finish the cut. Cores are split into two halves with a pair of guillotines and stored under refrigeration (4 °C). The sediment surface was cleaned using a glass microscope slides with rounded corners before the split cores were imaged. Images were taken by a line-scan CCD camera and a color card was included in the image for color correction. Magnetic susceptibility was determined in split cores by MSCL-XYZ automated core loggers with 0.5 cm resolution.

Sediment water contents were determined by comparing the sediment sample weights before and after freeze-drying:

$$WC(\%) = \frac{(W_1 - W_2)}{(W_2 - W_0)} \times 100\%$$

W_0 ---- weight of vials, g

W_1 ---- weight before freeze-dried of vial and sediment, g

W_2 ---- weight after freeze-dried of vial and sediment, g

Where appropriate, sediment porosity was calculated from the density of bulk sediments (gamma density measured by MSCL) and water contents:

$$\varphi = WC \times \frac{\rho}{\rho_{H_2O}}$$

Table 6. Sampling locations and times

1. Sediment cores taken from Robert Sterner's cruises, of which oxygen measurements and other processing were conducted 2 days after the cores were recovered; 2. WM_Jun10 cores were taken from two locations about 150 m apart, described as WM_Jun10-a and WM_Jun10-b in later text; 3. WM_Jul10-b and WM_Jul10-c were taken from locations ~150 m apart.

Date	Core	Depth (m)	Latitude	Longitude
6/3/2009	FWM_Jun09	170	47 02.90 N	91 14.97 W
11/10/2009	FWM_Nov09[1]	160	47 06.26 N	91 43.19 W
6/7/2010	FWM_Jun10	166	47 02.13 N	91 16.44 W
7/20/2010	FWM_Jul10	168	47 02.14 N	91 16.38 W
9/21/2010	FWM_Sep10	166	47 01.98 N	91 16.50 W
6/5/2009	EM_Jun09	218	47 32.54 N	86 34.31 W
10/6/2009	EM_Oct09	225	47 32.52 N	86 34.31 W
6/10/2010	EM_Jun10	229	47 33.38 N	86 35.76 W
7/22/2010	EM_Jul10	228	47 33.36 N	86 35.65 W
9/22/2010	EM_Sep10	226	47 33.37 N	86 35.68 W
6/4/2009	WM_Jun09	175	47 18.32 N	89 49.43 W
10/4/2009	WM_Oct09	170	47 18.29 N	89 49.73 W
6/11/2010	WM_Jun10[2]	169	47 19.01 N	89 50.73 W
7/22/2010	WM_Jul10[3]	174	47 18.26 N	89 49.33 W
9/25/2010	WM_Sep10	169	47 19.05 N	89 50.76 W
6/8/2010	IR_Jun10	234	47 58.41 N	88 28.01 W
7/21/2010	IR_Jul10	237	47 58.42 N	88 28.07 W
9/22/2010	IR_Sep10	235	47 58.41 N	88 28.08 W
6/8/2010	CM_Jun10	252	48 01.06 N	87 46.44 W
7/21/2010	CM_Jul10	236	48 02.84 N	87 47.32 W
9/22/2010	CM_Sep10	235	48 02.66 N	87 47.17 W
7/21/2010	ED_Jul10	316	47 31.81 N	87 07.81 W
9/22/2010	ED_Sep10	318	47 31.53 N	87 07.49 W
6/9/2010	KW_Jun10	84	47 09.85 N	88 05.32 W
6/4/2009	SI_Jun09	100	48 41.00 N	86 57.20 W
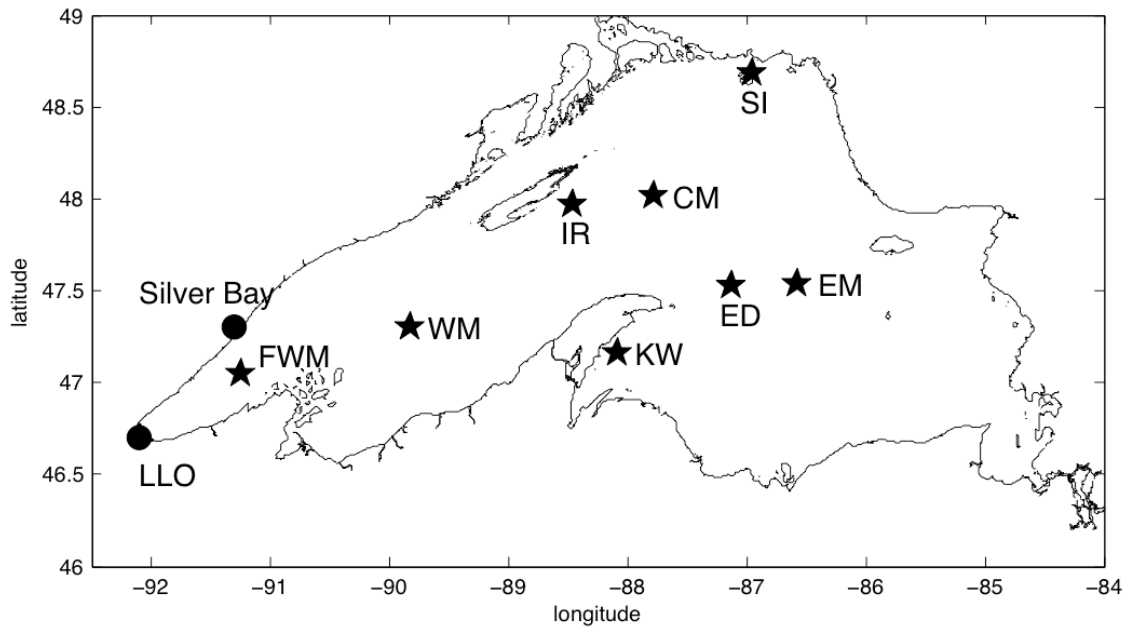
Figure 3. Sampling locations in Lake Superior.

Distances between sub-stations are smaller than the size of the symbol.

Figure 4. a. Sectioning of a sediment a core in a glove bag filled with N$_2$; b. Extracting sediment porewaters with Rhizon samplers in a N$_2$-filled glove bag; c. Rhizon sampler: hydrophilic porous polymer, pore diameter of 0.1 μm. The fluid sampled from the sediment flows into the tiny space between the porous tube and the supporting wire.

Oxygen measurements

Vertical distributions of dissolved oxygen in sediment porewaters were determined on board in sub-sampled cores (i.d. ~5 cm) that were kept at 4 °C and were thermostated following their recovery. Oxygen concentrations were measured using a Unisense (Clark-type) microelectrode (Revsbech 1989) positioned using a micromanipulator (Fig. 5). The electrode was calibrated in air-saturated and nitrogen-purged water at the temperature of measurement. Decrease of oxygen concentrations in overlying waters was measured to determine oxygen uptake rates (by S. A. Crowe).

Sub-cores after oxygen profiling were capped with stoppers and incubated under 4 °C and dark environment. Electrical tape was used to wrap around the tube ends to avoid contamination with atmospheric oxygen. Oxygen profiles were measured several times during incubations.

Figure 5. a. Measurement of sediment oxygen concentrations; b. Unisence (Clark-type) microelectrode (Revsbech 1989)

Organic carbon

The organic matter content was estimated in freeze-dried sediment samples by loss on ignition (modified from Dean 1974 and Niendorf 1998): powdered samples were dried in an oven at 60 °C in pre-weighed ceramic crucibles overnight and weighed after cooling to room temperature in a desiccator. Samples and crucibles were then heated in a muffle furnace at 550 °C for 5 hours. After cooling to room temperature in a desiccator, the samples were weighed again to get the weight of organic carbon ignited, which was the difference of the sample weight before and after ignition:

$$LOI(\%) = \frac{(W_1 - W_2)}{(W_1 - W_0)} \times 100\%$$

W_0 ---- weigh of crucibles

W_1 ---- weigh after drying at 60 °C overnight

W_2 ---- weigh after ignited at 550 °C for 5 hours

In selected samples, the total organic and inorganic carbon concentrations were also determined by coulometry using CM150 – TC/TOC/TIC Analyzer (by M. Kistner).

Nitrate and ammonium

Dissolved nitrate concentrations were measured using a Lachat Quickchem 8000 flow injection auto-analyzer (Diamond el al. 1999). Nitrate is quantitatively reduced to nitrite by passage of samples with appropriate dilution through a copperized cadmium column. Diazotized by sulfanilamide under acidic conditions, the reduced nitrate plus original nitrite form a diazonium ion which then is coupled with N-(1-

naphthyl)ethylenediamine dihydrochloride to result in a pink dye that absorbs at 520 um. Ammonium concentrations in porewaters were measured by the Orthophthaldialdehyde (OPA) fluorometric method (Holmes et.al. 1999): working reagent consisted of OPA, sodium sulfite and sodium borate was added to samples and incubated for 3 hours to give fluorescence with intensities proportional to concentrations of ammonium. Fluorescence was measured using a Fluoremeter TD-700.

Iron in solid phases and porewaters

Wet sediment samples were thawed and analyzed for an operationally defined biologically available iron fraction (amorphous Fe(III) oxides and solid-phase Fe(II) compounds) by a 0.5 N HCl extraction (Roden et al. 2002): ~8 mL of 0.5 N HCl were added to ~0.5 mL wet sediments and shaken for 2 hours. Iron speciation was also done by sequential extraction (modified from Poulton et al. 2005): 0.2 mg dried and ground sediments were sequentially extracted by magnesium chloride, sodium acetate, sodium dithionite and concentrated HCl to separate different species of iron. Sediments and extracts were separated by centrifuging. Dissolved Fe concentrations in porewaters and extracts were analyzed spectrophotometerically with Ferrozine (Viollier et al. 2000): the ferrozine reagent was added into samples with appropriate dilution to react with divalent Fe and form a stable magenta complex species with maximum absorbance at 562 nm. To determine both dissolved Fe(II) and Fe(III), spectrophotometric absorbance were measured using a Thermo Spectronic GENESYS ™ 6 Spectrophotometer before and after reduction of samples by hydroxylamine hydrochloride and buffered to between pH 4

31

and 9 with ammonium acetate (pH 9.5). The procedure was calibrated using Fe(III) standards under normal conditions of analysis. The non-reduced samples were used to determine the concentrations of dissolved Fe(II), whereas the reduced samples gave the total concentration of dissolved iron (Fe(III)+Fe(II)). Fe(III) concentrations in solution could be obtained by subtraction.

Phosphorus in solid phase and porewaters

Phosphorus sequential extractions were performed following the SEDEX procedure of Ruttenberg (1992): sedimentary P was separated into five pools: loosely sorbed or exchangeable P; ferric Fe-bound P; authigenic carbonate fluorapatite + carbonate fluorapatite + biogenic apatite + $CaCO_3$-associated P; detrital apatite P of igneous or metamorphic origin; and organic P. Dissolved phosphate concentrations in extracts and porewaters were measured using a Lachat Quickchem 8000 flow injection auto-analyzer (Diamond el al. 1995): Ammonium molybdate and antimony potassium tartrate reacted with phosphate under acid condition to form an antimony-phospho-molybdate complex, which was then reduced by ascorbic acid to a blue-colored complex with absorbance at 880 nm proportional to the phosphate concentration in the samples.

Scanning X-ray fluorescence

Split sediment cores (FWM_Jun09, EM_Oct09, WM_Jun10 and WM_Jul10) were scanned for major elements at a 200 μm spatial resolution using the X-ray

fluorescence (XRF) sediment analyzer at the Large Lakes Observatory, University of Minnesota Duluth.

Calculation of fluxes and rates

The diffusive fluxes of dissolved species within the sediment and at the sediment-water interface (SWI) were calculated from the concentration gradients using Fick's law of diffusion (Boudreau 1997):

$$F = -\varphi D_s \frac{\partial C}{\partial X}$$

F ---- Fluxes of dissolved species, mmol cm^{-2} yr^{-1}

φ ---- Porosity, cm^3 cm^{-3}

C ---- Concentration, μmol L^{-1}

X ---- Depth, cm

D_s ---- Temperature- and tortuousity- corrected diffusion coefficient, cm^2 yr^{-1}.

$$D_s = \frac{D_0}{1 - \ln \varphi^2}$$

where D_0 is the infinite dilution diffusion coefficients. D_0 for ions can be corrected for temperature as $D_0 = (m_0 + t\, m_1) \times 10^{-6}$ cm^2 s^{-1}, assuming in situ temperature t of 4 °C, and values of m_0 and m_1 refer to Boudreau 1997. D_0 for dissolved oxygen = (0.2604 + 0.006383 (T/u)) x 10^{-5} cm^2 s^{-1}, where T is the absolute temperature 277 K and u is the dynamic viscosity of 1.5648 centipoises (10^{-2} g cm^{-1} s^{-1}) (Boudreau 1997), assuming a salinity of 0 and pressure of 20 bars. The diffusion coefficients used for calculations in this study are listed in Table 7 (Boudreau 1997).

The oxygen consumption rates as functions of depth were calculated by taking a numerical derivative of the oxygen flux profiles (Sauter et al. 2001). With the typical $C:O_2$ stoichiometry of 1:1, sediment organic C:N ratio of ~13 (Heinen and McManus 2004), and $N:O_2$ ratio of 1:2 for ammonium oxidation, the carbon degradation rates can be estimated as proportional to oxygen consumption rates with a factor of 13/15=0.87, neglecting denitrification. Total carbon degradation rates can also be calculated from the decrease in organic carbon content with depth

$$R_c = \frac{\rho r_{sed}(1-\varphi)(C - C_{refr})}{x} \times \frac{10^6}{12 \bullet 365}$$

R_c ---- Rates of carbon degradation, μmol cm^{-3} d^{-1}

ρ ---- Density of dry sediments, g cm^{-3}

r_{sed} ---- Sedimentation rate, cm yr^{-1}

φ ---- Porosity, cm^{3} cm^{-3}

C ---- Total organic carbon content at the surface sediment layers, weight %

C_{refr} ---- Refractory organic carbon content (carbon content in the deep sediments), weight %

x ---- Thickness of sediment undergoing carbon decay, cm

The decay constants, k (yr^{-1}), of organic matter were calculated at the sediment surface from

$$R_c = k(C - C_{refr})$$

The characteristic half-decay time of organic C in the sediment was calculated as

34

$$t = \frac{\ln 2}{k}$$

Sediment burial fluxes can be calculated as follow:

$$F_b = \rho r_{sed}(1 - \varphi)C_{refr} \times \frac{10^7}{12 \bullet 365}$$

F_b ---- Sediment burial flux, mmol m^{-2} d^{-1}

ρ ---- Density of dry sediments, g cm^{-3}

r_{sed} ---- Sedimentation rate, cm yr^{-1}

φ ---- Porosity, cm^3 cm^{-3}

C_{refr} ---- Refractory organic carbon content, weight %

Table 7. Diffusion coefficients of dissolved oxygen, NO_3^-, NH_4^+ and SRP at the sediment-water interface and infinite dilution diffusion coefficient for Fe^{2+} in sediments. $(cm^2\ yr^{-1})$

D_0 are infinite diffusion coefficients. D_s are temperature and tortuousity- corrected diffusion coefficient. D_0 for SRP is the average of the diffusion coefficients for HPO_4^{2-} and $H_2PO_4^-$, as the concentrations of these species are similar at circumneutral pH. Porosity of 0.98 $cm^3\ cm^{-3}$ at the SWI is used for tortuousity correction. Ds for Fe^{2+} can be determined based on the appropriate porosity of the sediments.

	D_0	D_s
O_2	438	421
NO_3^-	349	335
NH_4^+	352	338
SRP	140	134
Fe^{2+}	123	

Chapter 3. Results

<u>Temperature and oxygen variability in the water column</u>

Water column temperature and oxygen concentrations are shown in Figs. 6 and 7. In June of 2009, at the beginning of spring overturn, temperature profiles reflected either a weak negative stratification (with surface water being colder than deep water, in the open lake) or a well-mixed water column (near-shore). In June 2010 the near-shore stations FWM and KW exhibited stratification, whereas other stations remained mixed. By July, in both years, temperatures in the surface water increased to ~ 15 °C and summer stratification was well developed. Between July and November, the lake remained stratified but the thermocline progressively deepened. The temperature of the bottom waters remained within a narrow range around 3.5 °C throughout the summer and down to 1 °C in the winter.

Oxygen distributions in the water column varied inversely with water temperature and their shapes reflected stratification. In June, oxygen concentrations were uniform throughout the water column where it was mixed (WM09, WM10, EM09, CM10, IR10); a slight decrease in oxygen concentrations in the bottom waters reflected a colder-over-warmer negative stratification at some stations (FWM09, EM09). Oxygen concentrations were lower in surface waters at sites where positive stratification had developed (FWM10, KW10). In September, October and November the lake exhibited orthograde oxygen distributions typical of oligotrophic dimictic lakes during summer stratification (Wetzel 2001). The anti-correlation of oxygen levels with temperature suggests that the

oxygen supply to the water column is regulated, to a large degree, by oxygen solubility, which decreases with increasing temperature. Oxygen saturation levels throughout the water column of Lake Superior remain above 85% year round. In bottom waters, oxygen concentrations were similar among sampling sites and varied temporally within a relatively narrow range (Table 8). In 2009, the bottom water oxygen concentrations dropped from 12.08 mg/L in June to 10.90 mg/L in October and 10.54 mg/L in November. In 2010, bottom water oxygen levels were similar between June and July and decreased by September. The decline from spring to fall is most likely attributable to the consumption of oxygen in the water column by settling organic matter during summer stratification.

Table 8. Bottom water oxygen concentrations (mg L^{-1})

	Jun	July	Sep	Oct	Nov
FWM_09	12.58				10.53
EM_09	11.55			10.95	
WM_09	12.10			10.85	10.55
Average	12.08			10.90	10.54
FWM_10	12.95	12.90	12.55		
EM_10	12.84	13.05	12.67		
WM_10	12.86	13.09	12.57		
CM_10	12.86	13.01	12.67		
ED_10		12.99	12.60		
IR_10	12.88	12.88	12.63		
KW_10	12.86				
Average	12.88	12.99	12.61		
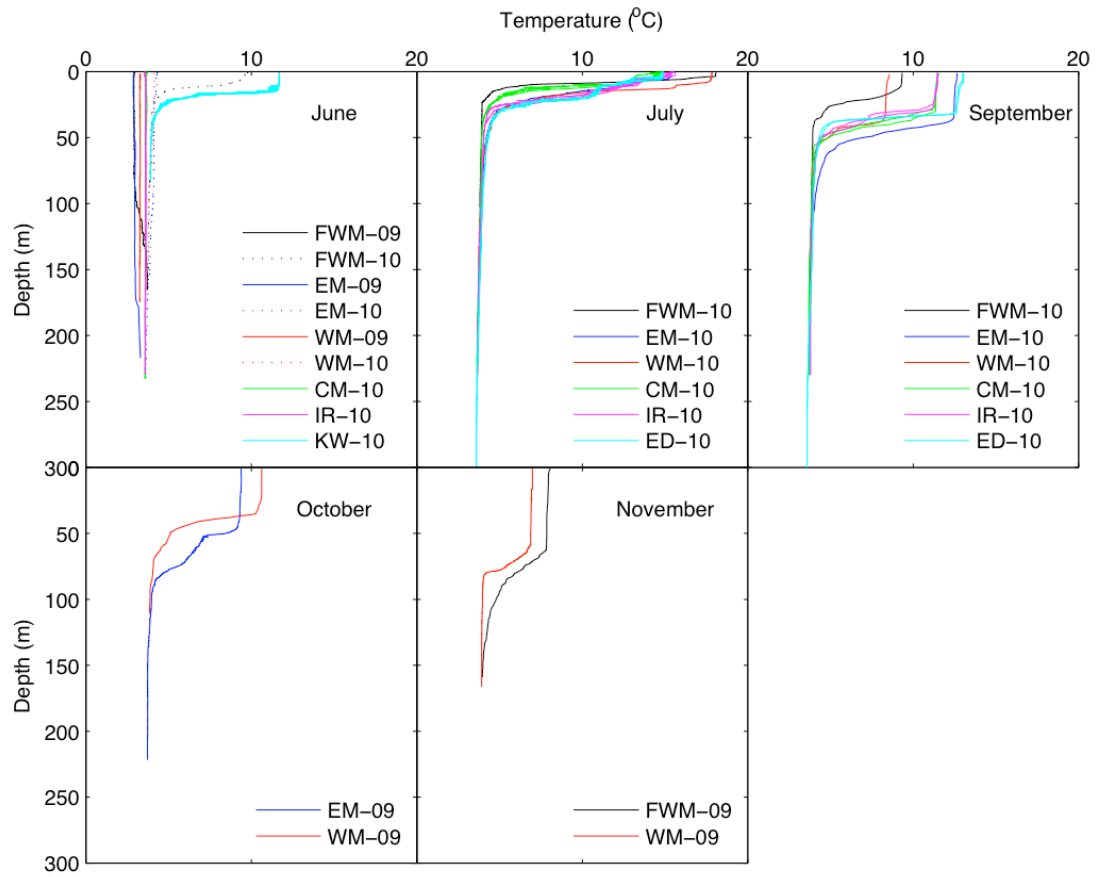
Figure 6. Vertical temperature variations in water column of Lake Superior
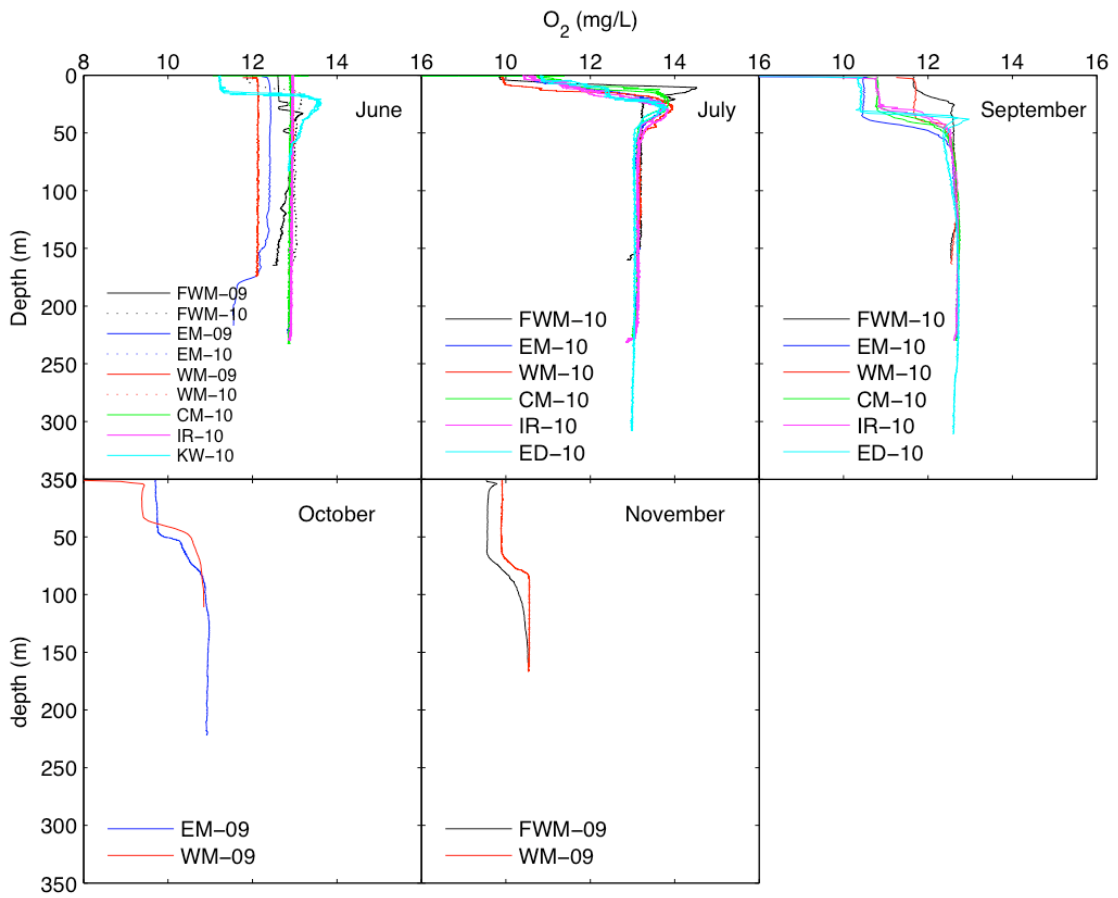
Figure 7. Vertical distributions of dissolved oxygen in water column of Lake Superior

40

Spatial variability in sediment physical properties

Sediment properties strongly varied among our sampling sites and, at several locations, among different cores within the same lake station. Our monitoring of the lake floor with shipboard echo-sounder during and between samplings indicated strong sediment heterogeneity in both eastern and western basins of the lake. Consistent with the topographical complexity, comparison of the recovered sediment cores indicates strong spatial variability (Fig. 8). The cores recovered relatively close to shores (FWM, KW and SI) were predominantly brown in color, whereas cores from IR, CM and ED under the black surface layer contained grey clays and narrow brownish metal-rich layers. Sediments around Stations EM and WM exhibited extreme variability, on spatial scales as small as hundred meters. For example, two cores from EM station in 2009 (EM_Jun09 and EM_Oct09) both contained brownish sediments overlain by a soft black surface layer, but the EM_Oct09 core had several visible metal-rich crusts at 6~7 cm depth, whereas the EM_Jun09 core had no such layers. Sediment cores recovered at the EM station in 2010 (within several hundred meters of each other and of the 2009 sampling sites) exhibited yet other features: the EM_Jun10 cores displayed multiple metal layers between 10 to 16 cm depth, which were underlain by gray clays, whereas EM_Jun10 cores showed no metal-rich layers and the sediment was uniformly gray below the depth of 3 cm. The WM cores WM_Jul10-b and WM_Jul10-c, taken within 150 m of each other, also looked different from each other: WM_Jul10-b had a prominent iron layer at ~7-8 cm depth and gray clays below, whereas WM_Jul10-c had no iron layer but contained brownish sediments sandwiched between the soft black surface layer (0-2 cm)

and gray clays underneath (> 30 cm). Neither of these cores was consistent with the WM_Jun10 cores, which contained prominent iron-rich layers underlain by brownish sediments. Even at stations where sediment properties were relatively consistent between sampling sites, the cores often noticeably varied in some detail. For example, two cores from Station CM differed in their depths of visible metal layers: CM_Jun10 had iron layers between 6 to 7 cm whereas in CM_Jul10 the metal layers resided between 9 and 10 cm.

Water content of sediments decreased from > 90% at the surface to 50-80% at 25 cm, with the exception of Station SI where water content fell below 40% below 12 cm depth (Fig. 9). Large differences in water contents among cores from the WM and EM sites were consistent with strong lateral variability in core appearances (Fig. 8). At the FWM, IR and CM sites, water contents in sediment cores were consistent among samplings. Magnetic susceptibility and gamma density profiles measured in our samples are shown in Figs. 10 and 11.
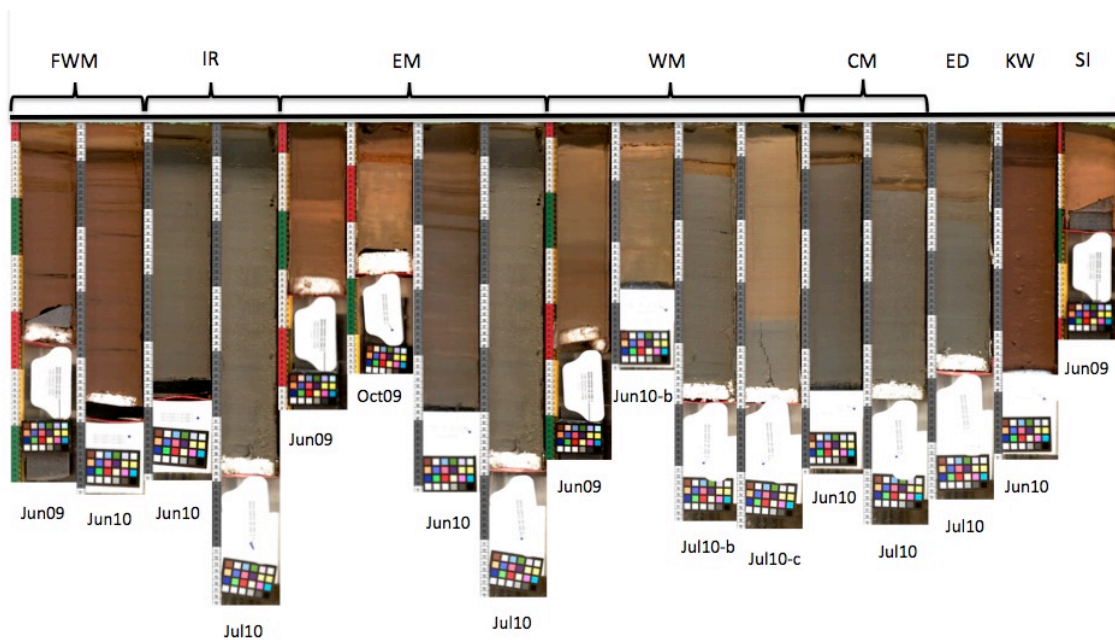
Figure 8. Optical images of Lake Superior sediment cores.

Note the strong variability in color and the presence of multiple metal layers that appear as distinct horizontal layers. The horizontal line indicates the position of the sediment-water interfaces. The vertical scale is the same for all cores.
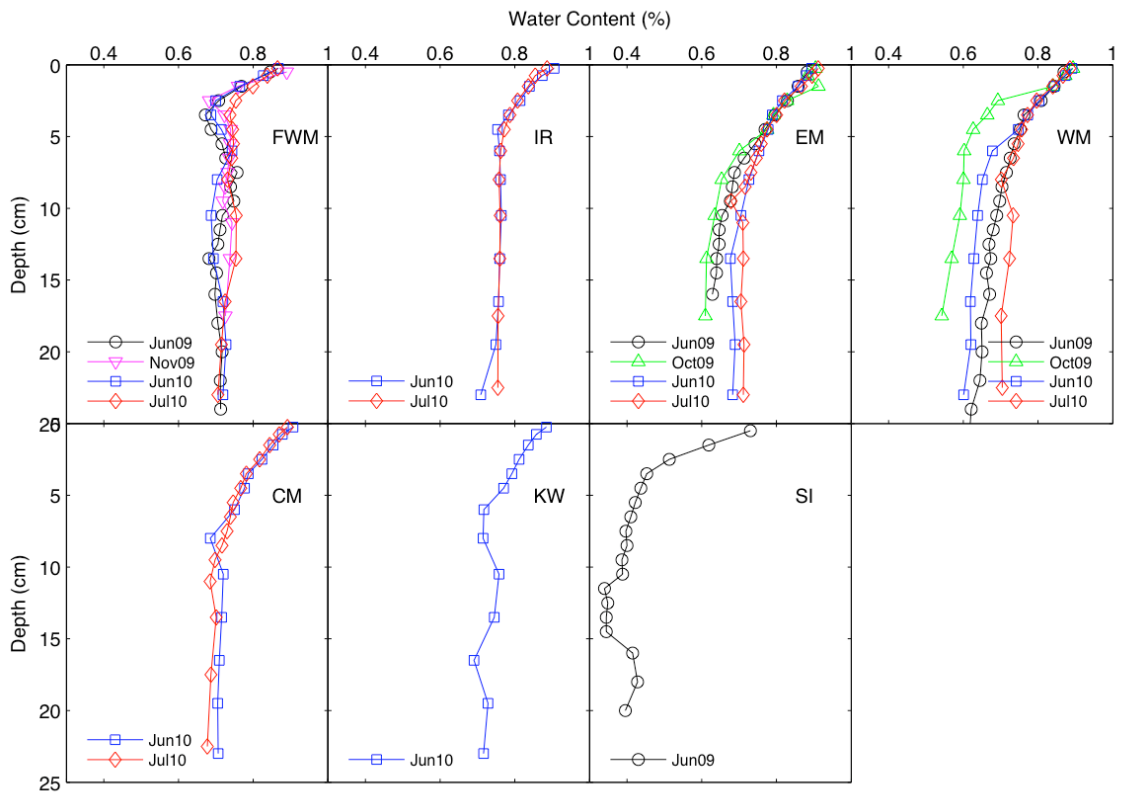
Figure 9. Water content in Lake Superior sediments.

For WM, the 2010 results are shown for WM_Jun10-b and WM_Jul10-b cores.
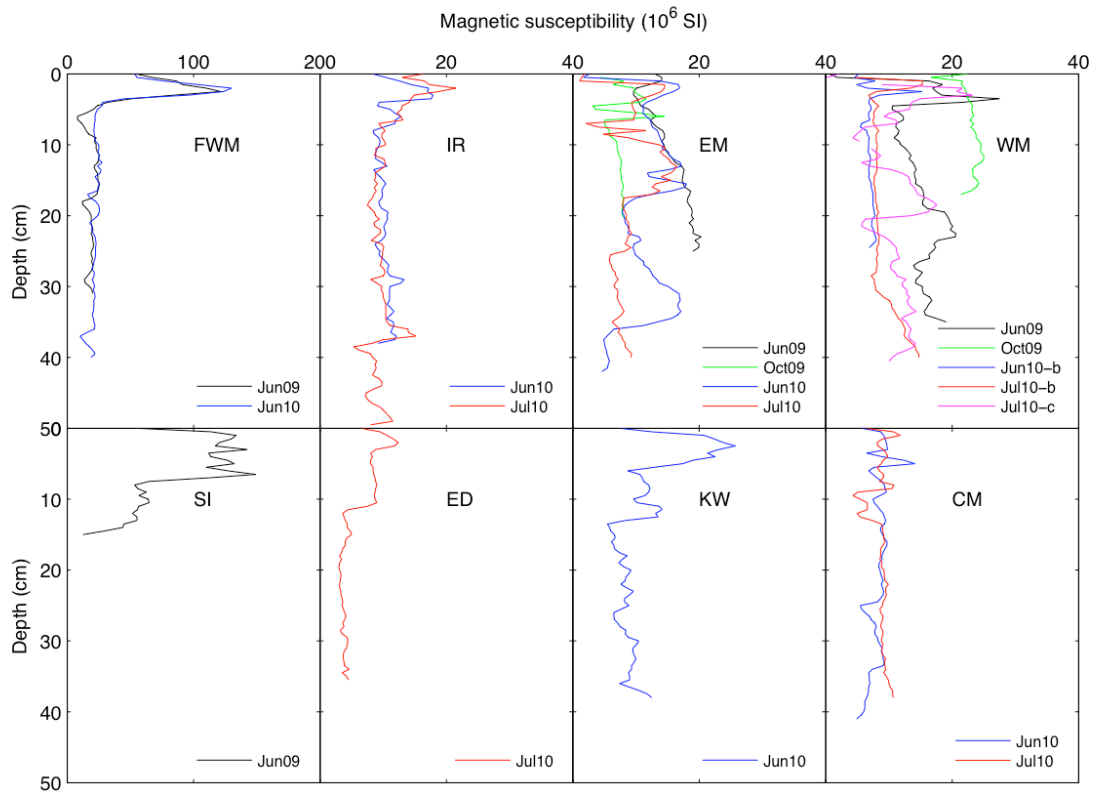
Figure 10. Magnetic susceptibility in Lake Superior sediments.

Notice a different scale for Station FWM.
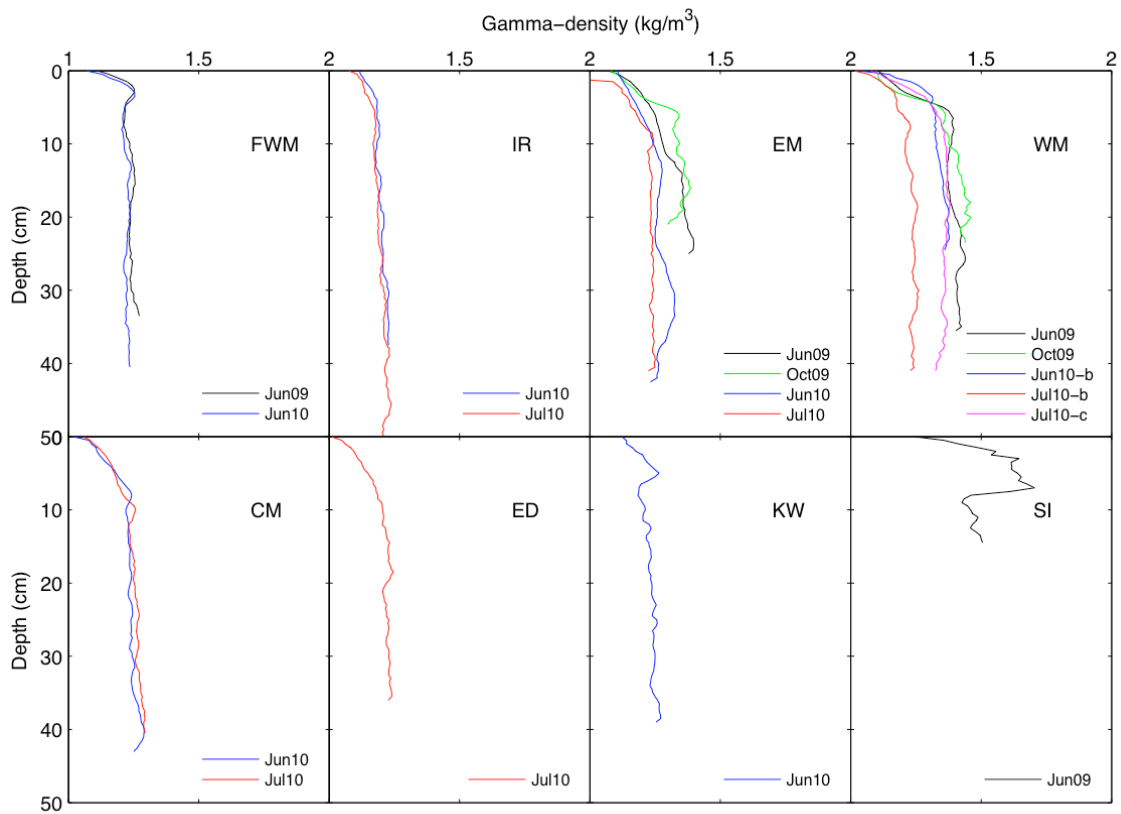
Figure 11. Gamma density in Lake Superior sediments.

Oxygen penetration into sediments

Despite the differences in sediment appearances, oxygen penetrated deeply into the sediment at all sampling locations: oxygen penetration depths (OPDs), defined at the detection limit of the microelectrode (2 μmol/L), varied from 3.5 cm at IR to > 12 cm at WM (Figs. 12.1-8). At FWM (Fig. 12.1), oxygen penetration was between 6 and 7 cm, except in May 2010, when it was 4.5 cm. The May 2010 core contained visible Fe-rich layers at the depth of ~ 4.5- 5 cm, whereas such Fe-rich layers in other FWM cores were located at ~ 7- 8 cm, consistent with their OPDs.

Oxygen profiles at the EM and WM sites had two distinct shapes. In EM 2010 cores, oxygen penetrated to ~7-8 cm; sediment below was gray, underlying the soft black surface layer and brownish iron layers (Fig. 8). In EM 2009 cores, oxygen concentrations remained high below 9 cm (Fig. 12.2), and the deep sediment was brown (Fig. 8). Sediments at WM all had deep (> 8 cm) oxygen penetration except in one July 2010 core (WM_Jul10_b). This core had OPD~ 8 cm (Fig. 12.3) and contained visible metal layers immediately below the OPD, underlain by gray clays (Fig. 8).

Oxygen penetration at CM and ED varied by a few cm between samples taken in different seasons (different cruises). At CM, it varied from 8 cm in June to > 12cm in September (Fig. 12.5). The visible metal layers in CM cores also varied in their position, although all sediment cores had visible metal layers below their OPDs (Fig. 8). At ED, OPD varied from 9 cm in July to 12 cm in September (Fig. 12.6). Both cores, however, had metal layers at ~ 11-12 cm (Fig. 8). Among the relatively near-shore sites IR, KW and SI, SI had an uncharacteristically deep oxygen penetration (Fig. 12.8). Interestingly,

the SI core was similar in appearance to the EM and WM cores with deep OPDs (e.g. EM_Jun09, WM_Jun09, WM_Jul10-c; Fig. 8). The IR cores had a relatively shallow OPD (~3.5 cm, Fig. 12.4) and KW cores had OPD~7 cm (Fig. 12.7).

Figure 12. 1. Porewater oxygen concentrations at Station FWM.

Multiple lines are replicate profiles measured at different locations within the same sediment core. May10 core was taken by R. Sterner at a location near FWM station. Jun10-b core was taken at the same location as Jun09 core. Jul10-a and Jul10-b cores were taken at sites located <50m apart.

Figure 12. 2. Porewater oxygen concentrations at Station EM.

Multiple lines are replicate profiles measured at different locations within the same sediment core. Jun10-a and Jun10-b cores were taken from sites located within 1 km of each other.
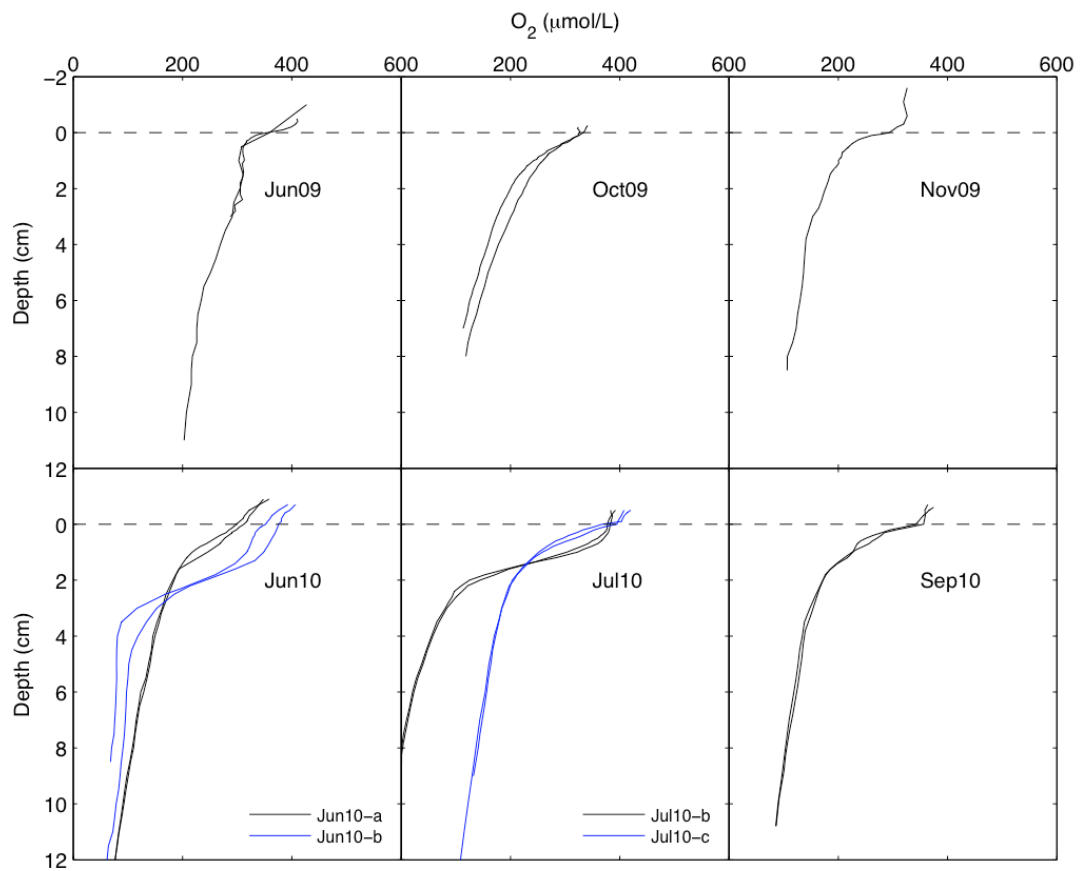
Figure 12. 3. Porewater oxygen concentrations at Station WM.

Multiple lines are replicate profiles measured at different locations within the same sediment core. WM_Jun10-a and WM_Jun10-b cores were taken from two locations about 150 m apart; WM_Jul10-b and WM_Jul10-c cores were taken from locations ~150 m apart.
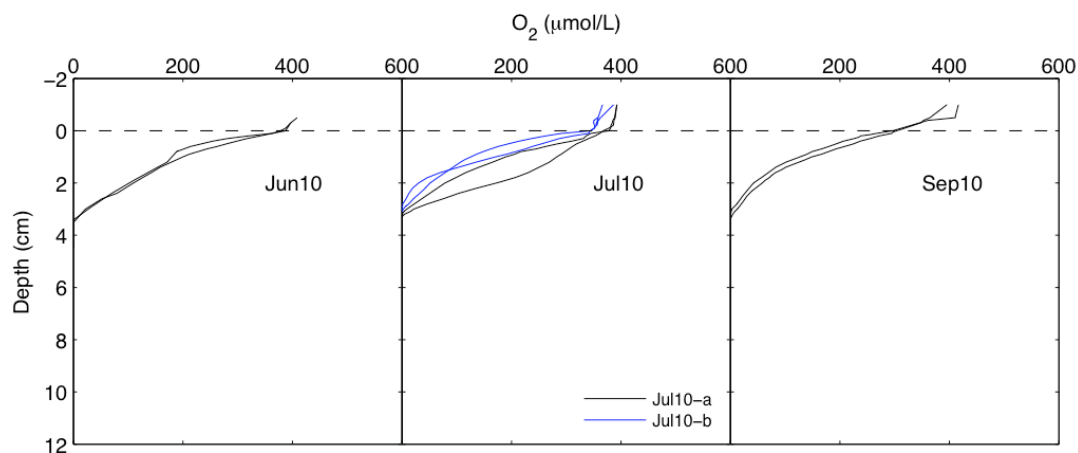
Figure 12. 4. Porewater oxygen concentrations at Station IR.

Multiple lines are replicate profiles measured at different locations within the same sediment core. Jul10-a and Jul10-b cores were taken from sites located within 1 km of each other.
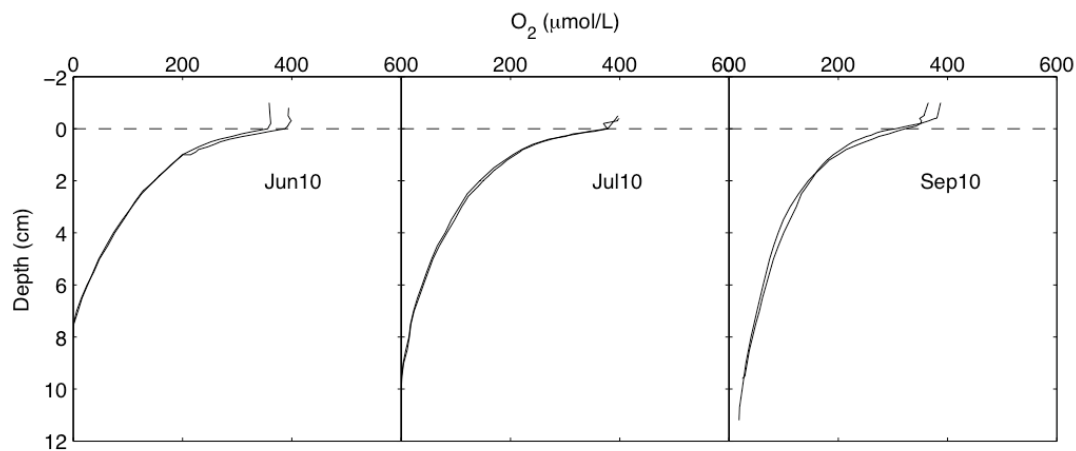
Figure 12. 5. Porewater oxygen concentrations at Station CM.

Multiple lines are replicate profiles measured at different locations within the same sediment core.
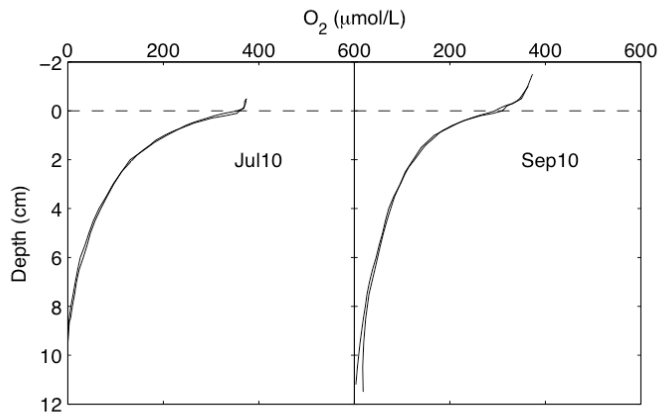
Figure 12. 6. Porewater oxygen concentrations at Station ED.

Multiple lines are replicate profiles measured at different locations within the same sediment core.
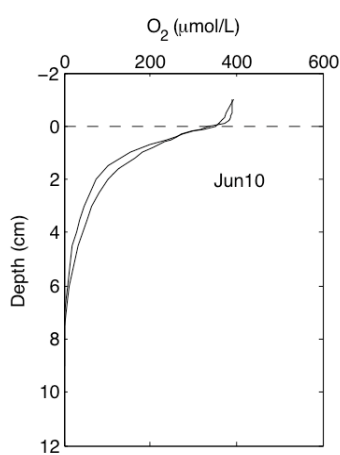
Figure 12. 7. Porewater oxygen concentrations at Station KW.

Multiple lines are replicate profiles measured at different locations within the same sediment core.
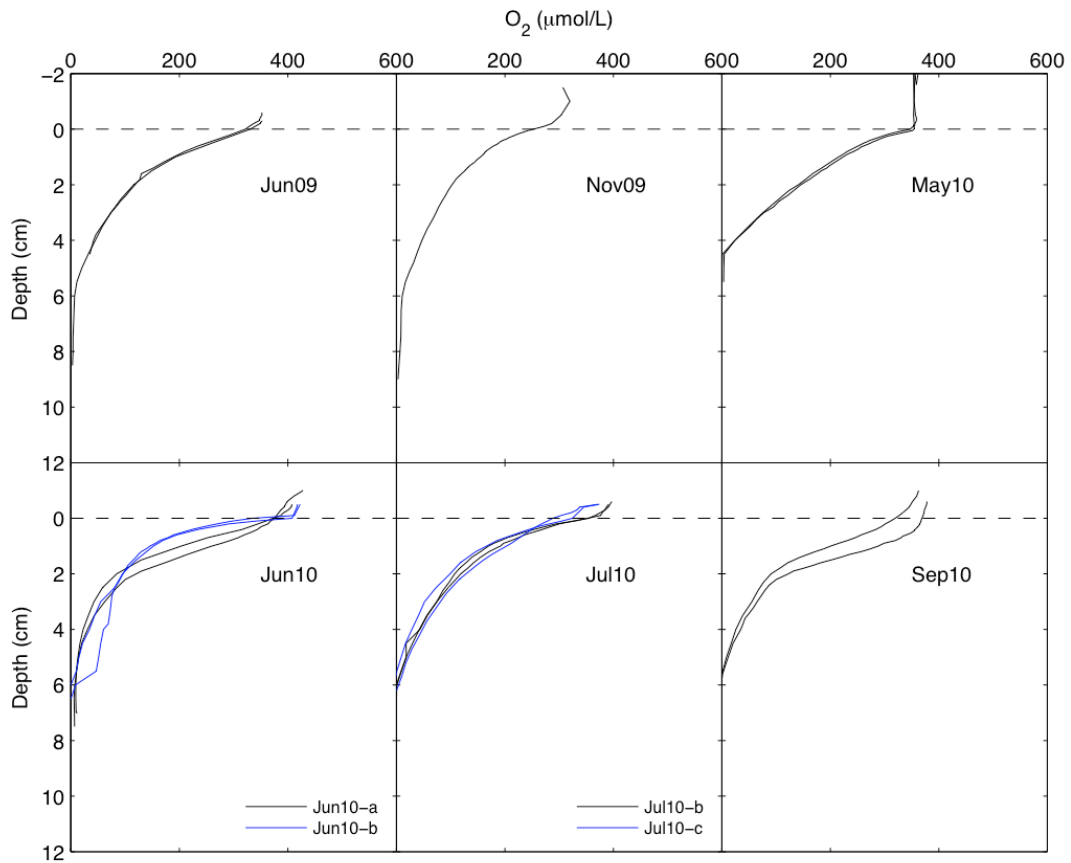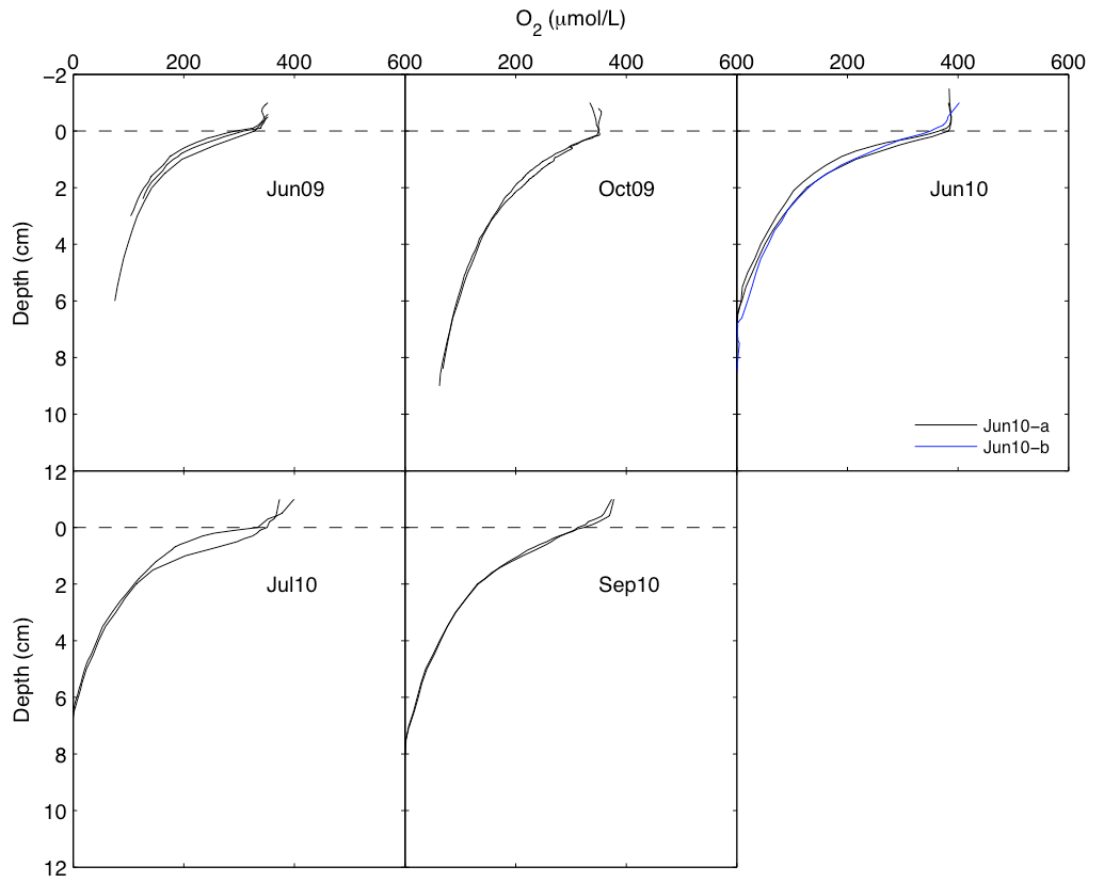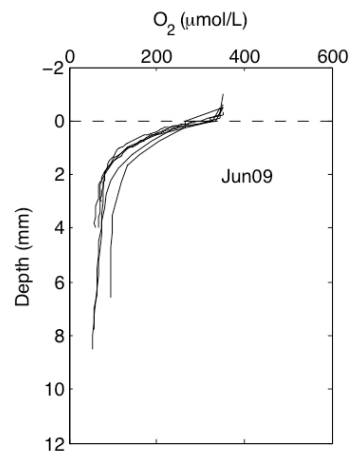
Figure 12. 8. Porewater oxygen concentrations at Station SI.

Multiple lines are replicate profiles measured at different locations within the same sediment core.

Oxygen fluxes and carbon degradation rates

Figure 13 (panels 1-8) shows the calculated diffusive fluxes of oxygen and oxygen consumption rates as a function of depth within the sediment. The diffusive oxygen fluxes, maximum carbon degradation rates, and reactivity of organic carbon at the SWI are listed in Table 9. Oxygen diffusive fluxes across the SWI ranged from 1.05 to 5.88 mmol m^{-1} d^{-1}, with an average of 2.92 mmol m^{-2} d^{-1} (Table 9). Oxygen diffusive fluxes in July were higher than in other seasons, with the exception of the WM station where oxygen fluxes in September and November were higher (Fig. 13.1-8; Table 9). Oxygen diffusive fluxes at the near-shore stations IR (average 3.96 mmol m^{-1} d^{-1}) and SI (average 4.08 mmol m^{-1} d^{-1}) were higher than at the offshore stations (averages ranging from 2.08 mmol m^{-1} d^{-1} at WM to 2.96 mmol m^{-1} d^{-1} at CM). The directly measured oxygen uptake rates ranged from 4.44 to 7.68 mmol m^{-2} d^{-1}, averaging 6.10 mmol m^{-2} d^{-1} (data courtesy of S. A. Crowe)

The oxygen consumption rates were highest within the top 1 cm of the sediments, with typical maximum values between 0.25 and 1 μmol cm^{-3} d^{-1} achieved near the sediment-water interface. The rates decreased downcore (Fig. 13.1-8). Maximum oxygen consumption rates were typically higher in June and July than in other seasons (peaked in July at stations EM, CM, IR; peaked in June at FWM), with the exception of WM where maximum oxygen consumption rate increased from July (0.27 μmol cm^{-3} d^{-1}) to November (0.98 μmol cm^{-3} d^{-1}). Maximum oxygen consumption rates were higher at near-shore stations (e.g. IR, SI) than at the open-water stations (FWM, WM, CM, ED).

The half-decay times, τ, for the organic matter in the surface sediment layer ranged from 0.31 to 1.40 years, with the average of 0.75 yr.

Table 9. Oxygen fluxes and carbon degradation rates

Listed diffusive oxygen fluxes are the maximum fluxes in Fig.13. Maximum carbon degradation rates are taken as equivalent to maximum oxygen consumption rates (Fig. 14). The reactivity of organic matter was calculated using porosity 0.95 and solid sediment density 2.5 g cm^{-3}. Where data were not available, the concentration of labile organic C was assumed 2 wt%. * A higher value of 8.3 mmol m^{-2} d^{-1} was obtained in a single core at St. EM, but the incubation appeared disturbed. This value was excluded from the average.

Station	Time of Sampling	Diffusive flux of oxygen (mmol m^{-2} d^{-1})	Total oxygen uptake (mmol m^{-2} d^{-1})	Max. carbon degradation rate, RC (μmol cm^{-3} d^{-1})	OC reactivity, k (yr^{-1})	Mineralization half-decay time, τ (yr)
FWM	May10	2.42		0.52	1.92	0.36
	Jun09	1.56	6.37	0.11	0.41	1.69
	Jun10	1.53; 4.11		0.20; 0.90	0.74; 3.33	0.94; 0.21
	Jul10	3.17; 2.14		0.66; 0.31	2.44; 1.15	0.28; 0.60
	Sep10	1.04	7.1±1.1	0.15	0.55	1.26
	Nov09	2.21		0.36	1.33	0.52
	Average	**2.27**		**0.40**	**1.48**	**0.73**
WM	Jun09	3.20	4.44			
	Jun10	1.05		0.15; 0.36	0.26; 0.63	2.67; 1.1
	Jul10	1.74		0.27	0.47	1.47
	Sep10	2.39		0.44	0.77	0.90
	Oct09	1.32		0.21	0.37	1.87
	Nov09	2.75		0.98	1.72	0.40
	Average	**2.08**		**0.40**	**0.70**	**1.40**

Table 9. Oxygen fluxes and carbon degradation rates (continued)

Station	Time of Sampling	Diffusive flux of oxygen (mmol m^{-2} d^{-1})	Total oxygen uptake (mmol m^{-2} d^{-1})	Max. carbon degradation rate, RC (µmol cm^{-3} d^{-1})	OC reactivity, k (yr^{-1})	Mineralization half-decay time, τ (yr)
EM	Jun09	2.63	8.29*	0.78	1.28	0.54
	Jun10	1.84; 1.64		0.37; 0.20	0.61; 0.33	1.14; 2.10
	Jul10	4.59		1.13	1.85	0.37
	Sep10	1.34		0.36	0.59	1.17
	Oct10	1.58		0.30	0.49	1.41
	Average	**2.27**		**0.52**	**0.86**	**1.12**
IR	Jun10	2.72		0.83	1.46	0.47
	Jul10	5.88		1.98	3.47	0.20
	Sep10	3.29	4.9± 0.8	1.51	2.65	0.26
	Average	**3.96**		**1.44**	**2.53**	**0.31**
CM	Jun10	2.84		0.49	0.86	0.81
	Jul10	3.74		0.77	1.35	0.51
	Sep10	2.30		0.48	0.84	0.83
	Average	**2.96**		**0.58**	**1.02**	**0.72**
ED	Jul10	2.96		0.69	1.27	0.55
	Sep10	2.73		0.59	1.04	0.67
	Average	**2.84**		**0.64**	**1.16**	**0.61**
KW	Jun10	2.89		0.29	0.51	1.36
SI	Jun09	4.08	7.68	0.83	1.46	0.47
Average		**2.92± 0.75**	**6.10**	**0.64**	**1.21**	**0.75**
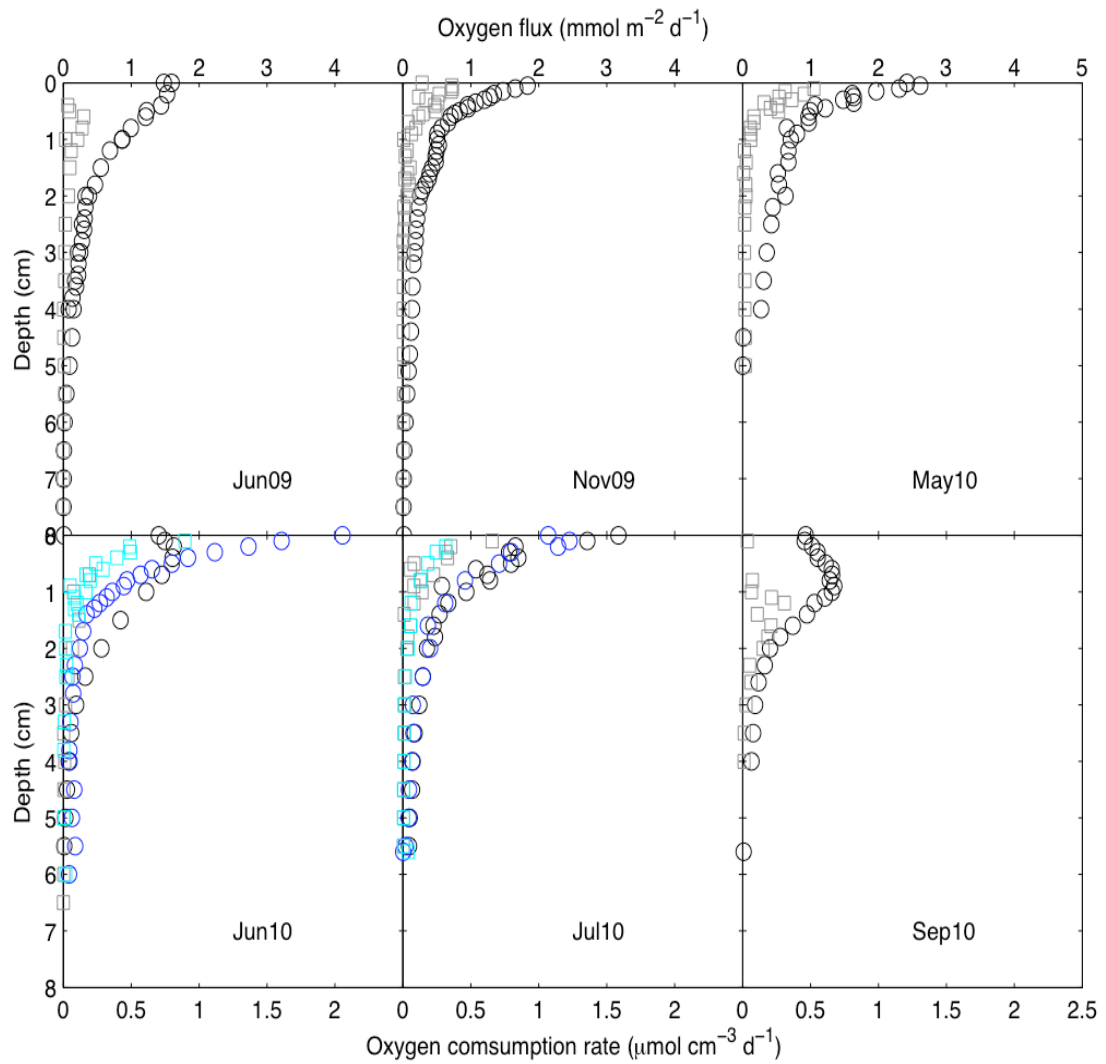
Figure 13. 1. Diffusive fluxes of oxygen (circles) and oxygen consumption rates (squares) in sediments at FWM.

Black and blue colors correspond, respectively, to Jun/Jul10-a and Jun/Jul10-b cores in Fig. 12.1
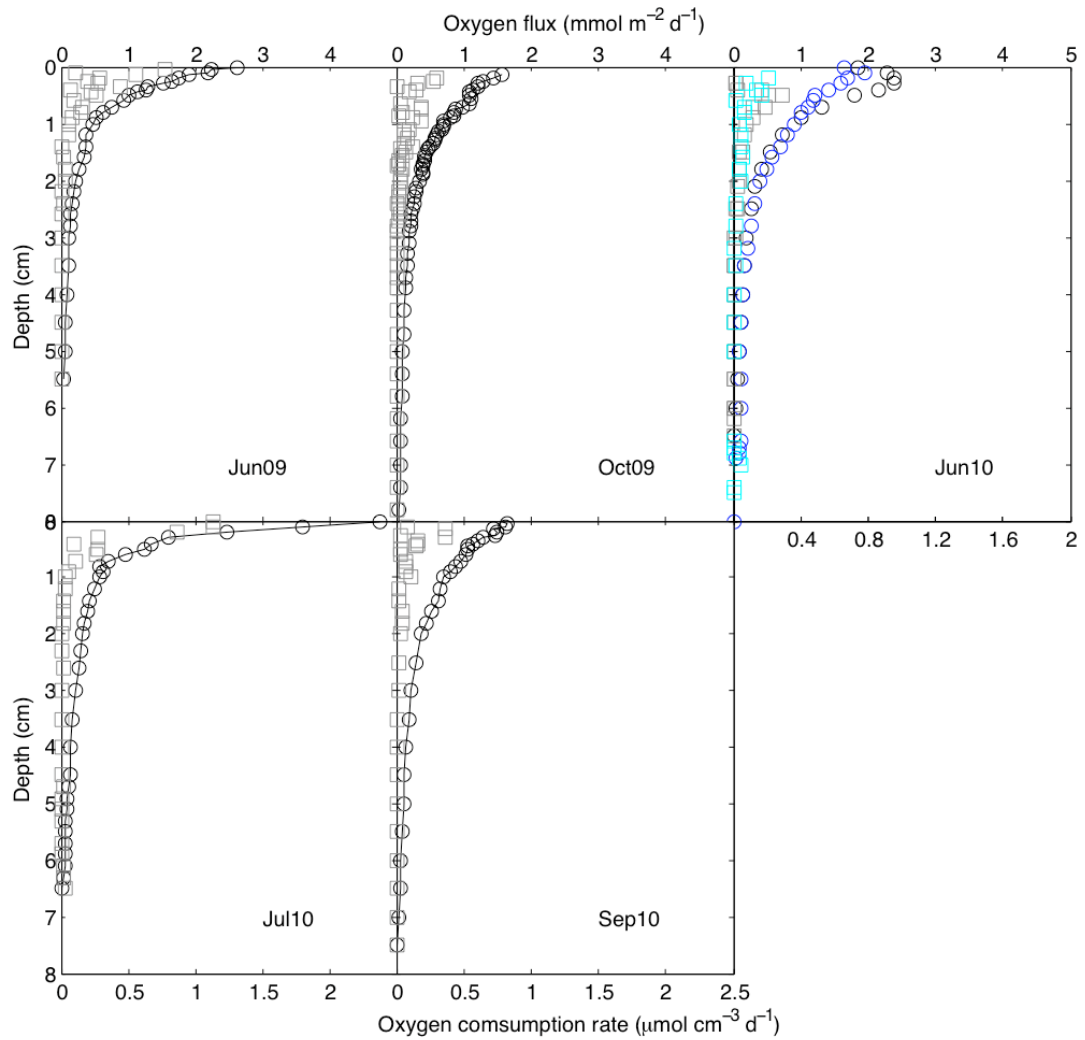
Figure 13. 2 Diffusive fluxes of oxygen (circles) and oxygen consumption rates (squares) in sediments at EM.

Black and blue colors correspond, respectively, to Jun10-a and Jun10-b data in Fig. 12.2.
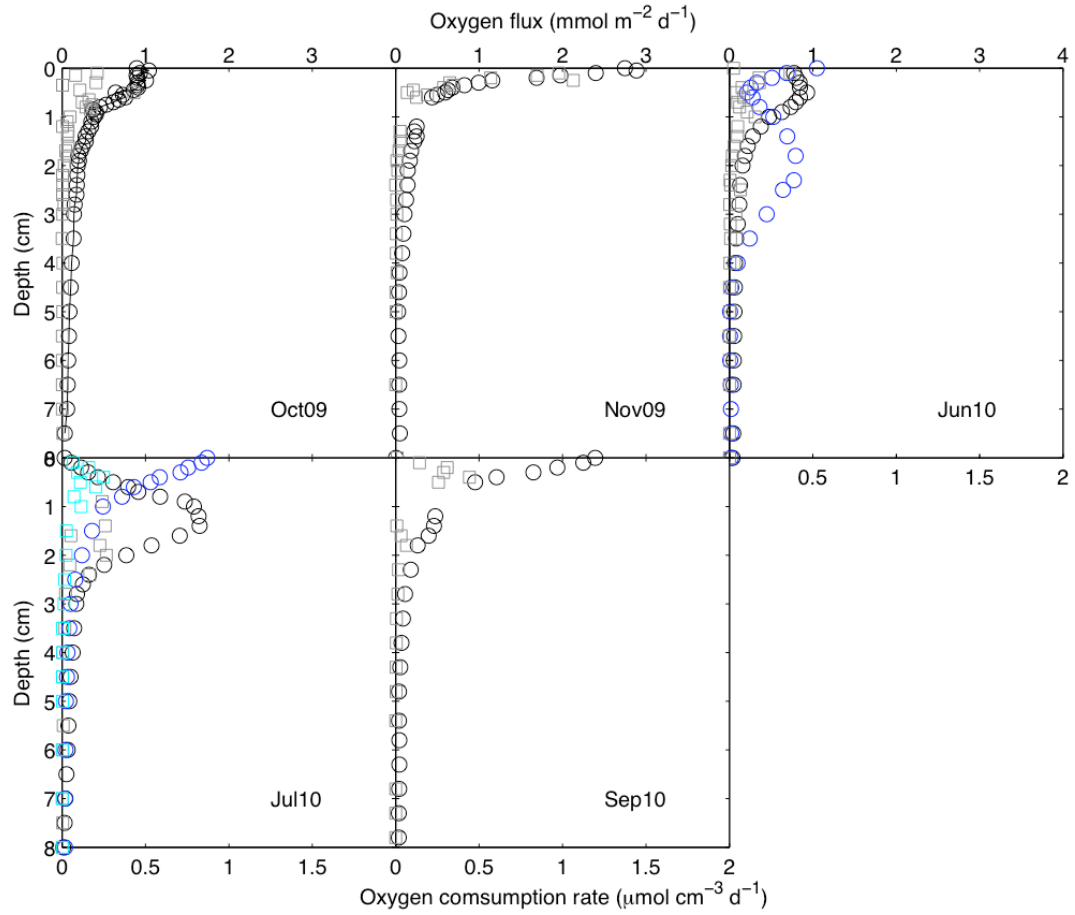
Figure 13. 3. Diffusive fluxes of oxygen (circles) and oxygen consumption rates (squares) in sediments at WM.

Black and blue colors correspond, respectively, to Jun/Jul10-a and Jun/Jul10-b data in Fig. 12.3.
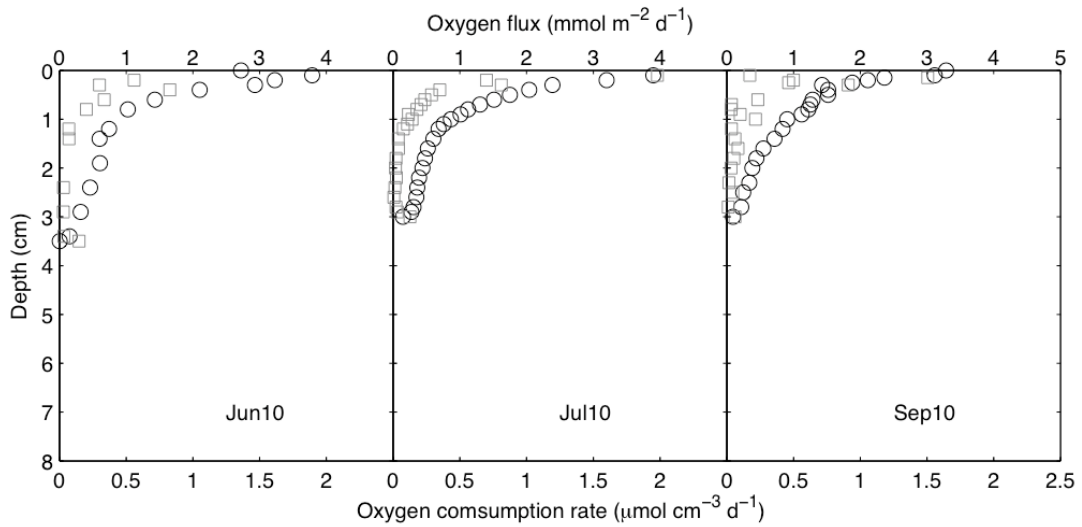
Figure 13. 4. Diffusive fluxes of oxygen (circles) and oxygen consumption rates (squares) in sediments at IR.
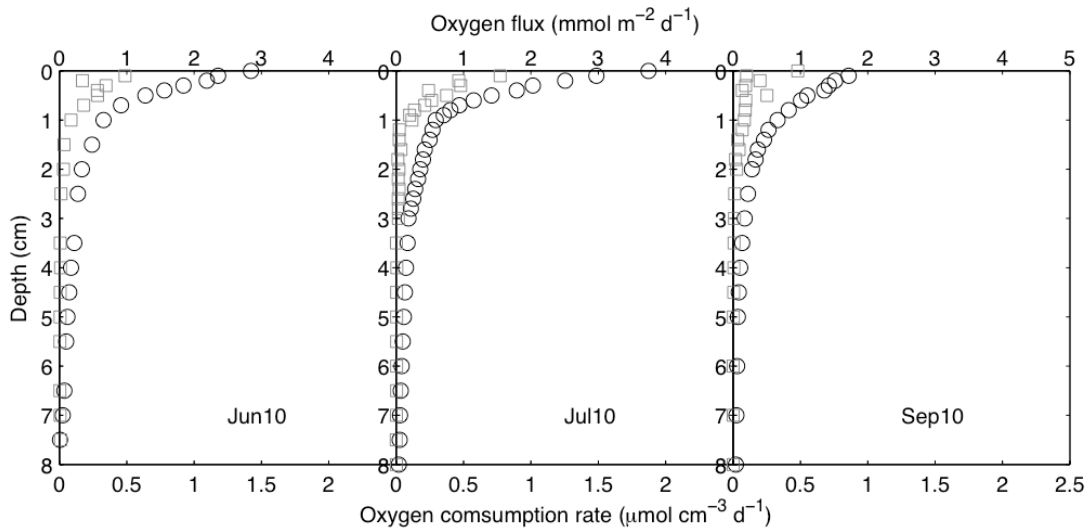
Figure 13. 5. Diffusive fluxes of oxygen (circles) and oxygen consumption rates (squares) in sediments at CM.
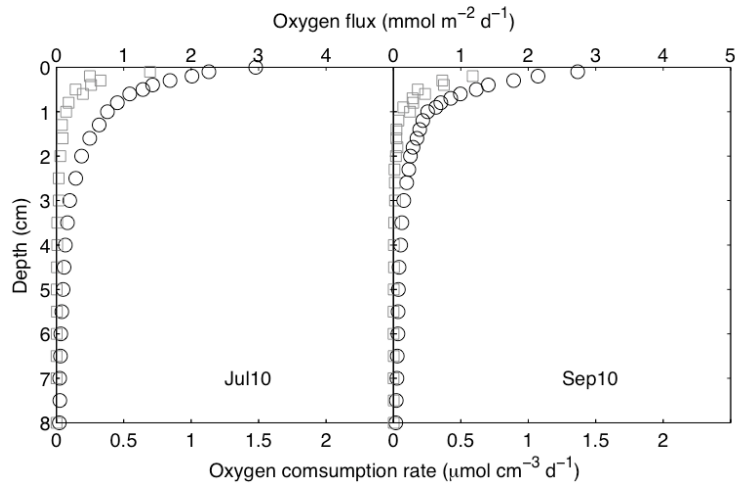
Figure 13. 6. Diffusive fluxes of oxygen (circles) and oxygen consumption rates (squares) in sediments at ED.
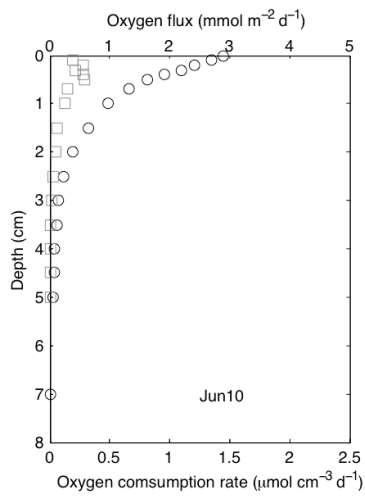
Figure 13. 8. Diffusive fluxes of oxygen (circles) and oxygen consumption rates (squares) in sediments at KW.
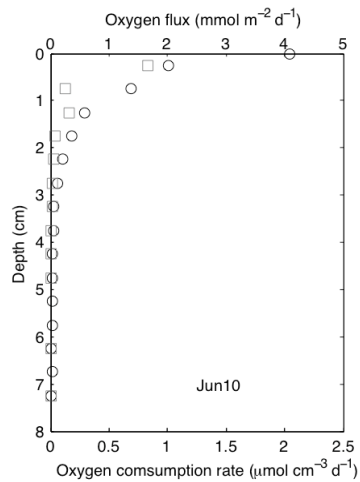
Figure 13. 7. Diffusive fluxes of oxygen (circles) and oxygen consumption rates (squares) in sediments at SI.

Oxygen in sediment incubations

Oxygen concentrations in the overlying waters and upper sediment layers (0-5 cm) decreased during whole-core incubations in sediments from all sites (Fig. 14). OPD became shallower at IR, but did not change appreciably at the sites with deeper OPDs (FWM, EM and CM). Increases in oxygen concentrations in the deeper sediments at some stations (KW-Jun10, EM-Sep10 and CM-Jun10) were enigmatic but could be due to contamination by oxygen from the atmosphere through or along the tube walls.
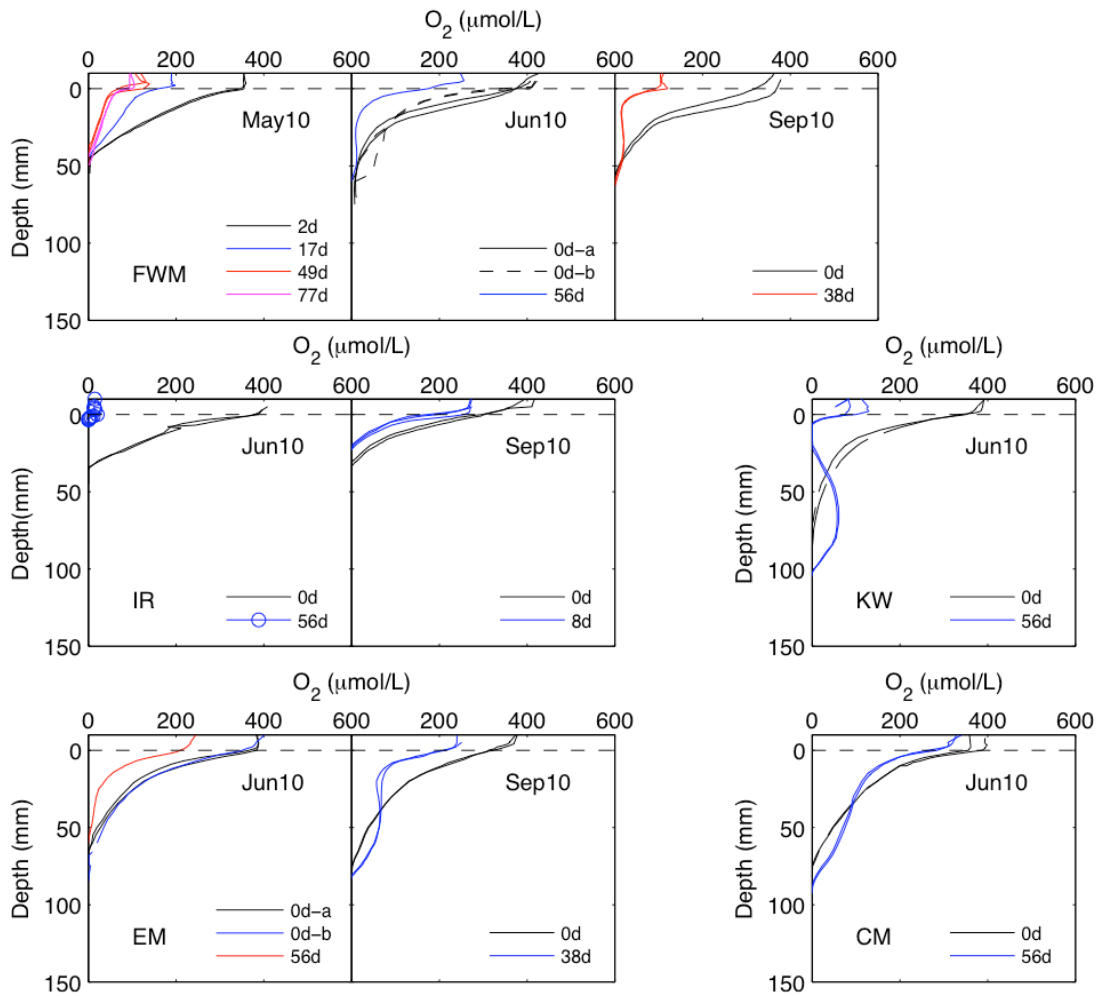
Figure 14. Changes in porewater oxygen concentrations during incubations (up to 77 days).

Organic carbon concentrations

Loss on Ignition (LOI) values ranged from 2.5% in the deep sediment to 10% at the sediment surface at FWM, EM and WM (Fig. 15). The LOI values were significantly higher than the TOC values obtained by coulometry (coulometry data courtesy of M. Kistner; Fig. 15). TOC contents varied in the range 1.5 - 2.8% at FWM_Jun09 and 2.0-4.5% at EM_Jun10. The TOC variation with depth within the sediment obtained by coulometry mimicked closely the trends observed in the LOI profiles (Fig. 15). This proportionality could be approximately described as

$$LOI = 2.5C_{org}.$$

Here, both LOI and C_{org} are in weight percent in dry sediment. OC concentrations in sediments from EM and WM decreased with depths within the top ~7 cm of sediment. The OC variations at FWM were non-monotonous (for reasons, see below). The total rates of carbon degradation ranged between 0.01 and 0.02 μmol cm^{-3} d^{-1}, based on the decrease in organic carbon (~ 2%) between the surface and deep sediment and the typical sedimentation rates at our sampling locations (~0.04 cm/yr at FWM, ~ 0.02 cm/yr at EM and 0.03 cm/yr at WM, Evans et al. 1981). These average rates of carbon degradation in the top 7 cm of sediment are an order of magnitude lower than the maximum carbon degradation rates achieved in the top 1 cm, as calculated from the rates of oxygen consumption. Carbon burial fluxes (into the deep sediment) averaged 0.49 mmol m^{-2} d^{-1}. The calculation assumed porosity of 0.85 cm^3 cm^{-3} in the deep sediments and dry weight density of 2.5 g cm^{-3}. These values are comparable with previous estimate

of 0.5 mmol m^{-2} d^{-1} by Heinen and McManus (2004) and 0.25-0.38 mmol m^{-2} d^{-1} by Baker et al. (1991).

At FWM, the organic carbon concentration varied with depth non-monotonously (Fig. 15). In the FWM-Jun09 core, the OC concentrations varied from 7% at the SWI to a minimum of ~2.5% at about 5 cm depth, and increased again to a secondary maximum of ~6% below 10 cm. The FWM-Nov09 core showed a similar pattern but with a steeper decrease: from 10% at the surface to < 5% below 5.5 cm. These variations at FWM can be explained by the deposition of taconite tailings discharged at Silver Bay, as discussed in the next Chapter.

Table 10. Carbon burial fluxes in Lake Superior sediments (mmol m^{-2} d^{-1})

Stations	Carbon burial flux
FWM	0.58
EM	0.37
WM	0.51
Average	**0.49**
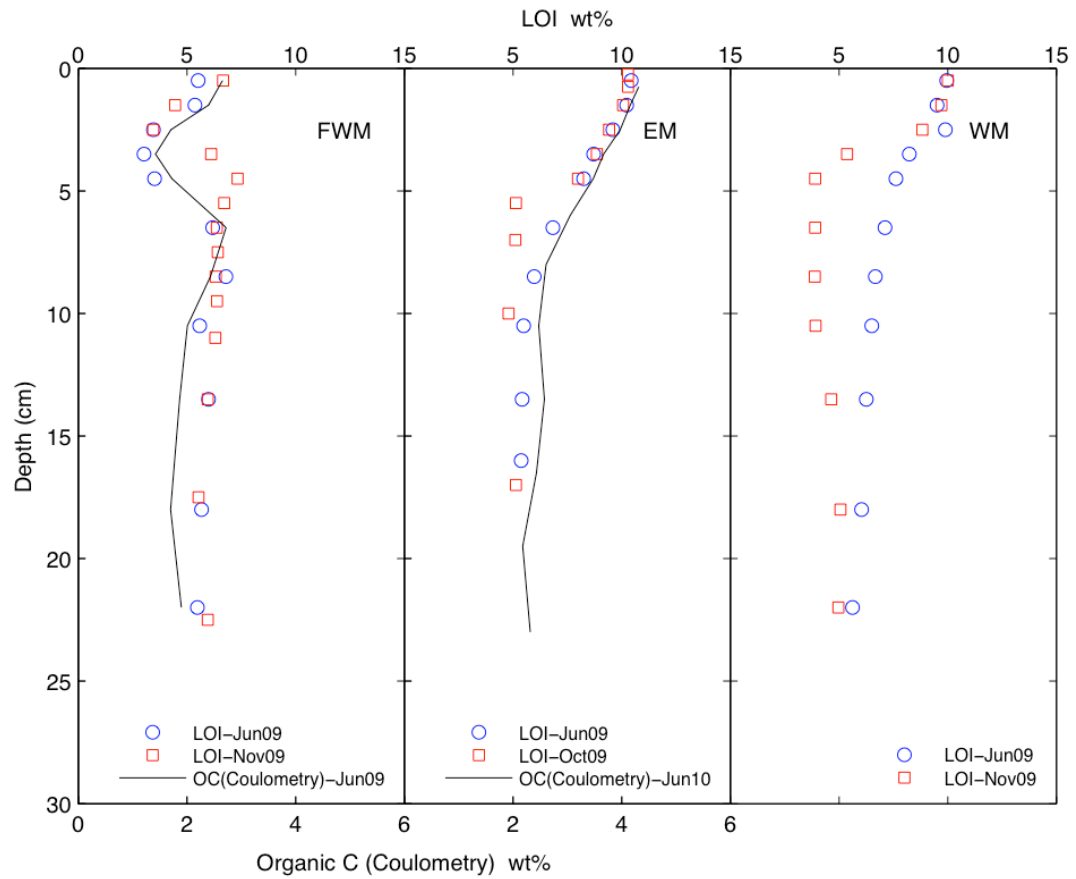
Figure 15. Organic carbon content (TOC) and loss-on-ignition (LOI) in Lake Superior sediments at Stations FWM, EM and WM.

(Coulometry data by M. Kistner)

Nitrate and ammonium concentrations and fluxes

The deep penetration of oxygen into the sediments leads to a correspondingly deep penetration of nitrate at all sampling sites (Fig. 16). Nitrate concentrations typically peak several mm below the SWI, decrease with depth to below the bottom-water nitrate levels, and disappear a few mm below the OPD (at FWM, EM-Jun/July10, WM-Jun10b, IR and CM). Where oxygen penetration is deep (> 12 cm), nitrate concentrations in the deep sediment porewater remain high, at about their bottom-water levels (EM-Jun/Oct09, WM-Jun/Oct09, WM_Jun10b). The porewater peak in nitrate seems to increase in magnitude from June to July (Fig. 16, e.g. FWM and IR). Ammonium concentrations increase monotonously with depth within the sediment, from below-detection or near-detection levels in the bottom waters to $\sim$ 5- 15 μmol L^{-1} in the deep sediment. An exception is the EM_Jun09 sample, where the ammonium profile exhibited a peak at $\sim$ 5 cm (Fig. 16).

The negative gradient of nitrate at the sediment-water interface indicates that sediments serve as sources of nitrate to the water column. The effluxes of nitrate (Table 10) calculated from nitrate gradients ranged between 0.05 and 0.36 mmol m^{-2} d^{-1}, averaging 0.17$\pm$0.07 mmol m^{-2} d^{-1}. This is consistent with previously reported estimates of 0.15$\pm$ 0.07 mmol m^{-2} d^{-1} in core incubations (Heinen McManus 2004). Nitrate effluxes at FWM did not exhibit any discernible seasonal pattern, whereas the nitrate efflux at IR in July was $\sim$ 3-4 times higher than in June (Table 11). Effluxes of NH$_4^+$ into the water column are an order of magnitude lower (from 1.2 x 10^{-2} to 2.7 x10^{-2} mmol m^{-2} d^{-1}, Table 12) than the effluxes of nitrate.
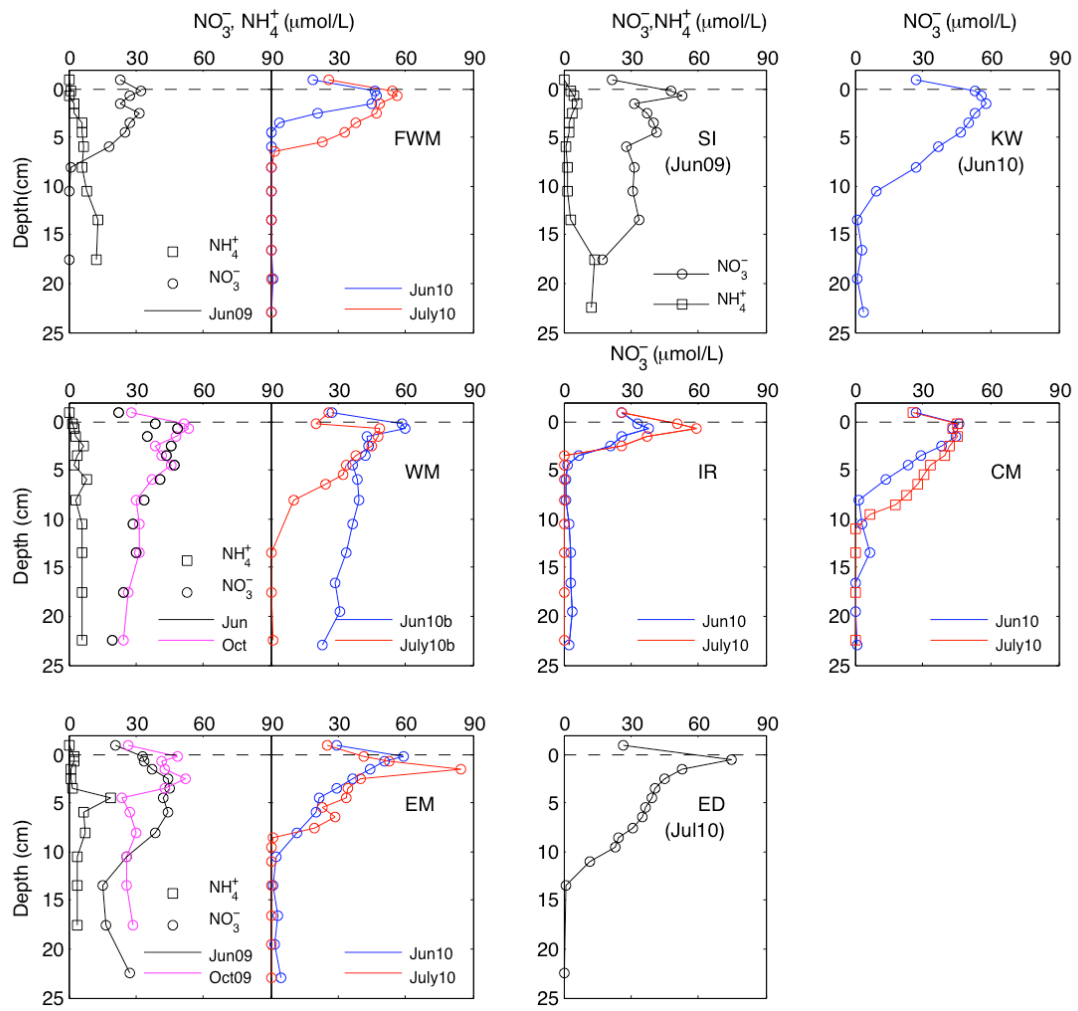
Figure 16. Distributions of nitrate and ammonium in porewaters of Lake Superior sediments.

Table 11. Nitrate effluxes from sediments into the water column (mmol m^{-2} d^{-1})

Stations	Jun09	Oct09	Jun10	July10	Consistency in OPD, physical properties
FWM	0.07		0.20	0.21	Yes
EM	0.09	0.16	0.22	0.12	No
WM	0.12	0.17	0.23	0.12	No
CM			0.14	0.15	OPD/metal layers shallower in June
IR			0.05	0.19	Yes
KW			0.19		
ED				0.36	
SI	0.19				

Table 12. Ammonium effluxes from sediments into the water column, (mmol m^{-2} d^{-1})

Stations	NH_4^+ effluxes
FWM	2.3 x 10^{-2}
EM	1.5 x 10^{-2}
WM	1.2 x 10^{-2}
SI	2.7 x 10^{-2}

Iron distributions and speciation

In sediments where oxygen and nitrate concentrations in the deep sediment remained high (below 12 cm at EM and WM), the sediments contained no dissolved Fe(II), indicating the absence of active iron reduction (Fig. 17). In sediments where oxygen and nitrate were depleted completely, dissolved Fe(II) increased in sediment porewaters below the depth of nitrate penetration. Such sediments contained solid Fe-rich layers, which were typically located near the depth of nitrate penetration.

Distributions of 0.5 N HCl-extractable iron fractions (amorphous Fe(III) oxides and solid-phase Fe(II) compounds) are shown in Fig. 18 . Increases in solid-phase Fe(II) below the OPDs are consistent with iron reduction. Enrichments in solid-phase Fe(III) at the depth of the sediment redox boundary are consistent with the oxidation of upward-diffusing Fe(II) at that depth. The Fe(III)-rich bands, often visible to a naked eye, are also revealed in the total Fe profiles obtained by high-resolution XRF scans (Fig. 19). Comparison of the XRF iron profiles with the distributions of Ti, which is typically associated with detrital sediment components, supports the idea that these Fe-rich layers formed diagenetically: Ti concentrations did not increase at the depths of the Fe-rich layers. Inconsistent with steady state diagenesis where a fixed redox boundary results in a single narrow metal layer, several sediment cores exhibited broad or multiple iron layers, as revealed by both high-resolution XRF profiles (Fig. 19) and visual observations (Fig. 8). Manganese layers located immediately above the uppermost iron layers were consistent with the diagenetic redox sequence. In cores EM-Oct09 and FWM-Jun09, the Fe- and Mn-rich layers were located within the oxidized sediment, above the depth of

oxygen penetration. The mechanisms and possible causes of this violation of the steady-state redox sequence are discussed in Chapter 4.
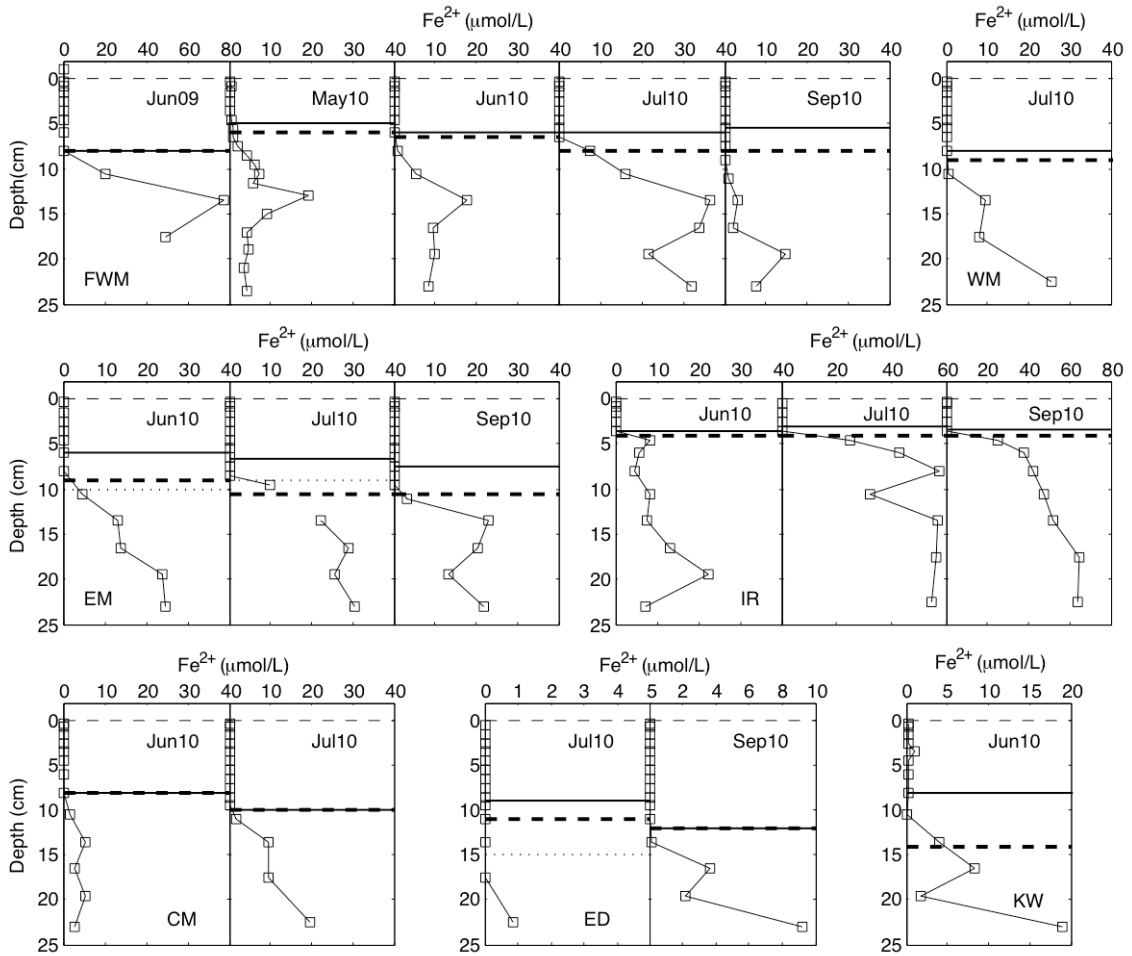
Figure 17. Distributions of dissolved Fe(II) in porewaters of Lake Superior sediments.

Thin horizontal dashed lines represent SWI; horizontal solid lines indicate OPDs; thick horizontal dashed lines mark the upper boundaries of iron-rich layers; dotted lines at EM_Jun10, EM_Jul10, and ED_Jul10 mark the depths of nitrate penetration.
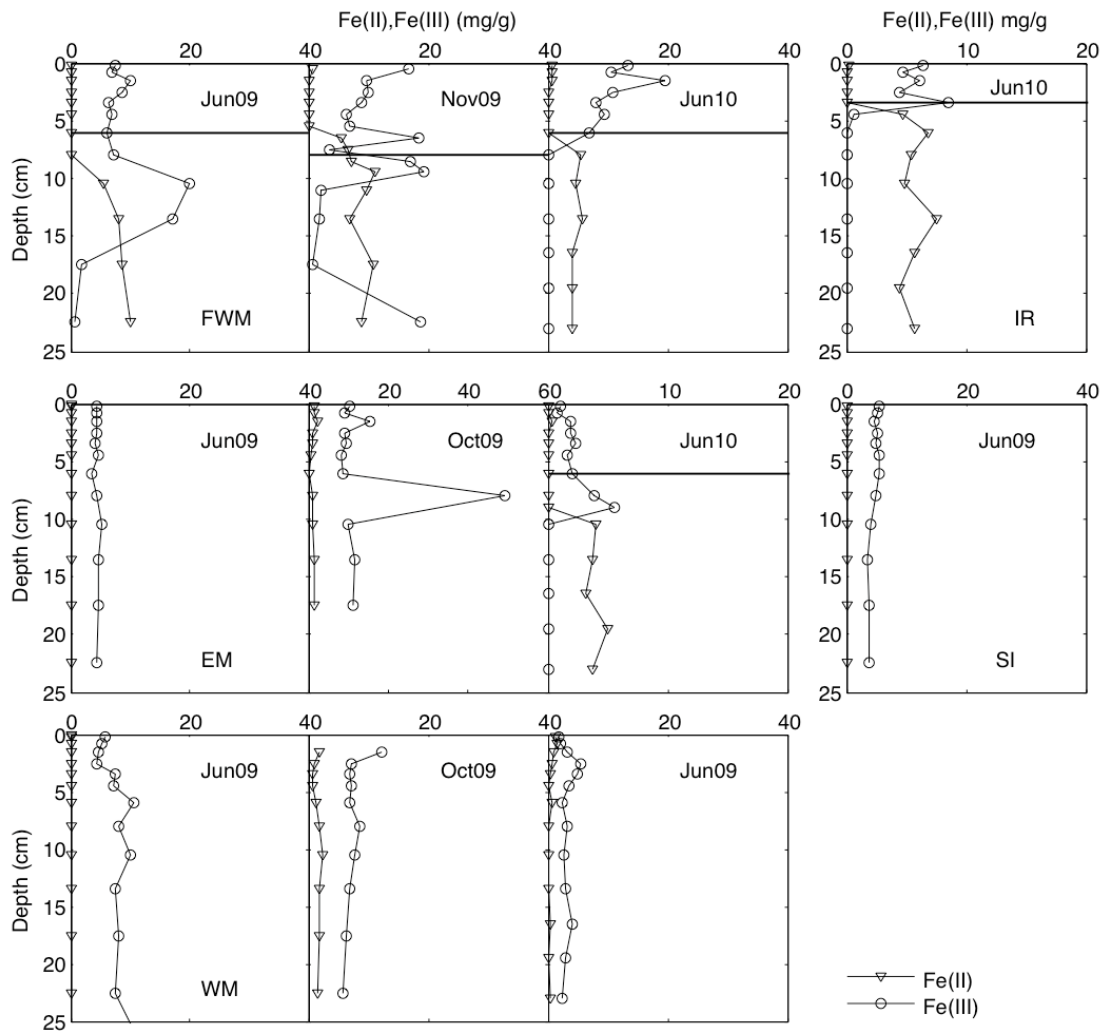
Figure 18. Distributions of 0.5N HCl-extractable solid Fe phases (typically corresponding to amorphous Fe(III) oxides and solid-phase Fe(II) compounds).
Horizontal solid lines indicate the OPDs.
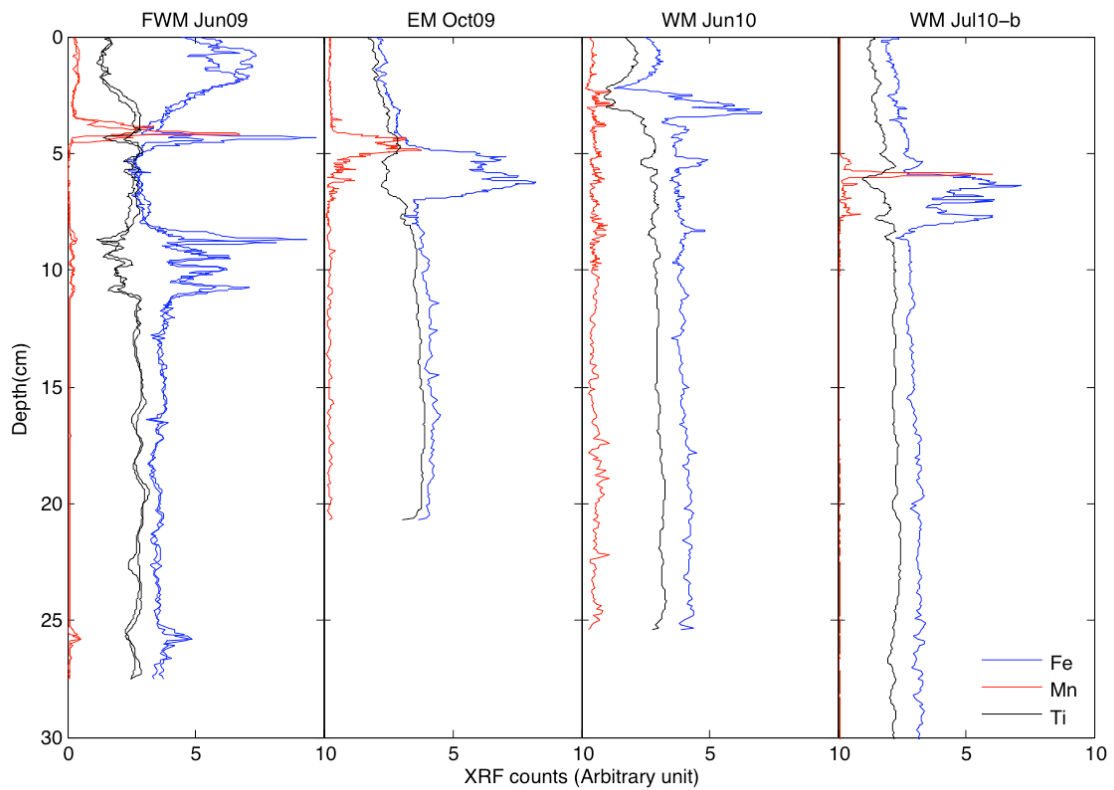
Figure 19. Scanning XRF counts for Fe, Mn, and Ti in sediments from FWM_Jun09, EM_Oct09, WM_Jun10 and WM Jul10-b.

Horizontal axes are in arbitrary units and individually scaled for each element, for visibility.

74

Phosphorus concentrations and fluxes

The concentrations of phosphate (SRP) in sediment pore waters increase with depth below the sediment redox boundary, concomitant with the increase in dissolved Fe(II) (Fig. 20). Dissolved phosphorus concentrations in the upper, oxidized, sediment layer are low, often < 1 μmol L^{-1} and close to the detection limit (on the order of 0.3 μmol L^{-1}). The SRP gradients at the SWI were similar among sediments with different OPDs. Fluxes of SRP into the water column, which were calculated from these gradients, were consistently small (< ~ 1.5 x 10^{-3} mmol m^{-2} d^{-1}; Table 13) for all stations where SRP profiles were determined. SRP concentrations in the bottom waters were close to or under the detection limit, therefore taken to be zero. Distributions of solid phase phosphorus phases obtained in sequential extractions are shown in Fig. 21. In the FWM-Jun09 core, which had a well-developed metal-rich layer, iron-bound phosphorus was the dominant P fraction, and the peak in the distribution of iron-bound phosphorus coincided with the location of the Fe(III) layer. In sediments with no iron layers, no enrichments in iron-bound phosphorus were observed (Fig. 21).
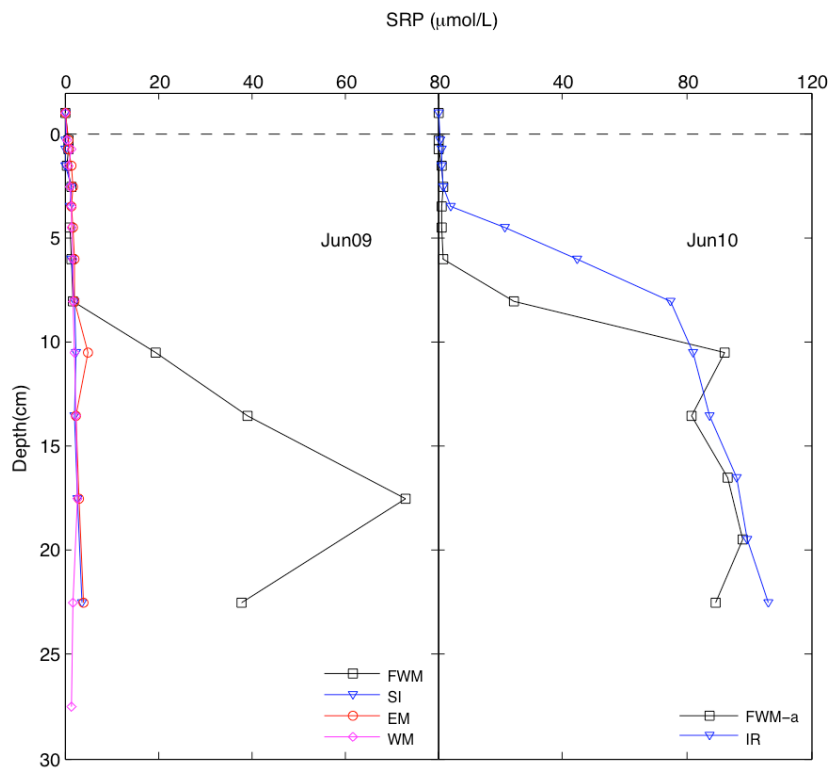
Figure 20. Soluble reactive phosphorus (SRP) in sediment porewaters at FWM, EM, WM, SI, and IR.

Table 13. Calculated SRP effluxes from sediments into water column, (mmol m^{-2} d^{-1})

Stations	SRP efflux
FWM_Jun09	1.5×10^{-3}
EM_Jun09	1.1×10^{-3}
WM_Jun09	1.2×10^{-3}
SI_Jun09	below detection
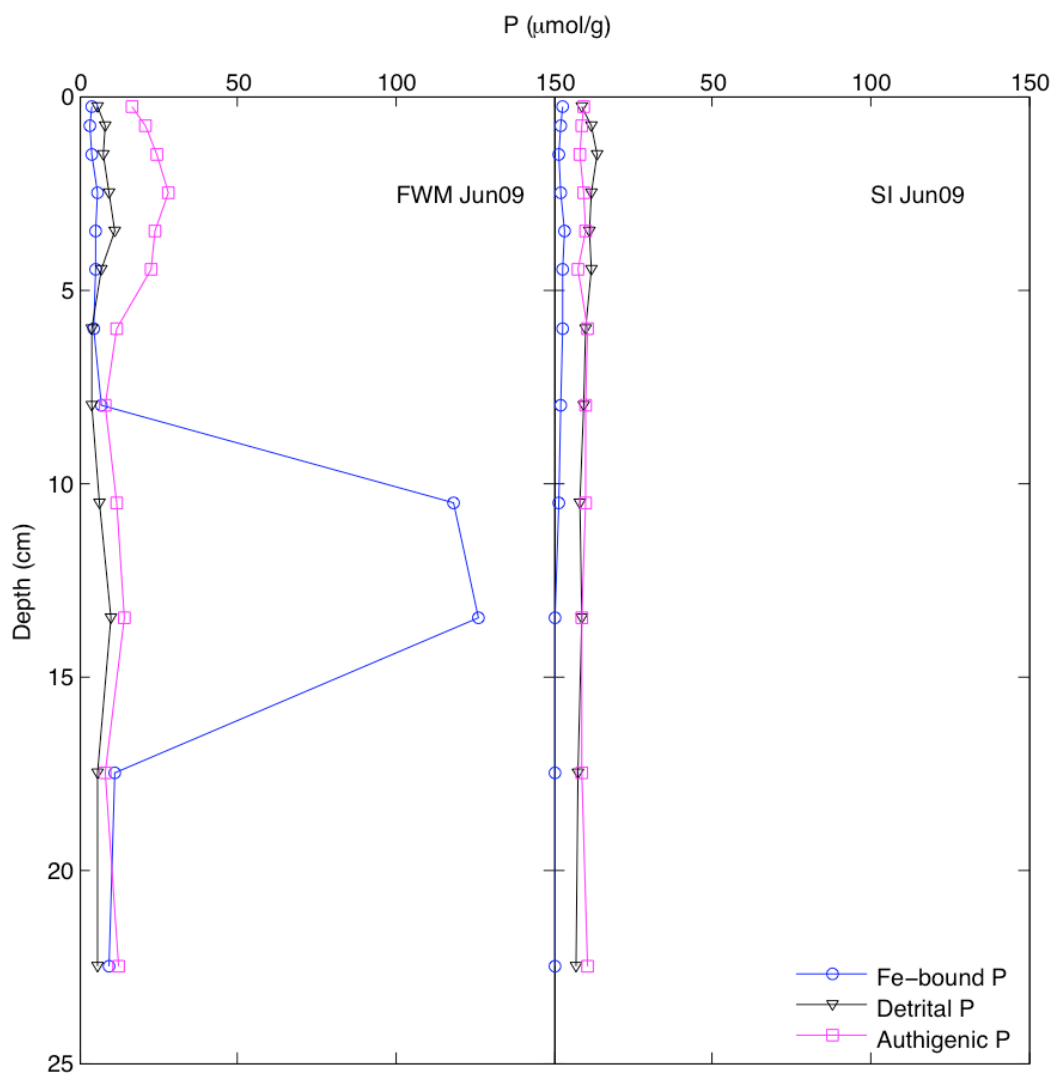
Figure 21.Solid-phase phosphorus speciation.

Fe-bound P represents easily reducible or reactive ferric Fe-bound phosphorus extracted by 0.30 M Na_3-citrate and 1.0 M $NaHCO_3$ (pH 7.6); Authigenic P represents Authigenic apatite plus $CaCO_3$- bound P plus biogenic apatite extracted by acetate buffer of pH 4; Detrital P represents detrital apatite phosphorus and other inorganic P extracted by 1 M HCl.

Chapter 4. Discussion: Sediment diagenesis in Lake Superior

Organic matter reactivity and carbon degradation rates

Despite the deep oxygen penetration, oxygen uptake rates in the upper sediments layers of Lake Superior are high (average 6.10 mmol m^{-2} d^{-1}). In marine sediments, oxygen fluxes of 2 -7 mmol m^{-2} d^{-1} are characteristic of the water depths of ~ 200 m, similar to the depths of our sediment samples (Fig. 22; Glud 2008). In such coastal marine sediments, oxygen penetration is only a few mm (Fig. 23). In contrast, in marine sediments with oxygen penetration of ~5 cm (typical of oceanic abyssal sediments at depths > 3000 m), total oxygen uptake is on the order of ~ 0.76 mmol m^{-2} d^{-1} (Glud 2008).

That directly measured oxygen uptake rates are higher than diffusive fluxes (2.92 mmol m^{-2} d^{-1}) suggests contribution from processes other than molecular diffusion. Such processes may include bioturbation and bioirrigation, or hydrodynamic forcing. Bioirrigation is typically weak in organic-poor sediments (Glud 2008) and weaker in freshwater than in marine environments. Bioturbation in lakes is conducted by smaller animals and is shallower than in the oceans where typical bioturbation depths exceed 10 cm. Our cores appeared bioturbated to no more than 2 cm below the interface. If results from stations WM and IR can be regarded as typical, the difference between the total and diffusive fluxes is ~ 30%.

The high oxygen uptake fluxes, in combination with deep oxygen penetration, indicate that the organic matter in Lake Superior consists of mostly reactive fractions that

become mineralized within the upper 1-2 cm of the sediment and that the sediment oxygen demand in the layers below is low. This is consistent with the high reactivity of organic carbon (typical maximum values between 0.4 and 1.4 $\mu mol\ cm^{-3}\ d^{-1}$, maximum k averages 1.21 yr^{-1}) in the upper 1 cm of sediment. These reactivity values are similar to those in marine sediments in similar water depths.

Significant seasonality in diffusive oxygen fluxes (Fig. 24; Fig. 13.1-8) could also reflect the presence of highly reactive material in the surface sediment where degradation rates vary over seasons. For example, the sediments in the North Atlantic (Smith and Baldwin 1984), where the organic material reaching the seafloor was very reactive ($k \sim$ 5-10 yr^{-1}), exhibited large seasonality in oxygen fluxes caused by seasonal variations in the rain flux of organic matter to the sediment.

That carbon degradation rates (0.01- 0.02 $\mu mol\ cm^{-3}\ d^{-1}$) calculated from organic carbon profiles were an order of magnitude lower than the maximum rates (0.64 $\mu mol\ cm^{-3}\ d^{-1}$) calculated from oxygen consumption suggests that more than 90% of the organic matter is consumed near the sediment-water interface. This reactive material may not appear in the organic carbon profile because of insufficient vertical resolution in the top sediment layer. Our results support the idea (Baker et al. 1991) that 80-90% of the organic matter reaching the lake floor is degraded near the sediment-water interface, aerobically.
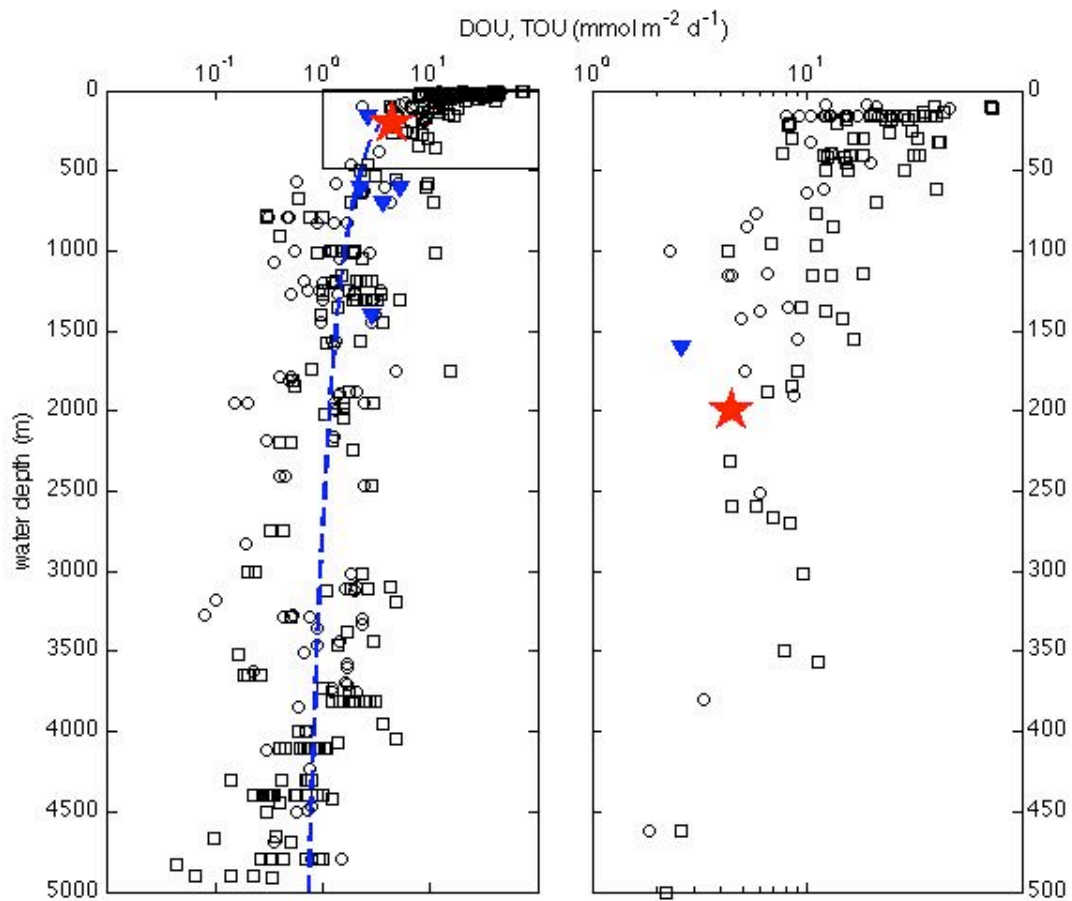
Figure 22. Lake Superior sediment diffusive oxygen uptake (DOU) and total oxygen uptake (TOU) in comparison to other lacustrine and marine systems.

Diffusive oxygen uptake (DOU, circles) and total oxygen uptake (TOU, squares) in marine sediments (replotted from Glud (2008)) and lake sediments (dotted line, from den Heyer and Kalff 1998). Stars are the results for Lake Superior from this study. Filled triangles are data in Lake Baikal (Maerki et al. 2006 and Müller et al. 2005).
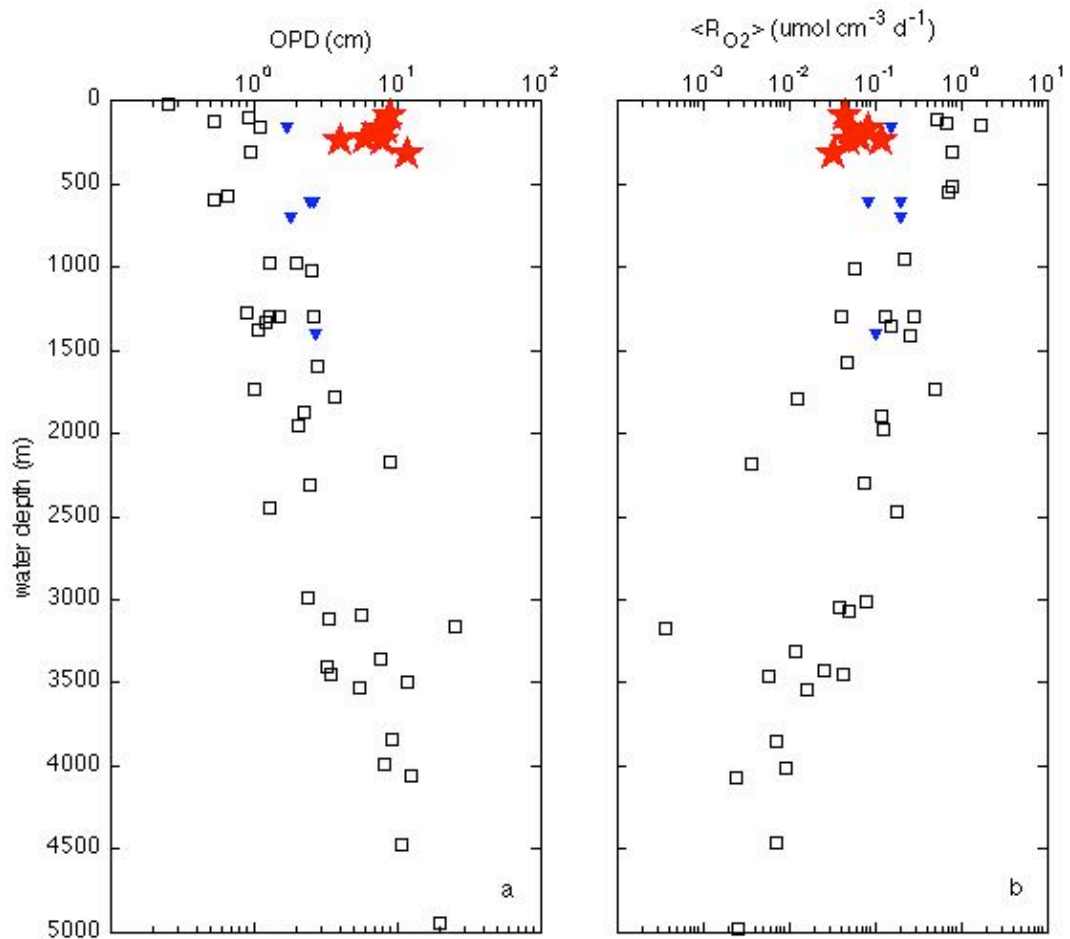
Figure 23. Lake Superior sediment oxygen penetration depth (OPD) and oxygen consumption rates (R_{O2}) in comparison to other lacustrine and marine systems.

Stars are the results for Lake Superior from this study. Filled triangles are data in Lake Baikal (Maerki et al. 2006 and Müller et al. 2005). a) Oxygen penetration depth. Data points are for marine sediments, from Glud (2008). b) Average carbon mineralization rates in the oxic sediment layer. Symbols are data in marine sediments (Glud 2008).
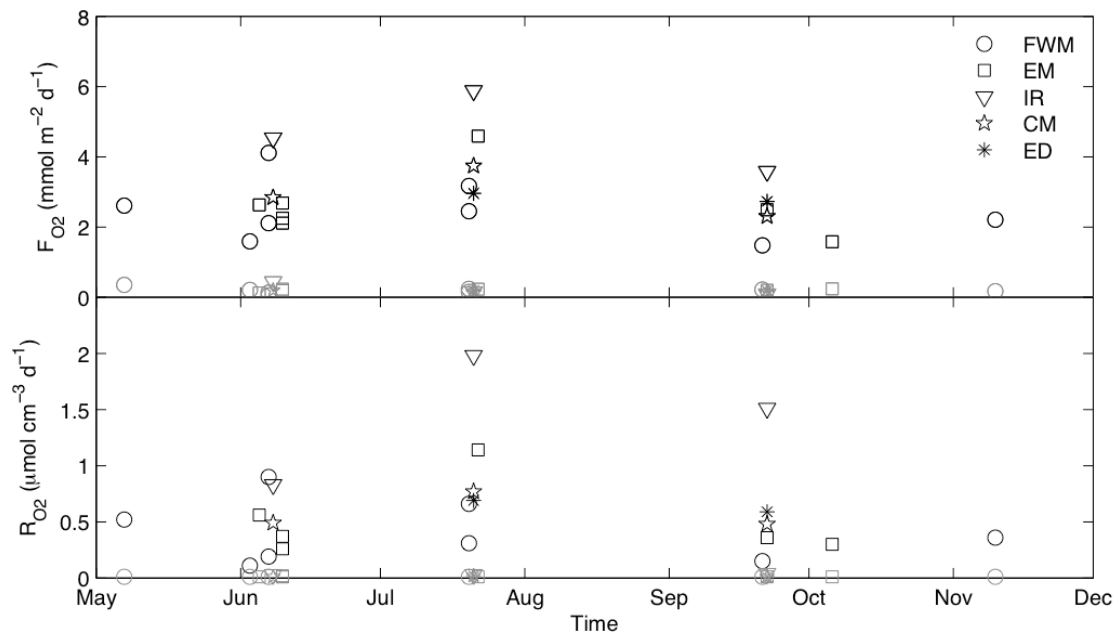
Figure 24. Seasonality in sediment oxygen fluxes (F$_{O2}$) and oxygen consumption rates (R$_{O2}$).

Black symbols are maximum values; grey symbols are values at 3 cm depth.

Nitrogen cycle and denitrification rates

The peaks in the nitrate concentrations several mm to cm below the sediment-water interface (SWI) indicate a locus of nitrification in that depth interval. In deeper layers, denitrification (Fig. 16) causes the depletion of nitrate from sediment porewaters, especially in sediments where oxygen penetration is relatively shallow. In sediments with deep OPDs, nitrate concentrations in the deep sediment remain high (at levels similar to those in the overlying waters). The sediment nitrogen cycle is illustrated in Fig. 25. The input of nitrogen to the sediments is primarily with organic sedimentation, as organic nitrogen. Degradation of organic matter within the sediment releases ammonium, which, to a large degree, is oxidized within the sediment. The nitrification reaction produces nitrate. In sediments with deep oxygen penetration (> 10 cm), ammonification and denitrification are negligible. In these sediments, nitrate produced by nitrification mostly fluxes out of the sediment into the water column. In anaerobic sediments, nitrate produced by nitrification is partly converted to N_2 via denitrification, but also diffuses upwards into the water column. The sub-interface peak in the nitrate concentration results in a positive nitrate gradient across the SWI, and the sediments in Lake Superior serve as net sources of nitrate to the water column (Table 11). Denitrification of downward-diffusing nitrate in the deeper sediment layers (down to ~15 cm depth at some locations) results in nitrate depletion there.

The amount of nitrogen removed from active circulation as N_2 via denitrification can be estimated by subtracting the sediment effluxes of nitrate and ammonium from the total ammonium production within the sediment. The latter can be estimated from the rate

83

of organic carbon mineralization by assuming a C:N ratio of 13:1 (Heinen and McManus, 2004). The rate of total carbon degradation can be calculated from the total oxygen uptake (Table 9) with a correction factor of 13/15=0.87 (see Chapter 2). In sediments with oxygen penetration of less than 10 cm, the total carbon degradation rate of $2.5 - 6.2$ m^{-2} d^{-1} translates into a total ammonium production of $0.19 - 0.48$ m^{-2} d^{-1}. Given the calculated effluxes of nitrate and ammonium (Table 11 and Table 12), the total amount of nitrogen released as N_2 is 0.18 mmol m^{-2} d^{-1} on average. In sediments with shallower OPD, ~2-8% of the total carbon degradation occurs by denitrification (Table 14), which is comparable to typical pelagic sediments with similar oxygen penetration (Burdige 2006).
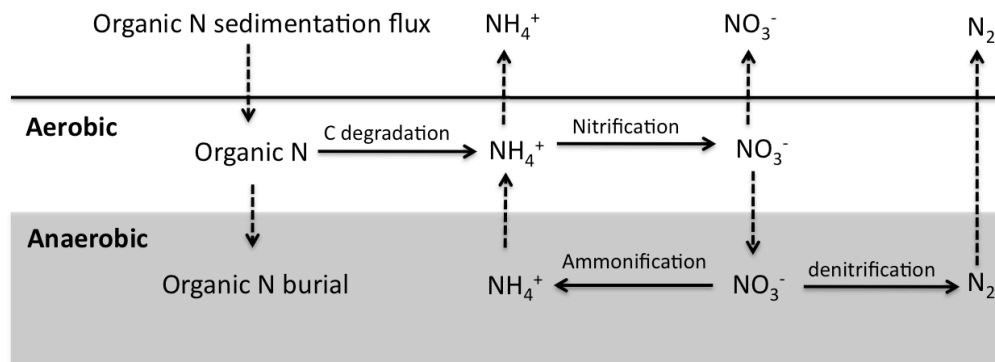
Figure 25. Schematics of the sediment nitrogen cycle

Horizontal solid line indicates the sediment-water interface; solid arrows indicate directions of diagenetic reactions; dotted arrows indicate sedimentation fluxes and diffusion processes.

Fe cycle and Fe reduction rates

The presence of dissolved Fe(II) and solid-phase Fe(II) below the depth of oxygen and nitrate penetration suggests active iron reduction there. In most of our sediment samples, Fe^{2+} appears in sediment porewater below the OPD, which is typical in aquatic sediments and suggests aerobic oxidation of upward-diffusing Fe(II) at the redox boundary. However, in some of our sediments (EM-Jun10, Jul10; KW-Jun10; ED-Jul10), the OPD and the depth of iron oxidation seemed to be separated by several cm. The depth of Fe oxidation in those samples seemed to coincide with the depth of nitrate penetration. This suggests an anaerobic oxidation of iron coupled to nitrate reduction (Burdige 1993; Straub et al. 1996). This is a relatively recently discovered pathway whose mechanisms, microbial mediators, and global contribution are still poorly quantified. Iron reduction,

whether aerobic or anaerobic, accounts for < 1% of total carbon degradation in Lake Superior sediments, with iron reduction rates ranging from 0.007 to 0.023 mmol m^{-2} d^{-1} (Table 14). The contribution of manganese reduction to carbon mineralization is expected to be even smaller, given the much smaller concentrations of Mn. As sulfate reduction rates are also low (Carlton et al. 1989), anaerobic pathways account for only a small percentage of carbon degradation in Lake Superior, with aerobic carbon degradation accounting for ~ 90- 95% of the total organic carbon degradation.

Table 14. Carbon degradation by anaerobic respiration pathways

Diffusive oxygen uptake was used as a measure of total oxygen consumption (carbon degradation) where data were not available (EM and CM). At stations where ammonium fluxes could not be calculated, ammonium fluxes were assumed to be small and negligible compared to nitrate fluxes, which are typically an order of magnitude higher. Carbon degradation by denitrification was estimated from the calculated rates of denitrification using a typical stoichiometry of the denitrification reaction of 5C:4N (Table 1). Iron reduction rates were estimated from fluxes of dissolved Fe(II) at the upper boundary of the iron reduction zone and the stoichiometry of the Fe reduction reaction 1C:4Fe (Table 1).

Station	Total carbon degradation (mmol m^{-2} d^{-1})	Input of N (mmol m^{-2} d^{-1})	N released from denitrification (mmol m^{-2} d^{-1})	Carbon degradation by denitrification (mmol m^{-2} d^{-1})	Carbon degradation by iron reduction (mmol m^{-2} d^{-1})
FWM	5.54; 6.18	0.42; 0.48	0.33; 0.26	0.41; 0.33 (7.4%; 5.3%)	0.0048
EM	4.0	0.31	0.19	0.23 (5.8%)	0.0017 - 0.0048
WM	3.86	0.29	0.17	0.21 (5.5%)	0.0018
CM	2.5; 3.3	0.19; 0.25	0.05; 0.1	0.06; 0.13 (2.4%; 3.9%)	0.0019
IR	4.3	0.33	0.14	0.18 (4.2%)	0.0058 - 0.0171
Average			**0.18**	**0.22 (5%)**	**0.4%**

The minimum time scale for the formation of Fe-rich sediment layers

The presence of Fe(III)-rich layers at the upper boundary of the iron reduction zone is consistent with the oxidation of upward diffusing dissolved Fe(II). The time scale required for the formation of these layers can be calculated from the estimated rates of iron reduction, as well as from the upward fluxes of Fe(II). The total amount of Fe(III) accumulated within such a layer is:

$$Fe(III)_{accumulation} = [Fe(III)] \times \rho_{sed} \times (1 - \varphi) \times \Delta X$$

where ρ_{sed} is the dry sediment density (3.0 g cm^{-3} was used for the iron-rich layer); φ is the porosity (0.7 cm^3/cm^3) and ΔX is the layer thickness. The average concentration of reactive iron within the layer, [Fe(III)], can be estimated (conservatively) from the amount of HCl-extractable ferric iron above the baseline. With a 1:4 (C:Fe) stoichiometry for microbial iron reduction, the required amount of labile organic carbon buried below the OPD into the iron reduction zone can also be calculated. Assuming 1% of organic carbon is available for Fe reduction ($\sim$ 0.4%; Table 11), the time required for reduction of these iron layers can be estimated as:

$$t = \frac{1}{4} \frac{Fe(III)_{accumulation}}{0.01 \times F_b}$$

where F_b is the organic carbon burial rate at the depth of iron reduction (mmol cm^{-2} yr^{-1}; For example, for the concentration of organic carbon of 1 wt%, burial rate of 0.04 cm/yr, dry sediment density of 2.5 g cm^{-3}, and porosity of 0.8 cm^3/cm^3, the carbon burial flux F_b is 0.017 mmol cm^{-2} yr^{-1}.).

Alternatively, the minimum time of iron layer formation can be estimated from diffusive fluxes of Fe^{2+} towards the redox boundary:

$$t = \frac{Fe(III)_{accumulation}}{F_{Fe(II)}}$$

The results from these two methods are compared in Table 15. Whereas in both cases the uncertainties are significant, it is clear that the formation of Fe-rich layers, as observed in the sediments of Lake Superior, requires at least several decades. The redistribution of sediment Fe(III) in response to potential variations in the sediment redox regime on seasonal time scale therefore must be insignificant. Any changes to the sediment redox regime that resulted in the formation of new metal-rich layers or diagenetic migrations of the previously formed layers need to have persisted for many years.

Table 15. Fluxes of Fe^{2+} at the upper boundary of the iron reduction zone and time required for the formation of iron-rich layers

1. Time for formation of iron-rich layers calculated from Fe(III) accumulation rates and carbon burial rates;

2. Time for formation of iron-rich layers calculated from Fe(III) accumulation rates and dissolved Fe(II) fluxes at the upper boundary of the iron reduction zone.

	Fe(III)-layer accumulation (mmol cm^{-2})	[1] Time for formation of Fe(III)-layer (yr)	Flux of dissolved Fe(II) (mmol cm^{-2} y^{-1})	[2] Time for formation of Fe(III)-layer (yr)
FWM_Jun09	0.15	225	7.04 x 10^{-4}	213
EM_Oct09	0.22	400		
EM_Jun10	0.053	100	2.55 x 10^{-4}	208
WM_Jun10	0.071	85		
IR_Jun10	0.019	60	8.45 x 10^{-4}	22

Phosphorus cycle. Phosphorus burial and recycling efficiency

Diagenetic mobility of phosphorus in Lake Superior sediments is strongly linked to the diagenetic cycling of iron. That porewater SRP concentrations increase with depth in concert with the increases in dissolved Fe(II) suggests that phosphate is mobilized by iron reduction (Fig. 20). Retention of phosphorus by iron oxyhydroxides is further suggested by a significant enrichment in iron-bound phosphorous within the iron-rich sediment layers (Fig. 21; FWM-09 in Fig. 18 and Fig. 19). The Fe:P ratio in the iron-rich layers ranged from ~30 to 60. This is higher than the typical ratio of < 15 at which the Fe oxides in sediments become saturated with phosphate (Jensen et al. 1992). This suggests that the phosphorus-retention capacity of these layers is not at its limit. In particular, this means that a partial dissolution of these layers would not be expected to result in phosphorus release. The consistently small fluxes of phosphorus across the SWI (average $(1.3 \pm 0.2) \times 10^{-3}$ mmol m^{-2} d^{-1}) support the idea that the sediment-water exchange fluxes of phosphorus can be only weakly affected by iron reduction. This could be expected in organic-poor sediments where oxygen penetration is deep and iron reduction occurs deep within the sediments. It is, nevertheless, in stark contrast to the situation in eutrophic lakes, where phosphorus mobilization in response to seasonally varying iron reduction rates is the primary supplier of phosphorus to the overlying water column (Katsev et al. 2006b; Hupfer and Lewandowski 2008.).

Contributions of sediment fluxes of carbon and nutrients to lake-wide budgets

Carbon -- The average oxygen uptake of 6.10± 1.39 mmol m^{-2} d^{-1} translates into a carbon degradation rate of 5.29± 1.20 mmol m^{-2} d^{-1} (with a factor of 13/15=0.87, see Chapter 2 for details). This is about a factor of two higher than the previous estimates in Lake Superior: 2.1 mmol m^{-2} d^{-1} estimated by Klump et al. (1989) and 1.7 ± 0.6 mmol m^{-2} d^{-1} estimated by Heinen and McManus (2004). At steady state, the rate of carbon degradation within the diagenetically active sediment layer and the rate of carbon burial into the deeper sediment (0.49 mmol m^{-2} d^{-1}) must add up to the rate of organic carbon supply to the sediment surface by organic sedimentation. This rate, 5.78± 1.20 mmol m^{-2} d^{-1}, suggests that the previous estimates for organic carbon sedimentation of 2.3-3.0 mmol m^{-2} d^{-1} obtained in Lake Superior in sediment traps (see Table 2; Heinen and McManus 2004; Johson et al. 1982) underestimated carbon sedimentation. The discrepancy is not entirely surprising, as sediment traps are known to have large uncertainties and methods based on sediment oxygen consumption may be more accurate in shallow water depths. The efficiency of sediment carbon mineralization is 5.3/5.8 = 90%, i.e. only 10% of the deposited organic carbon becomes buried into the deep sediments. Such high efficiency is not unusual in aquatic sediments, but is more typical of deep oceanic sediments where sedimentation rates are only a few cm per 1000 years (Reimers and Seuss 1983) rather than sediments in ~200 m water depth.

The average sediment carbon degradation rate of 5.29 ± 1.20 mmol m^{-2} d^{-1} is 19± 4% of the recently estimated gross primary production of 119 g m^{-2} yr^{-1} (Sterner 2010). This percentage of primary production exported to the sediments is higher than the

previous estimate of 5% (Baker et al.1991). The discrepancy, if real, may suggest that large areas of the lake are non-depositional and the lake-average decomposition rate in the sediments is lower than our estimate, or that the whole lake primary production was underestimated. However, this rate of export to the sediments ($\sim$ 20%) of organic carbon produced in the water column, matches the export efficiency in marine environments in 200 m water depth (Suess 1980). The burial flux of 0.49 mmol m^{-2} d^{-1} (0.18 Tg yr^{-1}) into the deep sediments represents $\sim$ 2% of the estimated gross primary production, which agrees well with the typical percentage of carbon burial in deep temperate lakes (Alin and Johnson 2007).

Nitrogen -- Our results suggest that the sediment nitrate effluxes are 0.17 $\pm$ 0.07 mmol m^{-2} d^{-1} and the organic nitrogen settling rates are 0.44 $\pm$0.01 mmol m^{-2} d^{-1}. (The N settling rates were calculated from the organic carbon settling rate of 5.78$\pm$ 1.20 mmol m^{-2} by assuming a C:N stoichiometry of 13:1). The nitrate effluxes agree with previous estimates (0.15 $\pm$0.07 mmol m^{-2} d^{-1}); our organic carbon settling rates, however, are greater than those obtained previously (2.3 mmol m^{-2} d^{-1} by Heinen and McManus (2004)) and, assuming a fixed C:N ratio, imply that the sedimentation of organic nitrogen in Lake Superior may be higher than previously thought. The corresponding correction to the lake-wide nitrogen budget moves the nitrogen budget toward balancing (Table 16). To further constrain the budget, the rates of nitrogen fixation and the DON fluxes need to be constrained better.

Table 16. Nitrogen budget of Lake Superior water column (mmol m^{-2} yr^{-1})

Table is modified from Table 3, with our results. Benthic fluxes of NO$_3^-$ are calculated using our estimate of 0.17±0.07 mmol m^{-2} d^{-1}. N sedimentation flux is calculated using our estimate for the organic carbon settling rate 5.63 ± 1.20 mmol m^{-2} d^{-1}, with a C:N ratio of 13 (Heinen and McManus 2004).

Source/Sink	Input	Output
Atmospheric deposition of NO$_3^-$ and NH$_4^+$	30.1	
Watershed input of Atmospheric deposition of NO$_3^-$, NH$_4^+$ and organic N	32.7	
Nitrogen fixation	Unknown	
Outflow of NO$_3^-$, NH$_4^+$ and organic N		28.6
Sedimentation flux		157 ± 33
Benthic flux of NO$_3^-$ [1]	62±26	
Benthic flux of DON [2]	100	
Total	**199-251**	**153-219**

94

Phosphorus -- Our calculated diffusive fluxes of phosphorus (1.3 ± 0.2) x 10^{-3} mmol m^{-2} d^{-1} are smaller than the fluxes that were previously estimated in sediment core incubations in the more productive western arm of the lake $(0.005 \pm 0.006$ mmol m^{-2} d^{-1}; Heinen and McManus, 2004), which had high uncertainty. Apart from spatial differences in phosphorus effluxes, some of the difference may be attributed to a non-negligible contribution from transport processes other than molecular diffusion, such as bioturbation. However, taking into account that such processes accounted for between 30 and 50% of the sediment oxygen fluxes, the phosphorus effluxes at our locations likely do not exceed 0.0026 mmol m^{-2} d^{-1}, which is still a factor of 2 smaller than the figure of Heinen and McManus (2004).

The consistency of the SRP fluxes across the SWI $((1.3 \pm 0.2)$ x 10^{-3} mmol m^{-2} d^{-1}) at a variety of locations, and the fact that phosphorus in the top several cm of sediment is bound to Fe(III) phases and relatively immobile, suggest that one may extrapolate SRP fluxes from a relatively small set of measurements to the entire lake. Our calculated diffusive effluxes of SRP are $\sim$ 2.4% of the estimated phosphorus sedimentation flux (0.053 mmol m^{-2} d^{-1}). The P sedimentation flux was obtained from the organic carbon settling rate 5.63 ± 1.20 mmol m^{-2} d^{-1} using a C:P ratio of 106 (Redfield 1934; Heinen and McManus 2004). That only a small percentage of the deposited phosphorus is returned to the water column suggests a high immobilization efficiency (97.6%) of phosphorus within the sediment, which is consistent with the immobilization efficiency of 80-95% in fresh water lakes. (The latter figure was obtained from a mmol dissolved P:mol DIC ratio of 1.2 ± 0.8 in the bottom waters of lakes (Caraco et al. 1990). Lower

values are typically found in marine sediments (< 50%; Sundby et al. 1992, Caraco et al 1990.). The contribution of sediments to the water-column phosphorus budget in Lake Superior is then estimated at ~ 16% of the total P input. The latter figure assumes that the atmospheric, point-source and riverine inputs of phosphorus to the lake are 200 Mmol yr^{-1} all combined (Table 4), but the uncertainty in this number is large, as atmospheric deposition rates, in particular, are poorly known.

Taconite deposition in the western arm

In the FWM sediment cores, millimeter-wide Mn- and Fe-rich layers reside within the oxic sediment layer, ~ 4 cm above the measured OPD. Below the depth of oxygen penetration, there are several more iron-rich layers (Fig. 26). This violation of the traditional redox sequence suggests that the OPD had been shallower in the past but at some point deepened to its present location. Our evidence suggests that the sediment redox chemistry at the FWM station is complicated by the deposition of taconite (depleted iron ore) tailings. Depleted iron ore was being discharged into the lake from 1955 to 1980 by the Silver Bay Mining Company, located ~30 km away from the FWM site. The narrow but prominent Mn- and Fe-rich layers at ~ 4.5 cm may be explained if one considers that oxygen demand exerted by the taconite particles is approximately double that of the regular sediment (Plumb and Lee 1983). Taconite deposition thus could shift the OPD upward, leading to the precipitation of Mn and Fe at the new redox boundary. Upon the cessation of taconite discharges after 1980 and the oxidation of the deposited taconite particles, the redox boundary would have migrated downward to its

present location. The taconite-affected layer contains the amount of iron that is in excess of the typical detrital inputs (relative to Ti). The broad peak in the bio-available Fe (0.5N HCl-extractable), however, is less pronounced than for the lower diagenetic Fe-rich layers (Fig. 26 and Fig. 18), suggesting the refractory character of this Fe. The taconite presence at FWM is further evidenced by high magnetic susceptibility in the upper 5cm of the FWM sediments (Fig. 26 and Fig.6), an order of magnitude higher than in typical Lake Superior sediments. The distribution of Pb in the sediments tracks historic trends in the atmospheric deposition of lead from gasoline (Graney et al. 1995; Niendorf 1998) and translates to a time interval between 1920 and 1970 for the sediment between 3.5 and 2 cm below the surface, which is consistent with the time interval of taconite deposition. The increase in copper concentrations at ~ 5 cm (Fig. 26) represents the time of the copper mine waste discharged to Lake Superior between 1895 and 1922 which had a significant effect on the western side of the Keweenaw Peninsula (Niendorf 1998). It agrees with the enrichment in taconite material at ~3.5 cm, assuming a sedimentation rate of 0.04 cm/yr: 1.5 cm/ (0.04 cm/yr) = 38 years. Taconite deposition explains the non-monotonous distribution of organic matter at FWM (Fig. 15), which is mirrored by the variation in sediment water content (Fig. 5): heavier taconite particles caused both a decrease in porosity and a decrease in organic carbon content per dry sediment weight.
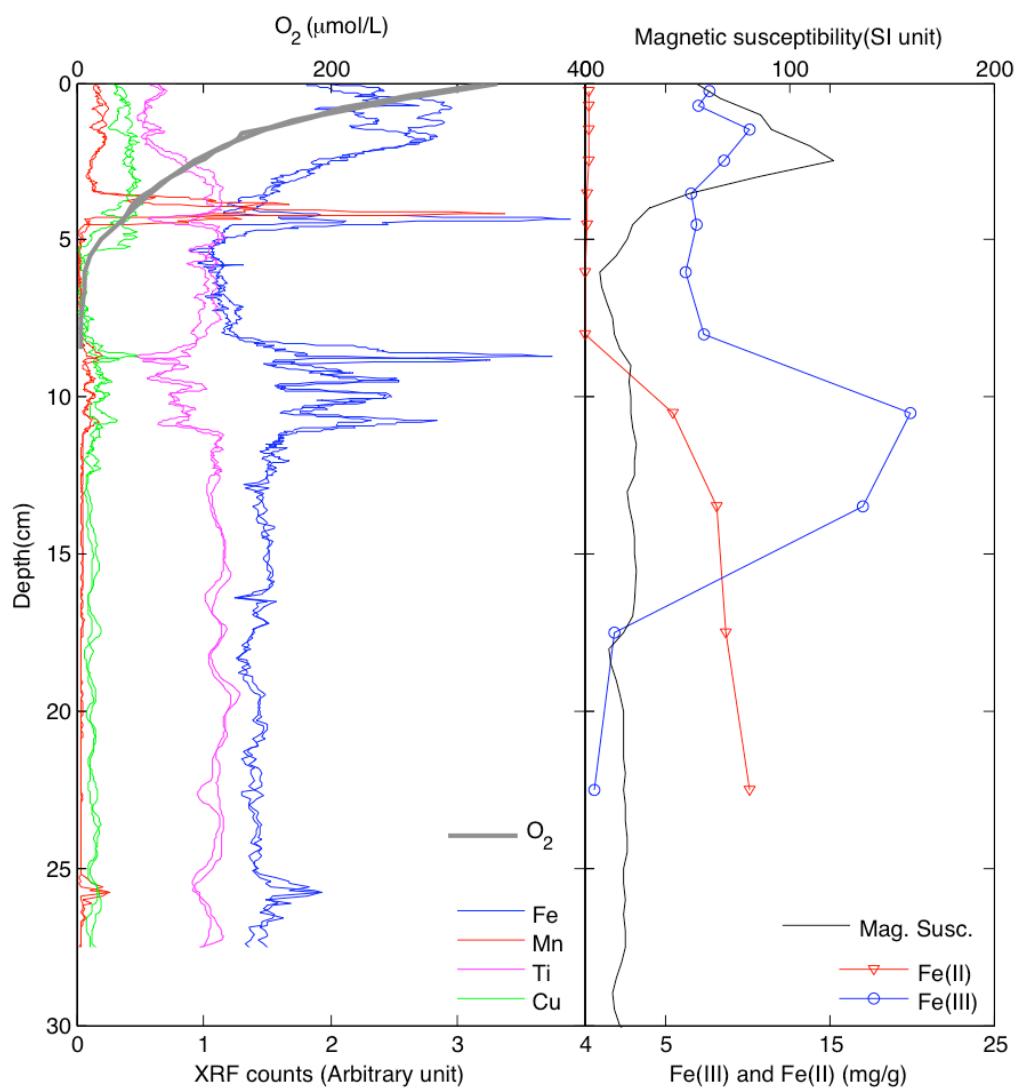
Figure 26. Distribution of dissolved oxygen, total Fe, Mn, Ti, and Cu (XRF), amorphous Fe(III) oxides and solid-phase Fe(II) compounds, and magnetic susceptibility at Station FWM.

Transient diagenesis: potential causes and time scales

At steady state, a single layer of manganese oxide precipitates at the depth of oxygen penetration, and iron (hydr)oxides precipitate immediately below (Burdige 2006). Multiple metal layers observed in Lake Superior sediments are incompatible with steady state diagenesis, suggesting that the redox boundary had migrated by as much as several centimeters. For example, the FWM_Jun09 sediment core had 4 iron-rich layers between 8-11 cm depth and a single layer at ~ 4.5 cm (Fig. 8 and Fig. 19). The mismatch between the present-day OPD and the locations of metal-rich layers suggest a non-steady state diagenesis. At locations other than in the taconite-affected western arm, for example in the EM_Oct09 core, diagenetic Fe and Mn layers are located within the oxic zone (Fig. 18 and Fig. 19), and the metal layers visible at 6 cm depth in the WM_Jun10-b core are inconsistent with the presently deep OPD (>12 cm, Fig. 8 and Fig. 12.3). A steady-state enrichment in diagenetic Fe (hydr)oxides requires a flux of Fe(II) from below and is impossible to reconcile with the absence of Fe(II) and the presence of O_2 in the underlying porewaters of these sediments. Therefore, these Fe-rich layers must have formed in the past: the OPD must have been shallower, allowing a flux of Fe(II) to the Fe (hydr)oxide enrichment. Subsequent changes must have allowed the redox boundary to migrate deeper into the sediment to its present position.

Given the great heterogeneity of the lake floor (van Alstine 2006), it is possible that the multiple metal-rich layers in Lake Superior and the mismatch between these layers and the OPD have resulted from physical disturbances to the sediments by bottom currents. For example, during strong storm events, upper sediment layers might have

been removed and redeposited at other locations. This would redistribute the sediment organic matter into different redox zones and alter the redox environment of sediments (Wakeham and Ganuel 2006). Whether the non-steady state features in Lake Superior have resulted from physical disturbances is difficult to test. It is useful, however, to assess the potential contributions of other common causes of sediment redox changes.

The depth of oxygen penetration into aquatic sediments is sensitive to the concentration of oxygen in the overlying water and the reactivity and sedimentation flux of organic matter. In Lake Superior, seasonal variations in oxygen levels in the bottom waters are small, on the order of 10% (Table 8), but they cannot be discounted as a driver for OPD migrations because in organic-poor sediments the OPD is highly sensitive to changes in oxygen concentrations in the bottom water (Katsev et al. 2006). The timing of the changes in bottom water oxygen concentrations, nevertheless, suggests that the mismatch between the observed OPD and the position of redox-sensitive metal enrichments has resulted from something other than seasonal variations in bottom-water O_2: the bottom water oxygen levels in Lake Superior increase after spring mixing in June and decline continuously as the summer stratification develops until an overturn in December re-supplies oxygen to the hypolimnion (Table 8; McManus et al. 2003; Russ et al. 2004). The oxygen penetration depths would be expected to follow the same trend: the OPD would reach its maximum after the mixing, then move upwards continuously until after the winter overturn. A time lag would be expected for oxygen diffusion but it would not exceed a few months. (For a typical diffusion coefficient of $D=400$ cm^2/yr, oxygen diffuses to $x=8$ cm in 1 month.) In contrast, in St. EM samples that were taken in June

(shortly before the Spring overturn) and in October 2009, OPDs were consistently deep (Fig. 9); in WM samples that were taken in June and September, oxygen penetration was deep and reaching far below the iron rich layers (Fig. 10). One of the WM_Jul2010 cores had an OPD of 8 cm, which matched the iron layer at ~9 cm, but this shallower OPD was not consistent with the relatively higher levels of bottom oxygen in July 2010 (Table 8). Thus, mismatches between the OPD and metal rich layers by several cm are unlikely to be seasonal but seasonal fluctuations in bottom water oxygen levels could be responsible for small-scale (< 1 cm) migrations of the OPD and thus for the formation of multiple closely spaced Fe peaks seen in the XRF profiles (Fig. 19).

The flux of organic matter to the sediment surface affects the OPD on a timescale that is determined by the sedimentation rates and reactivity of organic material (Sayles et al. 1994; Katsev et al. 2006). An episodic deposition of reactive organic carbon, e.g. caused by bottom currents, could potentially cause a single-time upward excursion of the OPD, which then could have resulted in the formation of new shallow metal-rich layers (e.g., similar to processes in marine turbidites (Burdige 2006)). A mass balance calculation, however, suggests that this scenario is unlikely to explain formation of new Fe layers in sediments where the OPD was sufficiently deep to suppress active Fe reduction. For example, reduction of iron required for the formation of iron layers in the EM_Oct09 core requires a burial of $0.22/4=0.055$ mmol cm^{-2} of labile organic carbon below the OPD. The sedimentation flux of organic carbon required to drive such a shift can be estimated as 1.1 mmol cm^{-2}, assuming 5% of the total organic carbon mineralization is through iron reduction (conservatively). For the wet sediment density of

~1 g/cm^3, water content of 90%, and the assumed thickness of 1 cm in organic-rich layer, it would need to have contained 13% of reactive organic carbon by dry weight. Given that typically less than half of all organic carbon is reactive and the organic carbon is typically less than 5%, the scenario of an episodic deposition or organic matter causing the redox migration of several cm is unlikely.

Large seasonal variations in OPD in response to organic sedimentation, e.g. during summer algal bloom or winter ice-melt, would be possible only if material reaching the lake bottom were sufficiently fresh and labile to allow its decomposition on the time scale of several months or shorter. Heinen and McManus (2004) reported minimum particle settling fluxes during winter (0.5 mmol m^{-2} d^{-1}) and maximum during spring (3.6 mmol m^{-2} d^{-1}), from sediment traps located in the western arm of the lake. The deepening of oxygen penetration from July to September in 2010 at stations EM and ED (Fig. 27), where sediment cores were consistent between seasons, suggests that the redox boundaries there may oscillate seasonally. That the locations of iron layers in these sediment cores (EM and ED) were deeper than the OPDs and seemed to match the depths of nitrate penetration suggests migrations of the nitrate penetration depths.

The high oxygen consumption rates in the upper 1 cm of the sediment (see Figures.13 and discussion above) suggest a higher reactivity of the organic carbon (average k ~ 1.2 yr^{-1}) than what was previously estimated (a time scale of 10-20 years for the remineralization of organic carbon at the SWI; Baker et al., 1991). The strong seasonality in oxygen fluxes and carbon degradation rates agrees with the high reactivity of organic material in the surface layers. Whether the magnitude of these fluctuations in

the amount of fresh organic material supplied to the lake floor is sufficient to shift the redox boundary is still an open question.

Besides the seasonally variable organic carbon fluxes, migrations of the sediment OPD may reflect a decrease in organic carbon sedimentation on a longer, e.g., decadal, time scale. At FWM, the organic carbon content at the sediment surface is lower than at ~5 cm, a layer that was "capped" by taconite deposition, which suggests that the organic carbon sedimentation fluxes at present are lower than they were before the taconite deposition in the 1950-60s. Organic sedimentation in Lake Superior may have followed the historical trends in the water column concentrations of phosphorus, the limiting nutrient that controls the lake productivity (Smith 1982; Dillon and Rigler 1974; Schindler 1977; Sterner 2004). Although the historical data on water column phosphorus levels and primary production are limited, documentation of total phosphorus loadings into the Great Lakes shows that the inputs of phosphorus have increased in the 1950-60s, peaked in the 1970s and declined since the 1980s, which correlates with the decline in the use of phosphate detergents (Lesht et al. 1991). The organic carbon fluxes to the Lake Superior sediments could be expected to follow a similar trend. The OPD therefore most likely became shallower in the middle of the 20th century, and then began to deepen in the late 1980s. In addition to the reduction in anthropogenic phosphorus inputs, the increase of open-water summer temperatures in Lake Superior by ~3.5 °C over the past century and the corresponding increase in the length of summer stratification (Austin and Colman 2008) could potentially decrease the primary production of Lake Superior by increasing the periods of nutrient limitation or light limitation (model of Lehman 2002). In

103

summary, the origin of the multiple iron-rich layers in Lake Superior sediments remains enigmatic: whereas iron-rich layers that are presently found within the oxic zone could have formed during the period of shallower OPDs in the 1950-60s, most sediments have metal-rich layers below the present-day OPD, which argues against a widespread deepening of the OPD since the 1980s.
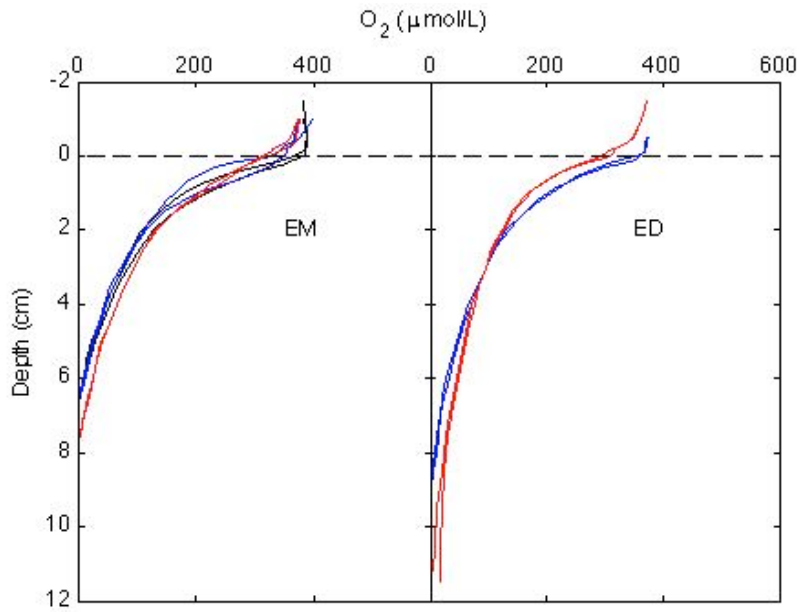

Figure 27. Seasonality in sediment oxygen penetration depths at EM and ED.

Chapter 5. Conclusions

- Sediments in Lake Superior exhibit strong spatial heterogeneity, especially in the open-water stations of western and eastern basins (EM and WM sites). Striking differences were observed in oxygen penetration depths, locations of metal-rich layers within the sediment column, and the color of sediment cores, on spatial scales as small as tens of meters.

- The sediments in Lake Superior contain multiple layers of Fe and Mn that form dense crusts often visible to the naked eye. Mass balance calculations suggest that these layers form over decades or longer. Mismatches between the depths of oxygen and nitrate penetrations and the positions of metal layers suggest non-steady state diagenesis. The causes and time scale of transient diagenesis remain open questions.

- Oxygen penetration into the sediments of Lake Superior is deep ($\sim$ 3.5 cm to > 12 cm). The average diffusive sediment oxygen uptake is $\sim 2.92 \pm 0.75$ mmol m^{-2} d^{-1} and the total oxygen uptake is $\sim$ 6.10 mmol m^{-2} d^{-1}. Our estimated carbon degradation rate of 5.29 ± 1.20 mmol m^{-2} d^{-1} is a factor of two higher than the previous estimates obtained in sediment traps. The calculated reactivity of the organic carbon in the upper 1 cm of sediments is ~ 1.2 yr^{-1}, suggesting that a significant fraction of the deposited material decomposes on a seasonal time scale.

105

The very top millimeters of the sediment are likely to contain large quantities of even more reactive material.

- The depth of oxygen penetration varies seasonally by several millimeters. A time lag of several weeks to months is expected between the variations in bottom-water oxygen levels and the OPD, with greater lags expected in sediments with deeper oxygen penetration. Oxygen fluxes into the sediments and the rates of oxygen consumption in the upper sediment layer also exhibit seasonality, with higher consumption rates in mid-summer.

- Aerobic respiration accounts for > 90-95% of the total carbon degradation. In sediments with shallower oxygen penetrations, denitrification rates average 0.22 mmol m^{-2} d^{-1}, contributing ~ 5% to the total carbon mineralization. Iron reduction rates in these sediments average 0.005 mmol m^{-2} d^{-1} and contribute < 1% to the total carbon degradation.

- Diffusive fluxes of nitrate from sediments into the water column average 0.17± 0.07 mmol m^{-2} d^{-1}, consistent with previous (Heinen and McManus 2004) estimates. Our estimated carbon sedimentation rate (5.63 ± 1.20 mmol m^{-2} d^{-1}) yields the organic nitrogen settling rate of 157 ± 33 mmol m^{-2} yr^{-1} (based on a 13C:1N ratio), which is higher than the previous estimate of 127 mmol m^{-2} yr^{-1}

(Heinen and McManus, 2004). The higher organic nitrogen settling rates move the nitrogen budget of Lake Superior closer to balance.

- Diffusive SRP fluxes across the SWI are smaller than previous estimates and vary little across locations (average $(1.3 \pm 0.2) \times 10^{-3}$ mmol m^{-2} d^{-1}).

- Lake Superior sediments are weaker carbon sinks than marine sediments in similar water depths. Whereas the total rates of carbon degradation in Lake Superior are similar to those in other freshwater and marine environments in similar water depths, the organic material is mineralized closer to the sediment-water interface. The prolonged exposure to oxygen results in a more complete carbon burndown. The resultantly low consumption of oxygen in the deep sediment allows oxygen to diffuse much deeper than in otherwise similar marine sediments.

References:

Alin, S., and T.C. Johnson. (2007) Carbon cycling in large lakes of the world: A synthesis of production, burial, and lake–atmosphere exchange estimates. Glob. Biogeochem. Cycles, 21: GB3002, doi: 10.1029/2006GB002881.

Alstine, van J.D. (2006) A high resolution study of the spatial and temporal variability of natural and anthropogenic compounds in offshore Lake Superior sediments. M.Sc. thesis. Univ. of Minnesota.

Archer, D. E., J. L. Morford, S. R. Emerson. (2002) A model of suboxic sedimentary diagenesis suitable for automatic tuning and gridded global domains. Glob. Biogeochem. Cycles, 16 (1): 10.1029/2000BG001288

Austin, J. and S. Colman. (2008) A century of temperature variability in Lake Superior. Limnol. Oceanogr., 53(6):2724-2730

Baehr, M. M. and J. McManus. (2003) The Measurement of phosphorus and its spatial and temporal variability in the western arm of Lake Superior. J. Great Lakes Res., 29(3): 479-487

Baker, J. E., S. J. Eisenreich and B. J. Eadie. (1991) Sediment trap fluxes and benthic recycling of organic carbon, polycyclic aromatic hydrocarbons, and polychlorobiphenyl congeners in Lake Superior. Environ. Sci. Technol., 25(3): 500-509

Bender, M. L. and D. T. Heggie. (1984) Fate of organic carbon reaching the deep sea floor: a status report. Geochmica et Cosmochimica Acta, 48: 977-986

Bennett, E. B. (1978) Characteristics of the thermal regime of Lake Superior. Internat. Assoc. Great Lakes Res., 4(3-4): 310-319

Bruland, K. W. and M. Koide. (1975) Lead-210 and pollen geochronologies on Lake Superior Sediments. Quaternary Research, 5: 89-98

Burdige, D. J. (1993) The biogeochemistry of manganese and iron reduction in marine sediments. Earth-Science Reviews, 35: 249-284

Burdige, D. J. (2006) Geochemistry of marine sediments. Princeton Univ. Press.

Boudreau, B. P. (1997) Diagenetic Models and Their Implementation. Modelling Transport and Reactions in Aquatic Sediments. Springer.

Canfield, D. E. (1994) Factors influencing organic carbon preservation in marine sediments. Chemical Geology, 114: 319-329

Carlton, R. G., G. S. Walker, M. J. Klug, and R. G. Wetzel. (1989) Relative values of oxygen, nitrate, and sulfate to terminal microbial processes in the sediments of Lake Superior. J. Great Lakes Res., 15(1): 133-140

Caraco, N., J. Cole, and G. E. Likens. (1990) A comparison of phosphorus immobilization in sediments of freshwater and coastal marine systems. Biogeochemistry, 9(3): 277-290

Caraco, N., J. Cole, G. E. Likens. (1993) Sulfate control of phosphorus availability in lakes. Hydrobiologia, 253: 275-280

Chapra S.C. and W.C. Sonzogni. (1979) Great Lakes total phosphorus budget for the mid 1970s. J. WPCF, 51: 2524-2532.

Colley, S., J. Thomson, T. R. S. Wilson and N. C. Higgs. (1984) Post-depositional migration of elements during diagenesis in brown clay and turbidite sequences in the North East Atlantic. Geochimica et Cosmochimica Acta, 48: 1223-1235

Cotner, J. B., B. A. Biddanda, W. Makino and E. Stets. (2004) Organic carbon biogeochemistry of Lake Superior. Aquatic Ecosystem Health and Management, 7:451-464.

Dalsgaard, T., B. Thamdrup and D. E. Canfield. (2005) Anaerobic ammonium oxidation (anammox) in the marine environment. Research in Microbiology, 156: 457-464

Dean, W. E. Jr. (1974) Determination of carbonate and organic matter in calcareous sediments and sedimentary rocks by loss on ignition: comparison with other methods. Journal of sedimentary petrology, 44(1): 242-248

Heyer, den C., and J. Kalff (1998) Organic matter mineralization rates in sediments: A within- and among-lake study. Limnol. Oceanogr., 43: 695–705.

Diamond, D. (1999) QuickChem Method 31-107-04-1-A: Determination of nitrate in brackish or seawater by flow injection analysis. Zellweger Analytics Lachat Instruments Division.

Diamond, D. (1995) QuickChem Method 31-115-01-3-C: Determination of orthophosphate in brackish or sea water by flow injection analysis. Zellweger Analytics Lachat Instruments Division.

Dickens, G. R., M. Koelling, D. C. Smith, L. Schnieders, and the IODP Expedition 302 Scientists, (2007) Rhizon Sampling of Pore Waters on Scientific Drilling Expenditions: An Example from the IODP Expedition 302, Arctic Coring Expedition (ACEX). Scientific Drilling, No. 4, March.

Dillon, P. and F. H. Rigler. (1974) The phosphorus-chlorophyll relationship in lakes. Limnol. Oceanogr., 19:767-773.

Evans, J. E. (1980) 210Pb geochronology in Lake Superior sediments: sedimentation rates, organic carbon deposition, sedimentary environments, and post-depositional processes. M.Sc. thesis. University of Minnesota

Evans, J. E., T. C. Johnson, E. C. Alexander Jr., R. S Lively and S. J. Eisenreich. (1981) Sedimentation rates and depositional processes in Lake Superior from ^{210}Pb geochronology. Journal of Great Lakes Research, 7: 299-310.

Froelich P. N., G. P. Klinkhammer, M. L. Bender, N. A. Luedke, G. R. Heath, D. Gullen, P. Dauphin, D. Hammond, B. Hartman and V. Maynard. (1979) Early oxidation of organic matter in pelagic sediments of the eastern equatorial Atlantic: suboxic diagenesis. Geochim. Cosmochim. Acta, 43: 1075-1090.

Gehlen, M., C. Rabouille, U. Ezat, and L. D. Guidi-Guilvard. (1997) Drastic changes in deep-sea sediment porewater composition induced by episodic input of organic matter. Limnol. Oceanogr. 42(5): 980-986.

Graney, J. R., A. N. Halliday, G. J. Keeler, J. O. Nriagu, J. A. Robbins, S. A. Norton. (1995) Isotopic record of lead pollution in lake sediments from the northeastern United States. Geochimica et Cosmochinmica Acta, 59(9): 1715-1728

Gobeil C., B. Sundby, R. W. Macdonald, And J. N. Smith. (2001) Recent change in organic carbon flux to Arctic Ocean deep basins: Evidence from acid volatile sulfide, manganese and rhenium discord in sediments. Geophys. Res. Lett., 28: 1743–1746.

Glud, R. N., J. K. Gundersen, H. Rφy and B. B. Jφrgensen. (2003) Seasonal Dynamics of Benthic O_2 uptake in semiencolsed bay: importance of diffusion and faunal activity. Limnol. Oceanogr., 48(3): 1265-1276

Glud, R. N. (2008) Oxygen dynamics of marine sediments. Mar. Biol. Res., 4: 243–289.

Hecky, R. E., (2000) A biogeochemical comparison of Lake Superior and Malawi and the limnological consequences of an endless summer. Aquat. Ecosyst. Health Manage., 3: 23-33

Heinen, E. A. (2002) Carbon and nutrient cycling in western Lake Superior. M.Sc. thesis. Univ. of Minnesota.

Heinen E.A. and J. McManus. (2004) Carbon and nutrient cycling at the sediment-water boundary in western Lake Superior. J. Great Lakes Res., 30 (Suppl. 1): 113-132.

Hulth, S., R. C. Aller, and F. Gilbert. (1999) Coupled anoxic nitrification/manganese reduction in marine sediments. Geochimica et Cosmochimica Acta, 63 (1): 49-66

Hupfer, M and J. Lewandowski. (2008) Oxygen controls the phosphorus release from lake sediments – a long-lasting paradigm in limnology. Internat. Rev. Hydrobiol., 93 (4-5): 415-432.

Holmes, R. M., A. Aminot, R. Kérouel, B. A. Hooker, and B. J. Peterson. (1999) A simple and precise method for measuring ammonium in marine and freshwater ecosystems. Can. J. Fish. Aquat. Sci., 56: 1801-1808

Jensen, H. S., P. Kristensen, E. Jeppesen, and A. Skytthe. (1992) Iron: phosphorus ratio in surface sediment as an indicator of phosphate release from aerobic sediments in shallow lakes. Hydrobiologia, 235/236: 731-743

Johnson, T. C., J. E. Evans, and S. J. Eisenreich. (1982) Total organic carbon in Lake Superior sediments: Comparisons with hemipelagic and pelagic marine environments. Limnol. Oceanogr., 27: 481-491

Katsev S., B. Sundby, and A. Mucci. (2006) Modeling vertical excursions of the redox boundary in sediments: Application to deep basins of the Arctic Ocean. Limnol. Oceanogr., 51:1581-1593.

Katsev, S., I. Tsandev, I. L'Heureux, D. G. Rancourt. (2006 b) Factors controlling long-term phosphorus efflux from lake sediments: Exploratory reactive-transport modeling. Chemical Geology, 234: 127-147

Kemp A.L.W., C.I. Dell, and N.S. Harper. (1978) Sedimentation rates and a sediment budget for Lake Superior. J. Great Lakes Res., 4: 276-287.

Keough, J. R., M. E. Rierszen, C. A. Hagley. (1996) Analysis of a Lake Superior coastal food web with stable isotope techniques. Limnology and Oceanography, 41: 136-146

Klump, J.V., P. Paddock, C. C. Remsen, S. Fitsgerald, M. Boraas, and P. Anderson. (1989) Variation in accumulation rates and the flux of labile organic matter in eastern Lake Superior basins. J. Great Lakes Res., 15:104–122.

Lesht, B. M., T. D. Fontaine III, D. M. Dolan. (1991) Great Lakes total phosphorus model: post audit and regionalized sensitivity analysis. J. Great Lakes Res., 17(1):3-17

Lehman, J. T. (2002) Mixing patterns and plankton biomass of the St. Lawrence Great Lakes under climate change scenarios. J. Great Lakes Res., 28(4):583-596

Maerki, M., B. Muller, and B. Wehrli. (2006) Microscale mineralization pathways in surface sediments: A chemical sensor study in Lake Baikal. Limnol. Oceanogr., 51(3): 1342-1354

Maier, W. J. and W. R. Swain. (1978) Lake Superior organic carbon budget. Water Res., 12: 403-412

Mangini, A., M. Jung, and S. Laukenmann, (2001) What do we learn from peaks of uranium and of manganese in deep sea sediments? Mar. Geol., 177: 63-78

Martens, C. S., and J. V. Klump. (1984) Biogeochemical cycling in an organic-rich marine basin – 4. An organic carbon budget for sediments dominated by sulfate reduction and methanogenesis. Geochim. Cosmochim. Acta, 48: 1987-2004

Martin, W. R., and M. L. Bender. (1988) The variability of benthic fluxes and sedimentary remineralization rates in response to seasonally variable organic carbon rain rates in the deep sea: A modeling study. Am. J. Sci., 288: 561-574

Matheson, D. H. and M. Munawar. (1978) Lake Superior basin and its development. J. Great Lakes Res., Internat. Assoc. Great Lakes Res., 4(3-4):249-263

McManus, J, E. A. Heinen and M. M. Baehr. (2003) Hypolimnetic oxidation rates in Lake Superior: Role of dissolved organic material on the lake's carbon budget. Limnol. Oceanogr., 48(4): 1624-1632

Middelburg, J, K. Soetaert, P. M. J. Herman, C. H. R. Heip. (1996) Denitrification in marine sediments: A model study. Global biogeochemistry cycles., 4: 661-673

Müller B., M. Maerki, M. Schmid, E.G. Vologina, B. Wehrli, A. Wüest, and M. Sturm. (2005) Internal carbon and nutrient cycling in Lake Baikal: sedimentation, upwelling, and early diagenesis. Global and Planetary Change, 46: 101-124.

Munawar, M. and I. F. Munawar. (1978) Phytoplankton of Lake Superior 1973. J. Great Lakes Res., Internat. Assoc. Great Lakes Res., 4(3-4): 415-442

Niendorf, C. R. (1998) An evaluation of anthropogenic trace metals in the western basin of Lake Superior. M.Sc. thesis. Univ. of Minnesota.

Ostrom, N. E., D. T. Long, E. M. Bell and T. Beals. (1998) The origin and cycling of particulate and sedimentary organic matter and nitrate in Lake Superior. Chem. Geol., 152: 12-28

Plumb, R. H. Jr., G. F. Lee. (1983) Oxygen demand of taconite tailings. Water Pollution Control Federation, 55(3): 317-322

Poulton S.W. and D.E. Canfield. (2005) Development of a sequential extraction procedure for iron: implications for iron partitioning in continentally derived particulates. Chem. Geol., 214: 209-221.

Rabouille C. and J.-F. Gaillard. (1991) A coupled model representing the deep-sea organic carbon mineralization and oxygen consumption in surficial sediments. Journal of Geophysical Research, 96(C2): 2761-2776

Redfield A.C. (1934) On the proportions of organic derivations in sea water and their relation to the composition of plankton. In *James Johnstone Memorial Volume*. (ed. R.J. Daniel). University Press of Liverpool, pp. 177-192.

Revsbech, N.P. (1989) An oxygen microelectrode with a guard cathode. Limnol. Oceanogr., 34: 472-476

Richardson, L. L., and K. H. Nealson. (1989) Distributions of manganese, iron, and manganese-oxidizing bacteria in Lake Superior sediments of different organic carbon content. J. Great Lakes Res., 15(1): 123-132.

Roden, E. E., and J. W. Edmonds. (1997) Phosphate mobilization in iron-rich anaerobic sediments: Microbial Fe(III) oxide reduction versus iron-sulfide formation. Arch. Hydrobiol., 139: 347-378.

Roden, E.E. and R.G. Wetzel. (2002) Kinetics of microbial Fe(III) oxide reduction in freshwater wetland sediments. Limnol. Oceanogr., 47: 198-211.

Russ, M. E., N. E. Ostrom, H. Gandhi, P. H. Ostrom, N. R. Urban. (2004) Temporal and spatial variations in R:P ratios in Lake Superior, an oligotrophic freshwater environment. Journal of Geophysical Research., 109, V10S12, doi:10.1029/2003JC001890

Ruttenberg K.C. (1992) Development of a sequential extraction method for different forms of phosphorus in marine sediments. Limnol. Oceanogr., 37: 1460-1482.

Sayles, F.L., W.R. Martin, and W.G. Deuser. (1994) Response of benthic oxygen-demand to particulate organic-carbon supply in the deep-sea near Bermuda. Nature, 371: 686–689.

Sauter, E. J., M. Schluter and E. Suess. (2001) Organic carbon flux and remineralization in surface sediments from the northern North Atlantic derived from pore-water oxygen microprofiles. Deep-Sea Research I, 48: 529-553

Schindler, D. W. (1977) Evolution of Phosphorus Limitation in Lakes. Science, 195: 260

Smith, V. H. (1982) The nitrogen and phosphorus dependence of algal biomass in lakes: An empirical and theoretical analysis. Limnol. Oceanogr., 27: 1101-1112.

Smith, K. L., and R. J. Baldwin. (1984) Seasonal fluctuations in deep-sea sediment community oxygen consumption: central and eastern North Pacific. Nature, 307(16): 624-626

Stark, R. A. (2009) Nitrate production and nitrogen and carbon cycling in Lake Superior Sediments. M. Sc. thesis. University of Minnesota.

Sterner, R. W., T. M. Smutka, R. M. L. McKay, X. Qin, E. T. Brown, R. M. Sherrell. (2004) Phosphorus and trace metal limitation of algae and bacteria in Lake Superior. Limnol. Oceanogr., 49(2):495-50.

Sterner R.W., E. Anagnostou, S. Brovold, G. S. Bullerjahn, J. C. Finlay, S. Kumar, R. M. Mckay, and R. M. Sherrell. (2007) Increasing stoichiometric imbalance in North America's largest lake: Nitrification in Lake Superior. Geophys. Res. Lett., 34: L10406.

Sterner, R. W. (2010) In situ-measured primary production in Lake Superior. J. Great Lakes Res., 36: 139-149.

Strous, M, J. A. Fuerst, E. H. M. Kramer, S. Logemann, G. Muyzer, K. T. van de Pas-Schoonen, R. Webb, J. G. Kuenen & M. S. M. Jetten. (1999) Missing lithotroph identified as new planctomycete. Nature, 400: 446-449.

Straub, K. L., M. Benz, B. Schink, and F. Widdel. (1996) Anaerobic, Nitrate-Dependent Microbial Oxidation of Ferrous Iron. Applied and Environmental Microbiology, Apr: 1458- 1460

Suess, E. (1980) Particulate organic carbon flux in the oceans: surface productivity and oxygen utilization. Nature, 288 (20): 260- 263

Sundby, B., C. Cobeil, N. Silverberg, and A. Mucci (1992) The phosphorus cycle in coastal marine sediments. Limnol. Oceanogr., 37(6): 1129-1145

Thomson, J. and N. C. Higgs, S. Colley. (1996) Diagenetic redistributions of redox-sensitive elements in northeast Atlantic glacial/interglacial transition sediment. Earth and Planetary Science Letter, 139: 365-377

Urban N.R., M. T. Auer, S. A. Green, X. Lu, D. S. Apul, K. D. Powell, and L. Bub. (2005) Carbon cycling in Lake Superior. J. Geophys. Res., 110: C06S90.

Viollier, E., P. W. Inglett, K. Hunter, A. N. Roychoudhury, P. Van Cappellen. (2000) The ferrozine method revisited: Fe(II)/Fe(III) determination in natural waters. Applied Geochemistry, 15: 785-790

Wakeham S. G. and E. A. Canuel. (2006) Degradation and preservation of organic matter in marine sediments. The Handbook of Environmental Chemistry, 2: 295-321

Weier, R. R. (1978) Chemistry of Lake Superior. J. Great Lakes Res., 4: 370-385

Wetzel, R. G. (2001) Limnology, Third Edition: Lake and River Ecosystems. Elsevier Science (USA).

Wilson, T. R. S., J. Thomson, D. J. Hydes, S. Colley, F. Culkin, J. Sϕrensen. (1986) Oxidation fronts in pelagic sediments: diagenetic formation of metal-rich layers. Science, 232(4753): 972-975